WIND-TUNNEL STUDY OF GAS DISPERSION
NEAR A CUBICAL MODEL BUILDING

by

Wen-Whai Li
Robert N. Meroney
Jon A. Peterka

Prepared for

Site Safety Research Branch
Office of Nuclear Regulatory Research
U.S. Nuclear Regulatory Commission
Washington, D.C. 20555

ABSTRACT

WIND-TUNNEL STUDY OF GAS DISPERSION
NEAR A CUBICAL MODEL BUILDING

The dispersion of effluent plumes emitted from the surface of a cubical model building into its near wake region ($\frac{x}{H} \leq 5$) has been examined. The model study was performed in a wind tunnel with a simulated neutrally stratified shear layer. Mean concentration measurements were made on the building surface and within the near wake region of the model building. Measurements of the concentration fluctuation intensity and the peak-to-mean concentration ratio were also conducted in the near wake.

The concentration level on the lee face of a model building is greatly reduced by the presence of a nearby sharp building edge. The optimum location for an intake vent on the building, for equal effluent exhaust to vent intake distances, is a position not directly downwind and at a location where the intake cannot "see" the exhaust vent.

The log-normal concentration probability model was found appropriate for measurements in the building wake ($1.0 \leq \frac{x}{H} \leq 5.0$). The concentration fluctuation intensity was found to be reduced by the presence of the model building from that of a plume released in an obstructed flow. A simple algorithm, based on the relation of the peak-to-mean concentration ratio and the local concentration fluctuation intensity, suggests an upper limit for the peak-to-mean concentration ratios near the ground centerline.

ACKNOWLEDGMENTS

TABLE OF CONTENTS

LIST OF TABLES

LIST OF FIGURES

LIST OF SYMBOLS

Symbol	Definition	Units
A	Area of building	cm^2
A_c	Cross-wind cross-sectional area of building	cm^2
A_e	Area of the exit vent	cm^2
A_{plume}	Cross-sectional area of the plume	cm^2
B_1	Constant	
D	Dilution factor	
D_e	Exhaust Vent ID	cm
E	Voltage output from a transducer	volts
F_r	Froude number	
g	Gravitational acceleration constant	$cm\ sec^{-2}$
g'	Velocity reduction factor	
H	Reference height of building	cm
H_c	Height of roof cavity above roof	cm
H_{rw}	Height of roof wake above roof	cm
h_b	Height of building	cm
h_s	Height of stack from ground	cm
I_c	Local concentration fluctuating intensity $$(\overline{\chi'^2})^{1/2}/\bar{\chi}$$	
$(I_c)_{1G}$	Absolute concentration fluctuating intensity $$(\overline{\chi'^2})^{1/2}/\bar{\chi}$$	
$(I_c)_{CL\infty}$	Centerline ground level local intensity far downwind	
J	Jet momentum factor	
K	Non-dimensional concentration coefficient (see Eq. 1)	
K_e	Non-dimensional concentration coefficient at (see Eq. 2) the effluent exit	

LIST OF SYMBOLS (CONTINUED)

Symbol	Description	Units
K_o	Nondimensional concentration coefficient in absence of cuilding (see Eq. 3)	
L	Reference length	cm
L_c	Roof cavity length	
L_1	Length of building along-wind	cm
M_r	Local concentration to source concentration ratio	
n	Exponent in power law velocity profile	
$p(\chi)$	Concentration probability density function	
Q	Volume flow rate of the effluent	cm^3/sec
R	Characteristic building length (se Eq. 25)	cm
Re	Reynolds number	
Ro	Rossby number	
R_r	RMS concentration fluctuations relative to source strength	
r	Air distance between vent exit and intake location	cm
s	"Stretched-String" distance between vent exit and intake location	cm
U	Free stream velocity	$cm\ sec^{-1}$
U_H	Wind velocity at building height	$cm\ sec^{-1}$
U_p	Mean speed in the neighborhood of the plume	$cm\ sec^{-1}$
W	Width of building	cm
W_e	Vent effluent exit velocity	$cm\ sec^{-1}$
x,y,z	Coordinates with origin at vent location	cm
z_o	Effective roughness height	cm
x',y',z'	Coordinates in plume relative to sampling location	cm
$\sigma_x, \sigma_y, \sigma_z$	Standard deviations of plume	cm
σ_ℓ	Logarithmic standard deviation	cm

Symbol	Description	Units
θ	Wind direction or building orientation	degrees
ρ_a	Density of air	$g\ cm^{-3}$
ρ_e	Density of effluent	$g\ cm^{-3}$
ω	Angular velocity	sec^{-1}
ν	Kinematic viscosity	$cm^2\ sec^{-1}$
δ	Boundary layer thickness	cm
γ	Intermittency factor	
χ	Mean gas concentration	ppm
χ_e	Gas concentration at the effluent exit	ppm
χ_p	Peak gas concentration	ppm
χ_{1G}	Mean gas concentration at x/H = 1.0, y/H = 0.0, z/H = 0.0	ppm
$\left(\dfrac{\chi_p}{\chi}\right)_{j\%}$	Peak-to-mean concentration ratio not exceeded j% of the time	
$(\overline{\chi'^2})^{1/2}$	RMS of gas concentration fluctuations	ppm
$\Omega(\chi)$	Cumulative probability density function	
Λ	Turbulent integral length scale	cm

Note: A number of nonrecurrent symbols are defined in the text when used.

Chapter 1

INTRODUCTION

The dispersion of effluent plumes emitted on or near buildings is a concern common to health physicists, regulatory agencies, and air conditioning engineers. When the exhaust gas contains toxic, flammable, bacteriological, or odorous material, one is interested not only in the average levels of concentration but their instantaneous peak values and the associated probability distributions.

There is relatively little guidance available in handbook format, and the problem is difficult to deal with theoretically. It is an aspect of dispersion which is ideally suited for study in wind tunnels or water channels. This report presents experimental results directed toward the following objectives:

(1) Determine building surface concentration distributions which result from different roof vent locations and building orientations for a simple building shape.

(2) Specify the concentration level and distributions which occur in the near wake region $(\frac{X}{H} \leq 5)$ behind a simple building geometry.

(3) Examine the instantaneous concentration fluctuations in the building wake and the resultant probabilities of exceeding various peak-to-mean concentration ratio values.

(4) Recommend simple dilution factor algorithms which account for building orientation, vent location, and exhaust to inlet vent separations.

A short literature review of related measurements and prediction algorithms is provided in Chapter 2. Wind tunnel facilities, simulation criteria imposed, and experimental techniques are discussed in Chapter 3. Experimental results are presented and discussed in Chapter 4. Chapter 5 summarizes the general conclusions and subsequent recommendations.

Chapter 2

LITERATURE REVIEW

2.0 Introduction

This chapter contains a review of building aerodynamics and gas dispersion near buildings. The physical models reviewed will be used to interpret the behavior of gas dispersion near the model building or to explain the physical flow structure in the near wake region behind a model building.

Section 2.1 presents the dilution theory and minimum dilution algorithms recommended by other investigators. The mean concentration levels in the near wake region reported by different authors are reviewed in Section 2.2. Results from recent measurements of concentration fluctuations are presented in Section 2.3. Section 2.4 is a brief summary of the flow structure in the near wake region around a model building.

2.1 Dilution Theory

When gaseous contaminants are discharged from building vents into the atmosphere near a building, the contaminants are initially transported by the mean flow in the zone near the building. The accompanying turbulent diffusion of contaminants is dominated by the turbulent motion within the wake. In the study of mean concentration behavior, the general nondimensional concentration coefficient, K, is defined as the ratio of the actual concentration at any point in the field, χ, to a reference concentration

$$K = \frac{\chi L^2 V}{Q} \qquad (1)$$

where   L : reference length

V : reference velocity

Q : contaminant release rate (Halitsky, 1968)

In the present study, L and V are chosen as $\sqrt{A_c}$, and U_H, respectively, where, A_c is the cross wind, cross-sectional area of the building for $\theta = 0°$ orientation and U_H is the velocity at the height of the building.

An effluent exit value for the parameter K may be defined as

$$K_e = \frac{\chi_e A_c U_H}{Q} \qquad (2)$$

where χ_e is the concentration of the effluent exit. A reference value for concentrations resulting from an equivalent source strength plume located at a similar location in the absence of the building may be defined as

$$K_o = \frac{\chi_o \, A_c \, U_H}{Q} \tag{3}$$

where χ_o is the concentration at an equivalent receptor location in the absence of the building.

A dilution factor D was defined by Halitsky (1961) as the ratio of gas concentration at the effluent exit, χ_e, to the concentration at the receptor point, χ, i.e.,

$$D \equiv \frac{\chi_e}{\chi} = \frac{K_e}{K} \tag{4}$$

Halitsky (1962) examined the geometry of a plume and suggested that the diameter of the plume cross section at a distance s (see Figure 1) from the center of the effluent vent is

$$D_p = f \, D_e + 2 \, m \, s \tag{5}$$

where, D_p : diameter of plume

D_e : diameter of exhaust vent

f : initial expansion factor for jet diameter

m : half-rate of plume expansion

He assumed that the lateral concentration distribution within the plume is conical with a maximum at the center and zero at the edge (thus, the maximum is three times the average), and he suggested that the mean speed in the neighborhood of the plume, U_p, will be less than the free wind speed, U, by some reduction factor, $g' = U_p/U$. Therefore, for a cubically shaped building the dilution factor can be expressed using conservation of mass and some algebraic manipulation, as

$$D_{min} = \frac{\chi_e}{\chi_{max}} = \frac{A_{plume} U_p}{3 A_e W_e} = [\alpha + \beta \, (\frac{s}{\sqrt{A_e}})]^2 \, (\frac{U}{W_e}) \tag{6}$$

where, α determines the initial dilution at $s/\sqrt{A_e} = 0$ and β is related to the rate of plume expansion as gas moves away from the vent. Later, Halitsky (1963) presented another expression of dilution factor for a rectangular block structure,

$$D = [\alpha + 0.11 \ (1 + \frac{\alpha}{5}) \ \frac{s}{\sqrt{A}_e}]^2 \tag{7}$$

For $\alpha = 1$, he obtained

$$D_{min} = (1 + 0.132 \ \frac{s}{\sqrt{A}_e})^2 \tag{8}$$

Halitsky conducted his verification experiments under conditions of non-turbulent, uniform, mean velocity profile and isothermal tempera-ture. Munn and Cole (1967) found that their field measurements for dispersion near a reactor complex were less than those predicted by Halitsky by a factor of 5; i.e., Halitsky's method overestimated the concentration level and predicted too low a dilution factor at the ground. The deviations have been examined by Wilson (1976) and Meroney (1979). They concluded that the discrepancies resulted from using constants derived during experiments which did not simulate the random fluctuations and the relative length scale of atmospheric turbulence.

Briggs (1973) has considered both the stack aerodynamic effect and the building effect. He employed a simplified diffusion model, where the plume cross section at any point is taken to be rectangular and the material is uniformly mixed (i.e., the "top hat" profile) and there is a uniform mean velocity profile. Briggs suggested that maximum concentration on the building can be approximated by $\chi_{max} = \frac{4Q}{U_H s^2}$. Restated in terms of a dilution factor, i.e.,

$$D_{min} = \frac{1}{4} K_e \ (\frac{s}{\sqrt{A}_c})^2 \tag{9}$$

Wilson (1976) adopted the suggestion by Gifford (1968) and the ASME (1973) that σ_y and σ_z for an effluent plume can be approximated at short distances by simple power functions:

$$\frac{\sigma_y}{L} \ \alpha \ (\frac{s}{L})^p \quad ; \quad \frac{\sigma_z}{L} \ \alpha \ (\frac{s}{L})^q \tag{10}$$

He argued that close to the building the plume dimension will be comparable to those of turbulent eddies which are diffusing from the gas vent, so that, $p \sim q \sim 1.0$. Combining Equation (3) and Equation (10), Wilson obtained

$$D_{min} = B_1 K_e \ (\frac{s}{\sqrt{A}_c})^2 \tag{11}$$

A value of $B_1 = 0.11$ was specified from model experiments for different vent locations in a simulated atmospheric boundary layer.

Hall (1980) examined the results of Read et al. (1963) and Munn et al. (1967). He subsequently proposed

$$\chi_{max} = \frac{7Q}{Us^2} \qquad (12)$$

In terms of a dilution factor the relation becomes,

$$D_{min} = \frac{1}{7} K_e \left(\frac{s}{\sqrt{A_c}} \right)^2 \qquad (13)$$

Evidently a consensus exists among many different authors that

$$D_{min} \sim B_1 K_e \left(\frac{s}{\sqrt{A_c}} \right)^2 \qquad (14)$$

where B_1 is a constant generally somewhere between 0.1 and 0.3.

2.2 Mean Concentration in the Near Wake Region Behind a Model Building

Yang and Meroney (1970) made concentration measurements in a cubical model building wake for gases released from a central roof vent. Data were taken downwind from $\frac{x}{H} = 3.0$ to $\frac{x}{H} = 25.0$. The ground level concentration variation with longitudinal distance in the wake region was found to follow $\log_{10} K = C_1 \log_{10} \frac{x}{H} + C_2$, where C_1 ranged from -0.6 to -0.7 and C_2 was an experimental constant. They reported that the orientation of the building to the approach wind had only a slight effect on the concentration distribution.

Meroney and Yang (1971) extended their original study to the effect of stack height and exit velocity over an isolated cubical building. They confirmed that $C_1 \sim -0.6$ provided a good estimate for ground level concentration in roof vent situations. A simple rule was suggested by them, i.e.,

$$\frac{K_{max}}{K_o} = \left(\frac{0.02}{\frac{h_s}{h_b} - 0.98} + 0.01 \right) \frac{U_\infty}{W_e} , \qquad (15)$$

where K_o is the concentration in the absence of the building for the same source locations.

For roof vent emission the relation implies that for $\frac{W_e}{U_H} > 1.3$ the downwash will be decreased, and hence the concentration level will be reduced.

Robins (1975) also conducted an experiment on plume dispersion in the vicinity of a cubical block with different release heights and building orientations. For releases from a vent at roof center, he concluded that (1), the downwash behind the cube is stronger for the

diagonal flow (θ = 45°) case, which tends to increase the surface concentration levels and brings the point of maximum concentration closer to the cube, and (2), for low emission velocity ratio, $\dfrac{U_e}{U_H}$ = 0.4, the maximum concentration for θ = 45° was approximately four times that for θ = 0°.

A fluid model study of the dispersion of roof-top emissions from a rectangular building was performed by Thompson and Lombardi (1977). Their conclusions can be briefly summarized as follows:

(1) The shape and size of the aerodynamic cavity region was significantly altered by a change of approach wind direction. A change of wind direction to θ = 45° increased the maximum ground level concentration by a factor up to 6 in the near wake region.

(2) Doubling the width of the building reduced the concentrations below the building height at a downwind distance of $\dfrac{x}{H}$ = 5.0 by about 20%. Doubling the height of the building had little effect on the concentrations, although slightly lower values were observed on the ground level.

Koga and Way (1979) conducted an investigation of the effect of stack height and position on pollutant dispersion in building wakes. They found that the stack position can affect local ground concentration by a factor of 6. The factor of variation was found to be only about 2 for a central roof vent release at θ = 45° orientation, as compared to a θ = 0° degree orientation. Maximum ground concentrations were found at a distance of 3 to 4 building heights from the building surface for the θ = 0° orientation, and at only 2 building heights from the downstream edge in the θ = 45° orientation.

The effect of plume exit momentum near a cube was considered by Robins and Fackrell (1980). They reported a rapid decrease in the near wake concentration with increasing exit momentum when the square root of the momentum flux ratio is about 0.1. On the other hand, Wilson (1977) reported a critical momentum ____ ratio of 0.004.

2.3 Concentration Fluctuations in the Near Wake Region Behind Buildings

Hinds (1968) conducted a short series of tests where a ground level point source was placed at the upwind stagnation point of a large building. It was reported that no detectable difference existed between the peak-to-mean ratios measured in unobstructed flow and those in the lee of a building. It is suspected that the release was located at the forward stagnation point of a building oriented 45 degrees to the wind; thus the gas may have been swept around the building and not participated significantly in the wake motion.

Ramsdell and Hinds (1971) examined concentration fluctuations and peak-to-mean concentration ratios in plumes from a ground level continuous point source in open terrain. It was found that: (1) near

concentration is only slightly larger than the mean concentration, but near the edge of the mean plume the standard deviation is more than triple the mean; (2) the absolute intensity of the concentration fluctuation is relatively constant near the center of the mean plume and decreases rapidly near the edge of the plume; and (3) general similarity of the concentration fluctuation intensity existed at distances from 200 m to 800 m from the source.

Csanady (1973) proposed that concentration fluctuations are log-normally distributed about the mean for a continuous ground level point source, and, further, that the distribution is a function of the logarithmic standard deviation only. The probability density function given by Csanady is

$$p(\chi) = \frac{1}{\sqrt{2\pi}\sigma_\ell \chi} \exp\left[- \frac{(\ell n(\frac{\chi}{\chi_o}))^2}{2\sigma_\ell^2}\right] \tag{16}$$

where χ_o, the median, is related to $\bar{\chi}$, the mean, by

$$\frac{\chi_o}{\bar{\chi}} = \exp\left(- \frac{\sigma_\ell^2}{2}\right) \tag{17}$$

and σ_ℓ, the logarithmic standard deviation, is related to $\sqrt{\overline{\chi'^2}}$, the RMS concentration, by

$$\frac{\overline{\chi'^2}}{\chi_o^2} = \exp(\sigma_\ell^2)[\exp(\sigma_\ell^2) - 1] \tag{18}$$

Therefore, the local concentration fluctuation intensity, I_c, is

$$I_c = \frac{\overline{\chi'^2}^{1/2}}{\bar{\chi}} = \sqrt{\exp(\sigma_\ell^2)-1} \tag{19}$$

The cumulative probability density function Ω is related to the probability that some specified peak concentration, χ_p, is not exceeded:

$$\Omega(\chi_p) = \int_o^{\chi_p} p(\chi)d\chi = \frac{1}{2}\left[1 + \text{erf}\left(\frac{\ell n(\frac{\chi_p}{\chi_o})}{\sqrt{2\sigma_\ell}}\right)\right] \tag{20}$$

whose inverse is

$$\frac{\chi_p}{\chi_o} = \exp\left\{\sqrt{2}\left[\text{erf}^{-1}(2\Omega(\chi_p) - 1)\right]\sigma_\ell\right\} \tag{21}$$

From Equation (17) and Equation (21), the peak-to-mean concentration ratio is obtained,

$$\frac{\chi_p}{\bar{\chi}} = \exp(-\frac{\sigma_\ell^2}{2}) \exp\left\{ \sqrt{2} \; [\text{erf}^{-1}(2\Omega(\chi_p) - 1)] \; \sigma_\ell \right\} \qquad (22)$$

Wilson (1977) measured concentration fluctuations on a building surface for a source at different roof vent locations. He reported that: (1) the concentration statistics are in good agreement with the log-normal probability distribution, and (2) the fluctuation intensity decreases as distance from the vent increases according to the relation

$$I_c = 0.71 \; (\frac{r}{\sqrt{A_c}})^{-0.81} \qquad (23)$$

Wilson used a fast-response sensor to measure the concentration fluctuations. The fluctuating concentrations were then normalized by the mean concentration, which was obtained from a thermal conductivity detector. The inaccuracy of the fast-response sensors, as reported by Wilson, was significantly greater below mean concentrations of approximately 100 ppm. This implies that data observed on the lee of the building, where low mean concentrations occurred, may be questionable.

Fackrell (1978) also reported concentration fluctuation behavior in an obstructed flow. He found that the fluctuation intensity increased with distance from the plume centerline and attained values in excess of 2 near the outer edges of the plume. One finds, however, that his reported fluctuation intensities near the model site ($\frac{x}{H} = 6.5$) were significantly different than data far downwind ($\frac{x}{H} = 19.5$). This indicates that the fluctuation intensities are strongly affected by the presence of a model building in the near wake region behind the building.

Netterville (1979) considered concentration fluctuation levels in a plume. The log-normal concentration probability was modified to include intermittency. The highest concentration peaks were observed to occur about 2/3 of the distance from the source to the point of maximum mean concentration.

Meroney (1979) examined Wilson's (1977) and Ramsdell and Hind's (1971) data and proposed an approximate asymptotic formula for the relation between local concentration intensity, I_c, and downwind distance from the source, $s/\sqrt{A_c}$,

$$(I_c)_{CL} = (I_c)_{CL\infty} + (4 - (I_c)_{CL\infty}) \exp(-2 \frac{s}{\sqrt{A_c}}) \qquad (24)$$

where s is the distance from vent to inlet found by stretching the shortest possible string between the two points and subscript CL indicates centerline values. Based on this algorithm, the concentrations do not exceed their mean value by more than a factor of 2 for more than 10% of the time at any reasonable distance from the vent.

2.4 Flow Structure Around and in the Near Wake of a Cubical Building

The presence of buildings in a turbulent boundary layer results in a highly disturbed flow region around the buildings. Mathematical descriptions of this flow do not exist to describe this phenomenon. Present understanding of flow near structures is primarily based on laboratory observations of smoke patterns, neutrally-buoyant bubble-streak photographs, and oil-film analysis. There are two major parameters which affect the flow around buildings, the nature of the upstream flow, and the shapes and orientations of the buildings.

2.4.1 Flow Structure Around a Cubical Building ($\theta = 0°$ orientation)

Quantitative estimates of flow patterns around structures were made by Halitsky (1965) and Wilson (1976, 1977, 1979) for exhaust gas recirculation and dilution. An extensive visualization study of roof flow patterns was performed by Wilson (1979). He classified the wake region above the roof into three zones: Recirculation Cavity, High Turbulence Region, and Roof Wake Region (see Figure 2). By defining two scaling factors, R and S, Wilson suggested a method to estimate the roof cavity length. L_c, the roof wake height, H_{rw}, and the roof cavity height, H_c.

$$L_c = 0.9R$$

$$H_{rw} = 0.57 \ H_s \ \phi \ (\frac{X}{R})^{0.33}$$

$$H_c = 0.22 \ R \ , \ \text{at} \ X = 0.5R$$

where,

$$\phi = [1 - \exp(- \ (\frac{H_L}{H_s})^{0.33} \ )] \tag{25}$$

$$R = H_s^{0.67} H_L^{0.33}$$

and H_s : smaller value of W and H

H_L : larger value of W and H

When this method is utilized to estimate L_c, H_{rw} and H_c for a cubical building, one finds that $L_c = 0.9 \ H$, $H_{rw} = 0.286 \ H$ and $H_c = 0.11 \ H$.

Flow over a building creates a positive pressure zone (in comparison with streamwise pressure outside the region influenced by the building) on the upstream face and negative pressure zones on the

roof, lee, and lateral sides. Although the pressure magnitudes change with wind speed within these zones for a given orientation, their relative magnitudes are unaffected (Akins et al., 1976).

2.4.2 Flow Models for the Near Wake of a Cubical Building

The complicated nature of a shear flow in the vicinity of a bluff body has been described by Hunt et al. (1978) and Woo et al. (1977) and is shown in Figure 3. This flow model is significantly different from the previously popular closed-bubble cavity concept. The new model reveals that mass transport into the cavity region can occur not only by turbulent transport, but also by advection along streamlines. Some important characteristics of the near wake region are:

(1) In the region upwind of a sharp-edged building, the main flow decelerates longitudinally and accelerates laterally and/or vertically to pass around the obstacle. This gross deflection of the incident flow strongly affects the shear-induced standing eddy. The size and strength of this vortex depend on the curvature of the incident velocity profile relative to the body height and on the width to height ratio of the obstacle (Hosker, 1979).

(2) When wind approaches a cubical building at some angle to the building face two strong counter-rotating vortices are induced at the upstream roof edges which tend to reduce the cavity height and increase wake centerline velocities as they sweep high velocity air downward (Hansen and Cermak, 1975).

(3) The addition of upstream turbulence and shear considerably reduces the size of the cavity zone for flow normal to the building (Castro and Robins, 1977).

(4) Huber (1978) examined available experimental data on building cavity size and shape. He proposed that the roof cavity and roof wake heights can be approximated by

$$H_c = H + 0.5 \, H_s$$
$$H_{rw} = H + 1.5 \, H_s \tag{26}$$

where H_s is the smaller value of W and H.

Hosker (1980) also examined the along-wind length of the cavity relative to the rear face of the building, X_r/H, and suggested that

$$\frac{X_r}{H} = \frac{A(W/H)}{1+B(W/H)} \tag{27}$$

If the flow does not reattach to structure's surfaces, then

$$A = -2.0 + 3.7 \, (L_1/H)$$
$$B = -0.15 + 0.135 \, (L_1/H) \tag{28}$$

where L_1 is the along-wind length of the building. If the flow does reattach, then

$$A = 1.75 \quad \text{and} \quad B = 0.25 \tag{29}$$

Combined with observations reported by previous researchers (Evans, 1957; Halitsky, 1963; Briggs, 1973), the size of the eddy zone of the cavity behind a cubical building varies depending upon building orientation, so that: (1) when the wind direction is perpendicular to the upstream face, the cavity region begins at the upstream edge. The cavity grows to a height of about 1.5 H and a width a little wider than the building, and extends over all lee sides of the building and downwind from 2 to 3 H, and (2) when the wind approaches the building at a 45 degree angle to the upstream face, the cavity region develops along the two upstream edges. It grows to a height of about 1.5 H and a width of about 2 to 2.5 H at a distance downwind of 2.5 H, and extends to 3 to 4 H from the leeward surface.

Chapter 3

EXPERIMENTAL FACILITIES AND MEASUREMENTS

3.0 Introduction

Three wind tunnels were employed during this study. The wind tunnel facilities are described in Section 3.1. Conditions required to assure boundary layer and diffusion similarity are discussed in Sections 3.2 and Section 3.3, respectively. Section 3.4 considers implications of model scale. Section 3.5 describes velocity measurement techniques. The receptor configuration are reviewed for mean concentration and concentration fluctuations in Section 3.6. Flow visualization with a helium bubble technique is described in Section 3.7. The last two sections cover data acquisition procedures and a summary of the test program.

3.1 Wind-Tunnel Facilities

Mean concentration measurements were conducted in the Thermal Stratified Wind Tunnel (TSWT) located in the Fluid Dynamic and Diffusion Laboratory (FDDL) at Colorado State University (CSU). A general view of the TSWT is shown in Figure 4a.

The TSWT was designed for simulation of a thermally stratified atmospheric boundary layer. The tunnel is an open-circuit facility driven by a 0.5 hp variable-speed motor and a fixed-pitch propeller. The test section lies 240 cm downwind from the entrance. Wind speed in the test region can be continuously adjusted from 40 cm/sec to 450 cm/sec. Vortex generators, barriers, and different surface roughnesses are available to produce various wind velocity profiles.

Visualization experiments were performed in the Industrial Aerodynamics Wind Tunnel (IAWT) in the FDDL at CSU. A detailed description of IAWT is given by Peterka and Cermak (1978).

Measurements of concentration fluctuations were conducted in the Meteorological Wind Tunnel (MWT) in the FDDL at CSU. A detailed description of the MWT is given by Plate and Cermak (1963). A general view of the IAWT and the MWT are shown in Figures 4b and 4c, respectively.

3.2 Boundary Layer Simulation

Although the TSWT and the MWT have the ability to produce thermal stratification, all the experiments in this study were performed under a neutral stratification condition.

3.2.1 IAWT and MWT

For the past few years many gas diffusion experiments have been done in the IAWT and the MWT. Both of these wind tunnels can simulate a wide range of atmospheric boundary layer conditions. Discussions of atmospheric simulation in wind tunnels are found in many reports, e.g.,

as Cermak (1973) and Plate and Cermak (1963). The procedures in the wind-tunnel simulations of this study was to adjust the TSWT to the desired conditions and then adjust the IAWT and the MWT to the same simulation conditions.

3.2.2 TSWT

Spires (made of 5 triangular wood plates, 10 cm base length, 30 cm height) and a barrier (3 cm x 60 cm) were installed at the entrance of the wind tunnel. A distributed surface roughness (0.25 cm height) was placed on the tunnel's floor. With this arrangement, a fully developed boundary layer approximately 30 cm deep with a power law exponent of 0.19 was obtained throughout the test section.

The vertical distributions of longitudinal mean velocity and turbulent intensity, without the model building present are shown in Figure 5. A mean velocity profile was also measured laterally at a height 30 cm above the floor to evaluate wall effects (as shown in Figure 6); the values were normalized using the centerline mean velocity at 30 cm above the tunnel floor, which corresponded to the top of the boundary layer. The roughness height $z_o \simeq 7.5 \times 10^{-3}$ cm was estimated by plotting mean velocity vs. height in semi-logarithmic coordinates according to the relationship $U \overset{\infty}{\underset{o}{\propto}} \log Z/Z_o$. An integral time scale, defined as $\tau = \int R_u(t)dt$, equal to 0.025 second at $\frac{z}{H} = 0.3$, was evaluated from an auto-correlation of the velocity fluctuations. Counihan (1975) has reviewed the meteorological literature on measurements in developed adiabatic boundary layers. He concluded that the main boundary layer characteristics can be derived from the effective roughness height. Characteristic parameters of the simulated atmospheric boundary layer are compared with Counihan's data in Table 1.

3.3 Diffusion Simulation

The concentration distributions obtained during building model tests of diffusion must be projected to appropriate prototype scales. To obtain concentration similarity, certain similarity criteria must be satisfied by the wind-tunnel flow and the model configurations. The criteria may be obtained from dimensional analysis of the momentum and energy conservation equations. Detailed discussions on the require- ments and limitations of similarity are given by Meroney (1967) and Cermak (1975), among many others. Three categories of simulation are required to model atmospheric gas diffusion, i.e., dynamic, kinematic and geometry similarity. In addition, initial-distributions and boundary-conditions of velocity, temperature, and concentration must be similar.

Dynamic similarity requires that the ratios of fluid forces at equivalent scaled locations be equivalent for the model and the proto- type, i.e., two criteria for the model, $R_e = \frac{UH}{\nu}$ and $R_o = \frac{U}{H\Omega}$ should

be equal to their counterparts for the atmosphere. The Reynolds number Re is interpreted as a ratio of reference inertia force to reference viscous shear force. In the wind tunnel it is not possible to obtain an equal Reynolds number for model and prototype, since length scale reductions are usually greater than 300:1. However, for "sufficiently large" Reynolds number, the effects on gas dispersion are small. For example, for tests over a sharp-edged building, reported by Golden (1961), there was no change in surface concentration patterns for values of reference Reynolds number greater than 11,000.

Although a larger Re number was desirable a minimum value of Re = 11,050 was necessary in this study due to wind-tunnel constraints. This value is marginally acceptable according to Golden's criteria. The Rossby number, $R_o = \frac{U}{H\Omega}$, is a quantity which indicates the effect of the earth's rotation on the flow field. The model Rossby number cannot be made equal to the atmospheric value. Generally, however, over the short distances typically considered, the Coriolis acceleration has little effect upon the flow. Accordingly, the requirement of equal Rossby number is relaxed.

Kinematic similarity requires similar streamline patterns of the flow over model and prototype. It was reported by Golden (1961) that for Re > 11,000, kinematic similarity is also independent of Reynolds number. Accordingly, the root-mean square value and correlation coefficient of the turbulence velocity components should be equal for the model and the prototype flows in the present study.

In building vent diffusion it is necessary to consider the exit gas buoyancy and the momentum effects. Equivalence of inertial to buoyancy forces from model to prototype are required. Golden, as cited by Halitsky (1963), states that gas buoyancy effects in building vent diffusion will not be significant when the Froude number is greater than 0.8

$$F_r = \frac{U_H^2}{Hg} \left[\frac{1}{1} - \frac{\rho_e}{\rho_a} \right] > 0.8 \tag{30}$$

The value, F_r = 25.8, utilized in this study should avoid any buoyancy effect on surface concentration measurements.

The vent gas exit momentum is an important parameter in concentration patterns around a model building. This parameter is expressed in terms of a jet momentum factor, J, which is the ratio of momentum flux from a vent to the horizontal wind momentum flux per unit area.

$$J = (\frac{\rho_e}{\rho_a} \frac{A_e}{A})^{\frac{1}{2}} \frac{U_e}{U_H} \tag{31}$$

Even small changes in the value of J were found by Wilson (1976) to significantly alter concentration patterns on a model building. Hence a range of values of J have been examined to assure parameter independence.

3.4 Model Scale

A plexiglass cube (5 cm x 5 cm x 5 cm) was constructed to simulate a cubical building in the TSWT. A larger plexiglass cube (15 cm x 15 cm x 15 cm) was employed in the IAWT and the MWT. The degree of wind-tunnel blockage was calculated based on the percentage of the cross section of the wind tunnel obstructed by the obstacles' cross wind cross-sectional area. The model intercepted at most 1.0 percent of the tunnel area in the TSWT, while less than 0.5 percent of the area was intercepted by the model in the IAWT or the MWT. The blockage values are considered well below that which might artificially accelerate the flow or deform the wake formations.

Geometric similarity requires that a constant ratio length scale and undistorted geometry be maintained for every dimensional quantity between model and prototype. However, for gases vented from the surface of a building, Wilson and Netterville (1976) reported that the diffusion process is not a strong function of scale factors; hence values ranging from 500:1 to 2000:1 may be used with reasonable accuracy. Thus results from the building models studies herein should be applicable to full-scale buildings with heights between 25 meters and 100 meters. The model parameters used in this study and the similarity criteria for wind tunnel testing are tabulated in Table 2.

3.5 Velocity Measurement

Measurements of longitudinal wind velocity were made with a Thermo-Systems, Inc., aneometer Model 1050 and a hot film probe Model 1210. The probe was calibrated every four hours by using a TSI flow calibrator Model 1125 and a MKS Baratron pressure transducer. Bridge output calibration data were fit to the King's law curve

$$E^2 = A + BU^n \tag{32}$$

A HP-1000 computer was employed to transform the voltage reading E from into wind speed U. The longitudinal turbulent intensities were obtained at the same time by interpreting the output from a RMS volt-meter, employing a 10 second averaging period.

A relation between pressure and the wind-tunnel reference velocity was established using a pitot-static probe positioned at the tunnel centerline 30 cm above the floor of the TSWT, and a hot film probe to detect the wind tunnel reference velocity. In the TSWT and the MWT the reference probe was positioned at the tunnel centerline and 110 cm above the floor of the wind tunnel. The reference velocity was recorded during each measurement series. All tests were performed under neutral stratification and at low wind speeds; hence detailed temperature measurements were not required. Room temperatures were approximately 20°C throughout the test series, as measured by a mercury in glass thermometer.

3.6 Concentration Measurements

3.6.1 Mean Concentration Measurements

3.6.1.1 Receptor Probe Configuration.

Ideally, the gases at a surface should be sampled directly at that surface, with zero withdrawal of fluid. Unfortunately, instrument response requires a finite sample flow rate at a finite distance away from the model surface. Wilson (1976) examined the variation of measured concentrations due to the sample probe configuration. It was reported that steep concentration gradients are often obtained near a building surface, with higher concentrations usually closer to the building. In the present experiments, a 1.47 mm O.D., 1.06 mm I.D. stainless steel hypodermic tube was positioned perpendicular to the surface at a distance of 0.3 mm. Concentrations measured in a similar manner by Wilson (1976) were lower than the readings produced at the building surface by about 10 percent. Thus, values presented in this study may have at least a 10 percent uncertainty.

A total system error can be evaluated by considering the mean deviation found for a set of measurements where a precalibrated gas mixture is monitored. For a gas of 100 percent helium, the average mean deviation from the TCGC was three percent. Since the source gas was premixed to the appropriate molecular weight and repetitive measurements were made of its source strength, the confidence in source strength concentration is similar. The flow rate of the source gas was monitored by Fischer-Porter flow meters which are accurate to 2 percent, including calibration and scale fraction error. The wind-tunnel velocity was constant to ± 10 percent at such low settings. Hence, the cumulative confidence in the measured values of the concentration coefficient K will be a mean deviation of about ± 9 percent, whereas the worst cumulative scenario suggests an error of no more that ± 20 percent.

The lower limit of measurement (approximately 200 ppm) is imposed by the instrument sensitivity and the background concentrations of helium in the air within the wind tunnel. Background concentrations were measured and subtracted from all measurements quoted herein.

The sampling probe was mounted in a traversing mechanism in the TSWT. The speed of traverse was controlled by a DC meter and set to 2.14 cm/min. Such a speed was experimentally found to be slow enough to prevent errors due to sampler time lag. After establishing the desired flow model configuration, pure helium was released at a flow rate of 12.5 cm^3/sec (exit velocity 63.6 cm/sec). The helium flow rate was controlled by a pressure regulator at the outlet of a supply gas cylinder, and monitored by a flowmeter. Diffusion patterns were allowed to stabilize for three minutes before any concentration measurement was taken. Gas samples were drawn through the probe to a thermal conductivity type gas chromotograph (GC).

3.6.1.2 Gas Chromotograph (GC).

Concentration of the tracer gas (helium) was determined by using a thermal-conductivity type GC. The GC (Carle Model 8000) was modified so that continuous sample anaysis was possible. The carrier gas was ambient air. The thermal conductivity detector is based on the principle that a heated thermistor will lose heat at a rate which depends upon the composition of the surrounding gas. The carrier-tracer gas mixture enters the GC through a metering valve and passes into the pre-heated inlet block before entering a 100 µl detector column. The inlet block is maintained at a fixed temperature a few degrees above the detector column temperature by a constant voltage supply. A pair of detector columns serve as two legs in a Wheatstone bridge circuit, providing a system having low baseline drift and noise. As the carrier-tracer (helium) gas mixture flows through the detector columns, the heat transfer from the heated detector thermistors changes their temperature and hence their resistance. A calibration curve was obtained using known air/helium mixtures; results are shown in Figure 7.

The GC bridge output was recorded by a X-Y recorder and monitored by a digital integrating voltmeter. The minimum detectable level of concentration imposed by instrument sensitivity is about 30 ppm. Background concentrations were checked before and after each measurement to correct for drift.

3.6.2 Concentration Fluctuation Measurements

An aspirated hot film probe was employed in this phase of the study. In an isothermal flow, film response is a function only of gas composition, for a fixed probe geometry. A detailed description is given by Neff and Meroney (1979). Argon was used as the tracer gas in this phase of study.

3.7 Flow Visualization

The purpose of the flow visualization was to provide a qualitative understanding of the complicated flow field about the building models. Visualization experiments were performed in a simulated atmospheric boundary layer, using a wind velocity profile with an power law exponent 0.2, and a model building Reynolds number in the IAWT equal to 13,300. This arrangement was considered consistent with the simulation employed for concentration measurements in the TSWT and the MWT. A Technovate Helium Bubble Generator, Model 9036, and a modified projector arc-lamp were employed for flow visualization. Soap bubbles filled with pure helium and swept out of the generator by an adjustable air flow. These bubbles reflected light only within the investigated region, which was illuminated by a slit-plane of light, width 2 cm, provided by the projection arc-lamp. Photographs were taken for different source locations and various light plane locations. Typical pictures are shown in Figures 8 through 10.

Flow separation and reattachment regions were sketched during the visualization experiments, and later confirmed for the second larger model scale by smoke visualizations in the TSWT.

3.8 Data Acquisition and Analysis

3.8.1 Mean Concentration Measurements

In order to provide a complete picture of the distribution of concentrations in the investigated region, a systematic method of interpolation to obtain data between any two observed points is required. An interpolation scheme developed from quasi-Hermite piece-wise continuous polynomials as suggested by Akima (1971), was employed to generate data at intermediate locations for contour plot generation. The method is based on a piecewise continuous function composed of a set of polynomials of degree less than or equal to three. It is applicable to successive intervals over the measured set of points. The slope at any given point is determined locally by the coordinates of five data points, with the data point in question as a center point, and two points on each side of it. A polynomial of degree three between each pair of given points is determined by the coordinates and slopes at the two points. Sufficient "data" to obtain a smooth countour plots can be interpolated from the resulted polynomials. An International Mathematical and Statistical Library Routine IQHSCU was utilized.

3.8.2 Concentration Fluctuation Measurements

Data obtained in this phase of the study were recorded on a HP-1000 minicomputer. A program was employed to evaluate the mean, standard deviation and probability distribution of the data for 5-minute sample periods (200 points per unit time).

3.9 Experimental Program

Experimental conditions for the present study are tabulated in Table 3.

Gas was released from three different vent locations for three different building orientations during the mean concentration measurements on the model building (Figure 11). Data were observed continuously in the z-direction for all the side surface measurements. On the roof surface, data were observed continuously in the y-direction.

Mean concentration measurements in the near wake of the model building were made in the TSWT for the case of $\theta = 0°$ and a top center release.   The sampling positions are shown in Figure 12. Data were obtained continuously in the z-direction at $\frac{x}{H}$ = 1.0, 1.5, 2.0, 2.5, 3.0, 4.0, 5.0 and $\frac{y}{H}$ = 0.0, 0.3, 0.6, 0.9, 1.2, 1.5, 1.8.

A $\theta = 0°$ top center release, a $\theta = 45°$ top center release, and a $\theta = 0°$ top downwind edge release were used during the measurments of the concentration fluctuations in the MWT. Data were obtained at $\frac{x}{H}$ = 1.0, 2.0, 3.0, 4.0, and 5.0. Only points at the wake centerline or on the ground were examined. The points are $\frac{z}{H}$ = 0.1, 0.5, 1.0, 1.5 along

the centerline and $\frac{y}{H}$ = 0.0, 1.0, 1.5 on the ground. Mean concentrations were also observed at these points. The equipment setup is shown in Figure 13.

Chapter 4

EXPERIMENTAL RESULTS AND DISCUSSIONS

4.0 Introduction

Results presented in this chapter have been divided into four sections:

Section 4.1 - Concentration measurements on the model building.

Section 4.2 - Concentration measurements in the near wake region behind a model building ($\frac{x}{H} \leq 5.0$).

Section 4.3 - Wind direction and jet momentum effects.

Section 4.4 - Concentration fluctuations, and peak-to-mean concentration ratios in the near wake of a model building.

Results obtained from the flow visualization experiments are incorporated in Sections 4.1 and 4.2 as appropriate, in order to facilitate the understanding of dispersion in the near wake.

4.1 Concentration Measurements on the Building

4.1.1 Concentration Isopleths

Figures 14 through 22 show isopleths of constant concentration coefficient K. Each K isopleth forms a closed contour about the vent location unless intercepted by the presence of the ground. These contours depend on vent location, effluent velocity and wind direction. Isopleth lines tend to retain a closed shape though they can be distorted into irregular lobes.

Bubble motions in Figure 8a suggest that the building wake develops from the sharp upper edges of the two upstream faces for a cubical building rotated less than 22.5 degrees from a normal position. No significant contamination was ever found on the upstream surfaces for such a configuration.

The concentration levels on a cubical building for different roof vent emissions, with wind normal to the frontal surface, are displayed in Figures 14 to 16. It was found that the concentration level on a building decreases greatly as the plume passes over a sharp building edge. The effect of the sharp edge on the surface concentration level is shown in Figure 23, where concentration coefficient as a function of distance from the vent location is plotted. A rapid decrease of concentration coefficient was found (see Figure 24) just past the edge point (as indicated in the figure). The effect of the sharp edge is anticipated, since a gas plume passing the sharp edge follows a trajectory similar to the general flow pattern around the building. Thus an "extra distance" is traveled by the plume after it leaves the edge and before it enters the wake proper. Moreover, the dispersion

process in the near wake tends to further reduce the concentration. Therefore, at an intake point which cannot "see" the vent location, one observes a lower concentration than at an intake point an equal distance from the exhaust vent, which can "see" the vent location. The concentration level at points are shown in Figure 24 which can "see" the vent location, for $\theta = 0°$, roof central release. By comparing points which can and cannot "see" the vent but are equal distances from the vent location, the effect of the sharp edges become obvious. The sharp edge effect was found most significant within the region 1/6 H from the edge of the lee face. It is implied that the plume, which dominated the concentration behavior on the building, reattached to the lee face of the building at a height 5/6 H from the ground level. However, the sharp edge effect is not significant for the side edge, since the flow mostly tends to advect the gas plume in the downwind direction.

Data for which the wind direction is normal to the building surface (Figures 14 to 16) have been compared with earlier results of Halitsky (1963) and Wilson (1976). Concentrations observed in the present study are larger than Halitsky's data by a factor of 2 to 5. However, Halitsky's data will be distorted from a properly atmospheric simulation, since a non-turbulent uniform approach velocity profile was used, modifing the shape and size of the reversed flow regions on the building. Data presented in this study were also found to be slightly different than those of Wilson (1976). Figure 24 compares concentration coefficients on the building using the present measurements and those of Wilson. The data were found to collapse into a common range of magnitude, which suggests that a similar concentration distribution existed for both experiments.

Figures 17 to 19 show concentration isopleths for buildings rotated 45 degrees to the wind direction. A similar tendency was found by Halitsky, (1968) with the exception of regions near the upstream edges. The wider spread of the isopleths of the present study indicates that the mean concentrations are higher than values at the same positions in Halitsky's report. A secondary peak occurring near the edge of the building roof is shown in Figure 17a. This phenomenon was significant for the $\theta = 22.5°$ and $\theta = 45°$ orientations (Figures 17a, 18a, 19a, and 22a). The bubble visualizations of Figure 10c, as indicated by the arrow, also gave evidence of this phenomenon. Perhaps a recirculation flow occurred in the separation zone, advecting the contaminants upwind across the top edge from the sides. This is because two counter-rotating vortices are induced at the upstream roof corner when the wind direction is not normal to the building face. These two vortices tend to return contaminants to the roof. The strength of the vortices increases as the speed of the approaching flow increases. The interaction between the recirculation flow and the roof vortices produces a secondary peak of concentration on the roof near the downstream edge.

The flow reattachment zone and the flow directions observed on the building during visualization are shown in Figure 25.

The optimum location for intake vents given different roof vent locations and different wind directions, with equal vent exhaust to vent intake separation distance, should be offset laterally from the downwind direction and at a position where it cannot "see" the exhaust vent.

4.1.2 Dilution Factor for Roof Vent

Surface concentration data in the form of dilution factors were plotted against the non-dimensional distance from the vent location $s/\sqrt{A_c}$, as shown in Figures 26 through 28. The minimum dilution factor corresponds to the maximum concentration which is expected at a given distance from a roof vent. Previous expressions proposed by different authors for this minimum dilution factor are noted on the figures. For the $\theta = 0°$ case, a value of $B = 0.11$ provides a lower bound to all measurements. Some recent measurements around two nuclear facilities were examined by Meroney (1979). Here too, $B = 0.11$ provided a lower bound to 99 percent of all measurements. Figure 28 indicates that $B = 0.11$ may not be a safe lower bound for buildings at large angles of orientation to the approach flow; $B = 0.11$ remains satisfactory for $\theta = 22.5°$, but, a few data at $\theta = 45°$ fall below the $B = 0.11$ line. These data originate in the boundary area at the rear roof corner where three edges intersect (the reattachment zone shown in Figure 25b).

At similar distances from the vent location, concentrations obtained for $\theta = 45°$ are higher than those observed for $\theta = 0°$ by a factor ranging from 3 to 9. Similarly for data at equal distances from the vent location, the results for $\theta = 22.5°$ tended to be 2 to 5 times larger than those at $\theta = 0°$ (as shown in Figure 23). Therefore, a correction factor for orientation is recommended, to adjust for orientation effect in Equation (14):

$$f(\theta) = \frac{1}{1+\theta/\frac{\pi}{4}} \qquad (33)$$

$$0 \le \theta \le \frac{\pi}{4}$$

$$D_{min} = B \, f(\theta) \, K_e \, (\frac{s}{\sqrt{A_c}})^2$$

Extension of Wilson's concept of the free stream line trajectory from roof to lateral face could not explain the total rate of decay of surface concentration. Trajectory adjustment by an order of magnitude could be necessary to account for the high dilutions produced by secondary motions and intense turbulence in the cavity region.

4.2 Concentration Measurements in the Near Wake Region ($\frac{x}{H} \le 5.0$)

Concentrations have been measured in the near wake region of a cubical model building, for gases released from a central roof vent, for orientations of $\theta = 0°$ and $45°$. For effluents emitted from a downwind roof vent, only the case $\theta = 0°$ was examined.

4.2.1 $\theta = 0°$, Central Roof Vent Release

Isopleths of constant K have been plotted on the y-z planes for different $\frac{x}{H}$ (Figure 29). Similar concentration distributions are found on the cross-wind planes in the near wake region. The longitudinal concentration distribution is displayed in Figure 30. The maximum concentration in the cross-wind plane occurred at ground level after $\frac{x}{H} = 7$ (extrapolated values obtained from Figure 31). The result is in good agreement with Robins (1975).

Figure 31 shows that the centerline ground concentration increases from the building lee edge to a maximum and then it gradually decreases with $\frac{x}{H}$. The maximum ground concentration in the near wake is also shown in Figure 31, where it occurs at $\frac{x}{H} = 4$ for $\theta = 0°$, and at $\frac{x}{H} = 2.5$ for $\theta = 45°$. The spread in K values among different experiments probably results from the jet momentum effect, which will be discussed in Section 4.3. The positions where the maximum ground concentration occurred have been confirmed in several experiments (Table 3).

Typical concentration profiles at $y = 0$ are compared with Thompson and Lombardi's experiments (1977) in Figure 32. Similar shapes of the concentration profiles were observed for $\frac{x}{H} = 2$ and $\frac{x}{H} = 5$. Data obtained in the present study are higher than those of Thompson and Lombardi by factors of a bit higher than 1, to as great as 2.

The lateral ground level concentrations obtained during this study are shown in Figure 33 for downwind distances between $\frac{x}{H} = 1$ and $\frac{x}{H} = 5$. Figure 34 presents concentration isopleths at ground level behind the model building.

4.2.2 $\theta = 0°$, Downwind Roof Vent Release

Vertical mean concentration profiles at $y = 0$ are presented in Figure 39a. In comparison with the vertical concentration profiles for $\theta = 0°$, top central vent release, in Figures 32 and 37a, a significant downwash effect (bringing higher concentrations nearer the ground) can be seen in Figure 39a. For the downwind roof vent release, most of the effluent is entrained by the downwash into the near wake region. Thus higher concentrations will be observed closer to the ground than with the central roof vent release, where a certain amount of effluent will be carried by the upper flow from the lee face of the building into the far wake region. As demonstrated in Figure 3, most of the center roof vent effluents are transported by flow pattern 1 while the downwind roof release is dominated by flow pattern 2. The maximum value of the cross-wind concentration distribution for the downwind roof vent

release occurred on the ground at $\frac{x}{H}$ = 5, and at $\frac{x}{H}$ = 7 for the roof center vent release. The plume dispersion along the lateral ground level is shown in Figure 40c for $\frac{x}{H}$ = 2 and $\frac{x}{H}$ = 3.

4.2.3 θ = 45°, Central Roof Vent Release

The vertical mean concentration profiles at y = 0 are displayed in Figure 38. The downwash effect due to a change in wind direction becomes more significant in comparison with the case of θ = 0° (Figures 37a through 38a). The maximum value of the cross-wind concentration distribution for θ = 45°, top center vent release, occurs at ground level for $\frac{x}{H}$ ≥ 3 (Figure 38cid). The cross-wind ground-level concentration profile is shown in Figure 40b. An interesting result is that two secondary peaks occurred near the edges of the plume. The two peaks are produced by a pair of counter-rotating vortices, which are due to the orientation of the building. The vortices originate at the upstream corner of the roof and travel along the wind direction passing by the edge of the near wake region. The rotation of the vortex tends to carry clean air from outside into the near wake region, resulting in a decrease of concentration level in the inner part of the vortex and an increase of concentration level at the outside (as indicated in Figure 40b).

4.3 Wind Direction and Exit Momentum Effect

Previous arrangements for model exhaust vent release conditions used by various authors are summarized in Table 3. Most conditions specified are quite similar. Wind direction and jet momentum effects are the only two significant parameters when the approach wind profiles are specified.

4.3.1 Effect of Wind Direction

A change of wind direction from the normal orientation, θ = 0°, shrinks the regions enclosed by isopleth lines and results in higher concentration near the upwind edge. Robins (1975) reported that for releases from a vent at the roof center, the maximum ground level concentration occurred when the building was rotated to an angle of θ = 45°. Examination of Robin's data suggests that for the θ = 45° orientation, the concentrations are higher by 2 to 4 times in the near wake region (see Figure 31). A similar result was found by Thompson and Lombardi (1977), but with a factor of 6. Data obtained in the MWT in the present study suggest a factor between 2 and 4. Overall a factor of 4, rather than 6, is more consistent with the data of the present study and of Robins.

The maximum concentration on the building was examined for various $s/\sqrt{A_c}$. An increase by a factor of 2 to 9 was found in the present study, between the θ = 45° and θ = 0° orientations (see Figures 27 and 28).

4.3.2 Effect of Exit Momentum

Sherlock and Stalker, cited by Wilson (1977), proposed a criterion which is generally accepted for the avoidance of significant downwash (for constant values of vent and building frontal area). When $(\frac{\rho_e}{\rho_a})^{0.5} \frac{U_e}{U_H} > 1.4$, stack tip downwash is avoided.

Meroney and Yang (1971) also supported this formula, since in Equation (16), if

$$\rho_e = \rho_a \quad \text{and} \quad h_s = h_b$$

then

$$\frac{U_e}{U_H} > 1.3$$

Wilson (1977) suggested this criterion may be too conservative. The first significant evidence of downwash effect reported by Wilson was when (constant values of vent and building frontal area)

$$(\frac{\rho_e}{\rho_a})^{0.5} \frac{U_e}{U_H} < 0.15$$

The jet momentum factor, $J = (\frac{\rho_e}{\rho_a} \frac{A_e}{A})^{\frac{1}{2}} \frac{U_e}{U_H}$, is a parameter useful as an indication of downwash effect, where $\rho_e U_e^2 / \rho_a U_a^2$ represents the effect of exit momentum, and $(\frac{A_e}{A})^{\frac{1}{2}}$ represents a parameter of length scale. The value of J is a criterion for comparison between different concentration measurements.

The value of J in the present study was found to be 6.25×10^{-3}, while J was equal to 1.6×10^{-3} for Wilson's data. Data presented in this study were compared to Wilson's for the $\theta = 0°$ roof vent release (as shown in Figure 24). The J value does not appear to be of importance in explaining the difference between these two experiments.

Data from various experiments in the near wake behind buildings were examined. Maximum ground concentration in the near wake was used as an indicator of concentration level in the near wake region. The relation between maximum ground concentrations and J values is shown in Figure 35. Note that a trend exists which indicates that the maximum ground concentration decreases as J increases. This coincides with the observations of near wake concentration levels reported by various authors. Note that in Figure 35, the maximum ground concentration reported by Koga and Way (1979) deviated from the trend both for $\theta = 0°$ and $\theta = 45°$ cases. The velocity ratios in

their study, which are high $(\frac{U_e}{U_H}$ = 1.3 to 5.2), seem to decrease the entrainment of contaminants into the wake region. Hence, their measurements in the near wake are not comparable with the present study.

The value $J \geqq 0.004$, reported by Wilson (1978), required to reduce the surface concentration on a building, seems to be an over-prediction of the jet momentum effect. Wilson measured his concentrations at a particular location at the center of the downwind edge. One reason for the overprediction, suggested by Robins and Fackrell (1980), was that at this specified position the concentration level is more sensitive to the ratio of $\frac{U_e}{U_H}$ than at other positions on the building. In addition, the effect of a nearby sharp edge also made the concentration on the lee side sensitive to a small variation of the downwash effect.

A value of $J \geqq 0.01$, seems more consistence with the present data for the prediction of negligible exit momentum effects, both on the building and in the building wake.

4.4 Concentration Fluctuations and Peak-to-Mean Concentration Ratios in the Near Wake behind the Model Building

The concentration fluctuations observed in this study were converted into local intensity and absolute intensity for convenience. Local intensity, I_c, is defined as the ratio of RMS value of the fluctuating concentrations to the mean concentration at that point. Absolute intensity, $(I_c)_{1G}$, is the RMS value of fluctuating concentrations normalized by the ground level mean concentration at $\frac{x}{H}$ = 1 for each case.

The "peak" concentration is that value which is not exceeded most of the time. Three values of the "peak" concentration which were not exceeded by 90 percent, 95 percent, and 99 percent of the sample period, respectively, were examined in this study.

4.4.1 Concentration Fluctuation Intensities (Both Local and Absolute Intensities, $1.0 \leq \frac{x}{H} \leq 5.0$)

Figure 36 displays measurements in the near wake region for the peak-to-mean concentration not exceeded by 99 percent of the samples as a function of logarithmic standard deviation as defined in Section 2. It is evident that the log-normal probability model is a reasonable approximation even in a building wake flow regime. (Note: It is assumed that the intermittency factor γ = 1 at every location in the wake, (Csanady, 1973).)

The local intensities were found to be less than 1 for most of the data in the near wake region behind a model building. Compared with data reported for continuous plumes in unobstructed flow, it appears that the fluctuation intensities are lower in the obstructed flow than in an unobstructed flow. That is, the presence of a building caused a decrease of fluctuation intensity rather than an increase.

A building adds turbulence to the wake, but at scales smaller than the boundary layer turbulence scales. The added scales are appreciably smaller close to the model than further downstream in the wake (Peterka and Cermak, 1975). If the concentration variance can be treated as a transportable quantity, then it can be transferred and dissipated in the same way as turbulence kinetic energy (Csandy, 1973). The energy dissipation rates are higher in the building wake than in the boundary layer, since they increase with decreasing turbulent length and time scales. Consequently, the fluctuation intensities observed in the near wake region dissipate faster than in unobstructed boundary layer. Perhaps it is the reason why lower fluctuation intensities were observed in the building wake in the present study.

The large eddies of the incident turbulent boundary layer are broken into many smaller eddies in the near wake region behind a building. Near the edges of a building wake, the smaller eddies recover to the boundary layer values rather quickly. Since the turbulence in the near wake region is dominated by the building effect, (in the inner building wake, $\frac{x}{H} \leq 4$, $\frac{y}{H} \leq 1$, $\frac{z}{H} \leq 1$), one would anticipate a small eddy size of the order of a characteristic dimension of the building. On the fringe of a building wake, the mechanism of transition of eddy size is rather complicated.

An empirical formula

$$R_r \leq 0.75 \ M_r^{1.2} \tag{33}$$

was found to provide an upper limit to the RMS concentrations observed in the inner building wake, where M_r is the ratio observed mean concentration to the source strength in percent, and R_r is the ratio of the observed RMS concentration to the source strength in percent. This simple formula only holds for the region where the dispersion process is dominated by small eddies. The RMS concentrations are plotted against mean concentrations in Figures 41 to 43. It can be seen in Figure 41 that the RMS concentrations near the fringe of a building wake significantly exceed the value of the upper limit of Equation (33). In Figure 42, $\theta = 0°$ downwind roof vent release, the deviation were not significant, since most of the contaminants were entrained into the inner building wake by downwash. In Figure 43 where $\theta = 45°$, roof central vent release, the building wake and the downwash effects were changed since a change in orientation of the building was made. However, Equation (33) still provides a reasonable upper limit for the RMS concentrations in the inner building wake.

Figure 40 displays a cross wind profile of local intensity and absolute intensity on the ground. The maximum local intensities were observed near the edge of the building wake ($\frac{y}{H} = 1$) on the ground level. Hence, the trend is for RMS concentrations to increase near the fringe of a building wake, while the downwash effect tends to reduce their magnitude. The absolute intensity is found to have its maximum magnitude at the point where the maximum mean concentration also exists.

The variation of fluctuation intensities at the ground level along the centerline is shown in Figure 44. By adopting $(I_c)_{CL\infty} = 0.35$ in Equation (25), the data support Meroney's (1979) prediction.

4.4.2 Peak-to-Mean Concentration Ratio

Fluctuation data were also expressed in terms of a probability distribution. From such results peak-to-mean values not exceeded by 90 percent, 95 percent, or 99 percent of the samples were obtained. These are shown in Figures 37 through 39 for both vertical and longitudinal directions. The shape of the local intensity curves in the figures is very similar to that of corresponding peak-to-mean concentration ratio curves. A fairly reliable estimate of the peak-to-mean concentration ratios in the near wake could be made by simply assuming it is some constant times I_c, i.e.,

$$\left[\frac{X_p}{\bar{X}}\right]_{99\%} = 5I_c \quad ,$$

$$\left[\frac{X_p}{\bar{X}}\right]_{95\%} = 4I_c \quad , \quad \left[\frac{X_p}{\bar{X}}\right]_{90\%} = 3I_c \tag{34}$$

A similar proposal by Fackrell (1978) was based on measurements over his Tilbury-Northfleet Site Model:

$$(X_p)_{99\%} \overset{\sim}{=} 4.5 \sqrt{\overline{X'^2}}$$

$$(X_p)_{95\%} \overset{\sim}{=} 3.0 \sqrt{\overline{X'^2}} \tag{35}$$

$$(X_p)_{90\%} \overset{\sim}{=} 2.0 \sqrt{\overline{X'^2}}$$

One notices that Fackrell conducted his experiments at two particular locations, $\frac{x}{H} = 6.5$ and $\frac{x}{H} = 19.5$, rather far downwind of the model site. Obviously, Equation (34) provides a safer upper limit on the peak-to-mean concentration ratio in the near wake region.

From Equations (33) and (34), an upper limit on the peak-to-mean concentration ratio in the inner building wake is

$$\left[\frac{\chi_p}{\bar{\chi}} \right]_{99\%} = 3.75 \ M_r^{0.2}$$

$$\left[\frac{\chi_p}{\bar{\chi}} \right]_{95\%} = 3.0 \ M_r^{0.2} \quad \text{and} \quad \left[\frac{\chi_p}{\bar{\chi}} \right]_{90\%} = 2.25 \ M_r^{0.2}$$

(36)

For receptors located on the ground centerline behind the building, it is reasonable to estimate the maximum peak-to-mean concentration ratios from the observed mean concentrations by following Equation (36):

$$\left[\frac{\chi_p}{\bar{\chi}} \right]_{99\%} \leq 3.0$$

$$\left[\frac{\chi_p}{\bar{\chi}} \right]_{95\%} \leq 2.5 \quad \text{and} \quad \left[\frac{\chi_p}{\bar{\chi}} \right]_{90\%} \leq 2.0$$

Figure 45 displays the peak-to-mean concentration variation at ground level, showing that the estimate from Equation (36) provides a reasonable upper limit to the ground centerline concentration measurements.

Chapter 5

CONCLUSIONS

Measurements of gaseous dispersion have been made on a cubical model building in a neutrally stratified shear layer and in the near wake region ($\frac{X}{H} \leq 5$) behind the model building for roof vent emissions. Based on the experimental results obtained in this study and a comparison with similar experiments by others, the following observations can be made.

5.1 Mean Concentration Measurements on the Surface of a Model Building

(1). Concentration isopleths on a building surface will appear as closed smooth curves with their centers at the vent location, unless intercepted by the presence of the ground. These isopleth shapes may be expanded, compressed, or distorted, depending on the particular flow condition or building configuration.

(2). For any intake located on the building surface, one may imagine a vector originating at the vent location and pointing toward the receptor location. For equal exhaust vent to recptor intake distance, the mean concentrations will decrease as the exhaust to intake vector deviats from the wind direction. The concentration level on the lee face of a model building is greatly reduced by the presence of a sharp building edge. The effects of the sharp edge become less significant as the exhaust to intake direction deviats from the direction of the main gas plume. Therefore, for different roof vent locations and different wind orientations, the optimum location for intake vents, given equal exhaust vent to intake vent distance, is a position rotated away from the downwind direction and a location where the intake cannot "see" the exhaust vent.

(3). Orientations of a building at an angle other than 0° to the mean wind increases concentrations near the two upstream edges.

(4). Wilson's suggestion for minimum dilution factor on a building, with $B_1 = 0.11$, is supported in this experiment for the $\theta = 0°$ orientation. The value $B_1 = 0.11$ provides a lower bound to more than 99 percent of the data. However, orientation of a building changes the minimum dilution factor. For a given approach flow and building configuration, a correction factor depending on orientation angle was able to adjust the prediction algorithm. A recommended factor for a cubical structure from this study is

$$f(\theta) = \frac{1}{1+\theta/\frac{\pi}{4}} \quad , \quad 0 \leq \theta \leq \frac{\pi}{4}$$

5.2 Mean Concentration Measurements in the Near Wake Region

(1). Nonnormal wind incidence on a building tends to increase concentration levels and the downwash effect in the near wake region. The maximum ground concentration in the near wake was found to occur between $\frac{x}{H} = 2$ and at $\frac{x}{H} = 4$.

(2). Orientation of the building at an angle of 45 degrees results in a secondary peak concentration in the cross-wind ground-level concentration distribution, at the edge of the near wake.

(3). The jet (or exit) momentum factor, $J = (\frac{\rho_e}{\rho} \cdot \frac{A_e}{A})^{\frac{1}{2}} \frac{U_e}{U_4}$, was found significant at values smaller than 0.01. As the J value increases downwash decreases; this results in a reduction of concentration levels in the near wake region.

5.3 Concentration Fluctuations and Peak-to-Mean Concentration Ratios

(1). The log-normal concentration probability model was found appropriate for measurements in the building wake. The local concentration intensity, I_c, tends to be reduced in a building wake, as compared to the local intensity in unobstructed flow, reported by other authors.

(2). The local intensities on the ground centerline were found to agree well with Meroney's (1979) prediction. The absolute intensity, $(I_c)_{1G}$, has its maximum value at the same location where the maximum mean concentration exists.

(3). The peak-to-mean concentration ratio was found to vary with the local concentration intensity. A simple algorithm is suggested:

$$\left[\frac{\chi_p}{\bar{\chi}}\right]_{99\%} = 5I_c \; ,$$

$$\left[\frac{\chi_p}{\bar{\chi}}\right]_{95\%} = 4I_c \; , \quad \text{and} \quad \left[\frac{\chi_p}{\bar{\chi}}\right]_{90\%} = 3I_c$$

(4). Data from this study suggest that, near the ground-level centerline behind the model building, an upper limit on the peak-to-mean concentration ratios is,

$$\left[\frac{\chi_p}{\bar{\chi}}\right]_{99\%} \leq 3.0$$

$$\left[\frac{\chi_p}{\bar{\chi}}\right]_{95\%} \leq 2.5$$

$$\left[\frac{\chi_p}{\bar{\chi}}\right]_{90\%} \leq 2.0$$

REFERENCES

Akima, H., 1970. "A New Method of Interpolation and Smooth Curve Fitting Based on Local Procedures," J. of the Assoc. for Computing Machinery, Vol. 17, pp. 589-602.

Akins, R. E., Peterka, J. A., and Cermak, J. E., 1976. "Mean Force and Moment Coefficients for Buildings in Turbulent Boundary Layers," J. of Industrial Aerodynamics, Vol. 2, pp. 195-209.

ASME, 1973. Recommended Guide for the Prediction of the Dispersion of Airborne Effluents, Am. Soc. of Mechanical Engineers, New York, 2nd edition.

Briggs, G. A., 1973. "Diffusion Estimation for Small Emissions," Atmospheric Turbulence and Diffusion Laboratory Report No. 79, NOAA, Oak Ridge, Tennessee, 61 p.

Cermak, J. E., 1975. "Applications of Fluid Mechanics to Wind Engineering--A Freeman Scholar Lecture," J. of Fluid Engineering, Vol. 97, pp. 9-38.

Counihan, J., 1975. "Adiabatic Atmospheric Boundary Layer: A Review and Analysis of Date from the Period 1880-1972." Atmospheric Environment, Vol. 19, pp. 871-905.

Csanady, G. T., 1973. Turbulent DIffusion in the Environment, Vol. 3 in Geophysics and Astrophysics Monographs, B. M. McCormac, editor, 248 p.

Evans, B. H., 1957. "Natural Air Flow around Buildings," Texas Engineering Experimantal Station Research Report No. 59, College Station, Texas.

Fackrell, J. E., 1978. "Plume Concentration Statistics Measured on the Tilbury-Northfleet Model," Marchwood Engineering Laboratories, R/M/N 1016, TF 212.

Gifford, F. A., 1968. "An Outline of Diffusion in the Lower Layers of the Atmosphere," Chapter 3, Meteorology and Atomic Energy--1968, D. H. Slade, ed., U.S. Atomic Energy Commission, TID-24190 pp. 65-116.

Halitsky, J., 1961. "Vent to Intake Short Circuit," Air Conditioning, Heating and Ventilation J., 81 p.

Halitsky, J., 1962. "Diffusion of Vented Gas around Buildings," J. of APCA, Vol. 12, pp. 74-80.

Halitsky, J., 1963. "Gas Diffusion near Buildings," ASHRAE Trans., Vol. 69, pp. 464-485.

Halitsky, J., 1968. "Gas Diffusion near Building," Chapter 5.5 Meteorology and Atomic Energy--1968, D. H. Slade, ed., U.S. Atomic Energy Commission, TID-24190 pp. 221-255.

Halitsky, J., 1965. "Estimation of Stack Height Required to Limit Contamination at building Air Intakes," Am. Ind. Hygiene Assoc. J., Vol. 26, pp. 106-116.

Hall, D. J., 1980. "The Discharge of Fume Cupboard Effluents into the Atomsphere," LR 845(AP), Warren Spring Laboratory, Department of Industry, Heitfordshire, SGI2BX.

Hansen, A. C. and Cermak, J. E., 1975. "Vortex-Containing Wakes of Surface Obstacles," Project THEMIS Technical Report No. 29, Civil Engineering Department, Colorado State Universiyt, ADAO 19785, 163 p.

Hinds, W. T., 1969. "Peak-to-Mean Concentration Ratios from Ground-Level Sources in Building Wakes," Atmospheric Environment, Vol. 3, pp. 145-156.

Hosker, R. P., Jr., 1981. "Flow and Diffusion near Obstacles," Atmospheric Turbulence and Diffusion Laboratory, NOAA.

Hosker, R. P., Jr., 1980. "Dispersion in the Vicinity of Buildings," Atmospheric Turbulence and Diffusion Laboratory, NOAA.

Huber, A. H., 1978. "Determination of Good Engineering Practice Stack Height," presented at the 70th Annual Meeting of the APCA, June 25-30, 1978, Houston, Texas.

Hunt, J. C. R., Abell, C., J., Peterka, J. A., and Woo, H., 1978. "Kinematical Studies of the Flow around Free or Surface Mounted Obstacles; Applying Topology to Flow Visualization, " J. Fluid Mech., vol. 86, Part I, pp. 170-200.

Koga, D. J. and Way, J. L., 1979. "Effects of Stack Height and Position on the Dispersion of Pollutants in Bulding Wakes," IIT Fluids and Heat Transfer Rport R79-2, Illinois Institute of Technology.

Meroney, R. N., 1979. "Turbulent Diffusion near Building," Chapter 11 in Engineering Meterology, E. Plate, editor, Colorado State University, CEP78-78RNM33.

Meroney, R., N. and Cermak, J. E., 1967. "Wind-Tunnel Modeling of Flow and Diffusion over San Nicolas Island, California," Colorado State University, CER66-67RNM-JEC44.

Meroney, R. N. and Yang, B. T., 1971. "Wind-Tunnel Study on Gaseous Mixing Due to Various Stack Heights and Injection Rates above an Isolated Structure," Colorado State University, CER71-72RNM-BTY16.

Munn, R. E. and Cole, A. F. W., 1967. "Turbulence and Diffusion in the Wake of a Building," Atmospheric Environment, Vol. 1, pp. 33-43.

Neff, D. E. and Meroney, R. N., 1979. "Dispersion of Vapor from LNG Spills--Simulatin in a Meterologic Wind Tunnel of Spills at China Lake Naval Weapons Center, California," CER78-79DEN-RNM41, Colorado State University.

Netterville, D. D. J., 1979. "Concentration Fluctuations in Plumes: A Wind-Tunnel Study," Ph.D. Dissertation, Department of Mechanical Engineering, University of Alberta.

Peterka, J. A. and Cermak, J. E., 1975. "Turbulence in Building Wakes," CEP74-75AJP-JEC34, Colorado State University.

Peterka, J. A. and Cermak, J. E., 1978. "Wind Tunnel Study of Town Center Project, Phase II, Southfield, Michigan," CER78-79JAP-JEC6, Colorado State University.

Plate, E. J. and Cermak, J. E., 1963. "Micrometeorological Wind-Tunnel Facility, Description and Characteristics," CER63EJP-JEC9, Colorado State University.

Ramsdell, J. V. J. and Hinds, W. T., 1971. "Concentration Flucturations and Peak-to Mean Cncentration Ratios in Plumes from a Ground-Level Continuous Point Source," Atmospheric Environment, Vol. 5, pp. 483-495.

Read, L. E., Barret, C. F., and Walling, S. C., 1965. "An Experimental Chimney for the Study of Dispersion of Gaseous Pollutants," Paper given to the Conference of the National Society for Clean Air, UK, pp. 8-11.

Robins, A. G., 1975. "Plume Dispersion in the Vicinity of a Surface Mounted Cube," R/M.R220, Central Electricity Generating Board.

Robins, A. G. and Fackrell, J. E., 1979. "Continuous Plumes--Their Structures and Prediction," MM/MECH/TFR8, Central Electricity Generating Board.

Thompson, R. S. and Lombardi, D. J., 1977. "Dispersion of Roof-Top Emissions from Isolated Buildings," EPA-600/4-77-006, U.S. Environmental Protection Agency.

Wilson, D. J., 1976. "Contamination of Building Air Intakes from Nearby Vents," Department of Mechanical Engineering, Report No. 1, University of Alberta.

Wilson, D. J., 1977. "Dilution of Exhaust Gases from Building Surface Vents," ASHRAE Trans., Vol. 83, pp. 168-176.

Wilson, D. J., 1979. "Height and Location of Exhaust Stacks to Reduce Recirculation to Air Intakes," Department of Mechanical Engineering, Report No. 15, University of Alberta.

Wilson, D. J. and Netterville, D. D. J., 1976. "Influence of Downwind High-Rise Buildings on Stack Design," J. of APCA, Vol. 26, pp. 976-980.

Woo, H. G. C., Peterka, J. A., Cermak, J. E., 1976. "Wind-Tunnel Measurements in the Wakes of Structures," CER75-76GCW-JAP-JEC40, Colorado State University.

Yang, B. T. and Meroney, R. N., 1970. "Gaseous Dispersion into Stratified Building Wakes, CER70-71BTY-RNM8, Colorado State University.

TABLES

Table 1. Characteristic Parameters of the Simulated Atmospheric
Boundary Layer

	Model Scale (1/2000)	Prototype	Field Result Counihan (1975)*
n	0.19	0.19	0.17
δ (m)	0.30	600	600
z_o (m)	7.5×10^{-5}	0.15	0.15
$\Lambda_{at}\ \frac{z}{\delta} = \frac{1}{20}$	0.0667	134	148
$\left(\frac{\sqrt{\overline{u'^2}}}{U}\right)_{\frac{z}{\delta} = \frac{1}{20}}$	0.152	0.152	0.188
$\left(\frac{\sqrt{\overline{u'^2}}}{U}\right)_{\frac{z}{\delta} = \frac{1}{6}}$	0.118	0.118	0.153
$\left(\frac{u_*}{U_\infty}\right)^2$	2.44×10^{-3}	2.44×10^{-3}	2.26×10^{-3}

*$n = 0.096 \log_{10} z_o + 0.016(\log_{10} z_o)^2 + 0.24$

$\Lambda_{at}\ \frac{z}{\delta} = \frac{1}{20} = 108\left(\frac{1}{z_o}\right)^{1/6}$

$\frac{\sqrt{\overline{u'^2}}}{U} = 0.4 \times 2.49 \times \left(\log_e \frac{z}{z_o}\right)^{-1}$

$\left(\frac{u_*}{U_\infty}\right)^2 = 2.75 \times 10^{-3} + 6 \times 10^{-4} \log_{10} z_o$

Table 2. Information of Test Condition in the TSWT

1.	Boundary Layer Thickness	(δ)	:	30 cm
2.	Free Stream Velocity	(u_∞)	:	450 cm/sec
3.	Wind Velocity Profile Exponent	(n)	:	0.19
4.	Thermal Stratification		:	Neutral
5.	Model Size		:	5 cm x 5 cm x 5 cm
6.	Exhaust Vent ID		:	0.5 cm
7.	Tracer Gas		:	Helium
8.	Emission Rate		:	12.5 cm^3/sec
9.	Density of Helium	(ρ_{He})	:	1.66 x 10^{-4} g/cm^3
10.	Density of Air	(ρ_a)	:	1.205 x 10^{-3} g/cm^3
11.	Kinematic Viscosity of Air	(v_a)	:	15 x 10^{-2} cm^2/sec
12.	Reynolds Number Based on Building Size	(R_{eH})	:	11,050
13.	Froude Number	(Fr)	:	25.78
14.	Jet Momentum Factor	(J)	:	0.006
15.	Sample Probe	I.D.	:	0.10 cm
		O.D.	:	0.15 cm
16.	Traverse Speed		:	2.14 cm^3/sec
17.	Sampling Rate		:	0.5 cm^3/sec
18.	Test Section		:	120 cm x 30 cm x 30 cm
19.	Temperature		:	20°C
20.	Velocity at Building Height	(U_H)	:	330 cm/sec

Table 3. Comparison of Experimental Conditions

	Halitsky (1963)	Meroney & Young (1971)	Robins (1975)*	Wilson (1976)****	Thompson & Lombardi (1977)**	Koga & Way (1979)***	Present Study TSWT	Present Study MWT
1. δ (cm)	⨄	65	200	25	180	100	30	110
2. n	Uniform	0.2	0.23	0.23	0.14	0.16	0.19	0.2
3. Model (cm^3)	38 x 38 x 38	15 x 15 x 15	20 x 20 x 20	7.5 x 5 x 5	18 x 18 x 18	10 x 20 x 20	5 x 5 x 5	15 x 15 x 15
4. H (cm)	38	15	20	7.5	18	10	5	15
5. u_∞ (cm/sec)	120	200	750	1441	200	200	450	240
6. Tracer	SO_2	k-85	Propane	Helium	Methane	Helium	Helium	Argon
7. ρ_e/ρ_a	1.0	1.0	1.0	0.138	0.98	0.176	0.138	1.38
8. D_e (cm)	1.27	0.635	1.54	0.1	2.54	0.9	0.5	1.25
9. w_e/u_H	1.0	0.32, 0.64	0.41	0.3	0.0915	1.315	0.19	0.47
10. A_e/A	8.77×10^{-4}	1.41×10^{-3}	4.66×10^{-3}	2.09×10^{-4}	1.56×10^{-2}	3.18×10^{-3}	7.85×10^{-3}	5.45×10^{-3}
11. Stratification	Neutral	Neutral	Neutral	Neutral	Neutral	Neutral	Neutral	Neutral
12. J	2.96×10^{-2}	1.2×10^{-2}, 2.4×10^{-2}	2.8×10^{-2}	1.6×10^{-3}	1.13×10^{-2}	3.11×10^{-2}	6.25×10^{-3}	4.07×10^{-2}
13. Max GLC. (K_c) $\theta = 0°$	--	--	0.45	--	0.42	0.44	0.67	0.57
$\theta = 45°$	--	--	1.7	--	2.4	0.96	--	1.91
14. Location of Max GLC. $\theta = 0°$	--	--	3.5H	--	5H	4H	4.5H	4H
$\theta = 45°$	--	--	2.5H	--	2H	2.5H	--	2H
15. Buoyancy	Neglected	Neglected	Neglected	Neglected	Neglected	Neglected	Neglected	Neglected
16. $(Re)_H$	2.9×10^4	1.5×10^4	6×10^4	2.1×10^4	1.75×10^4	1.34×10^4	1.1×10^4	1.4×10^4

*Only lowest w_e/u_H case is listed
**Only cubic building is listed
***Only lowest w_e/u_H case is listed
****Listed only one case

40
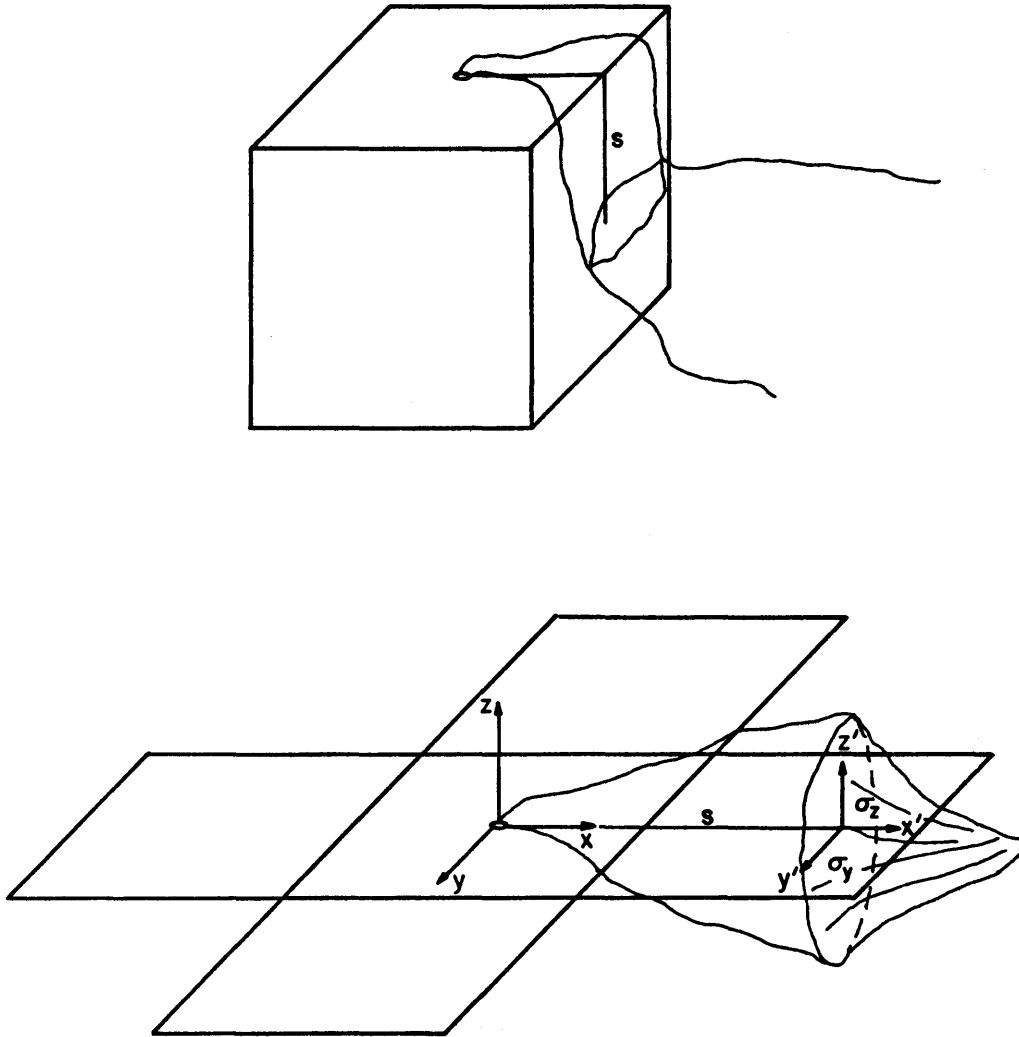
FIGURES

Figure 1. Coordinate system for vent gas dispersion.
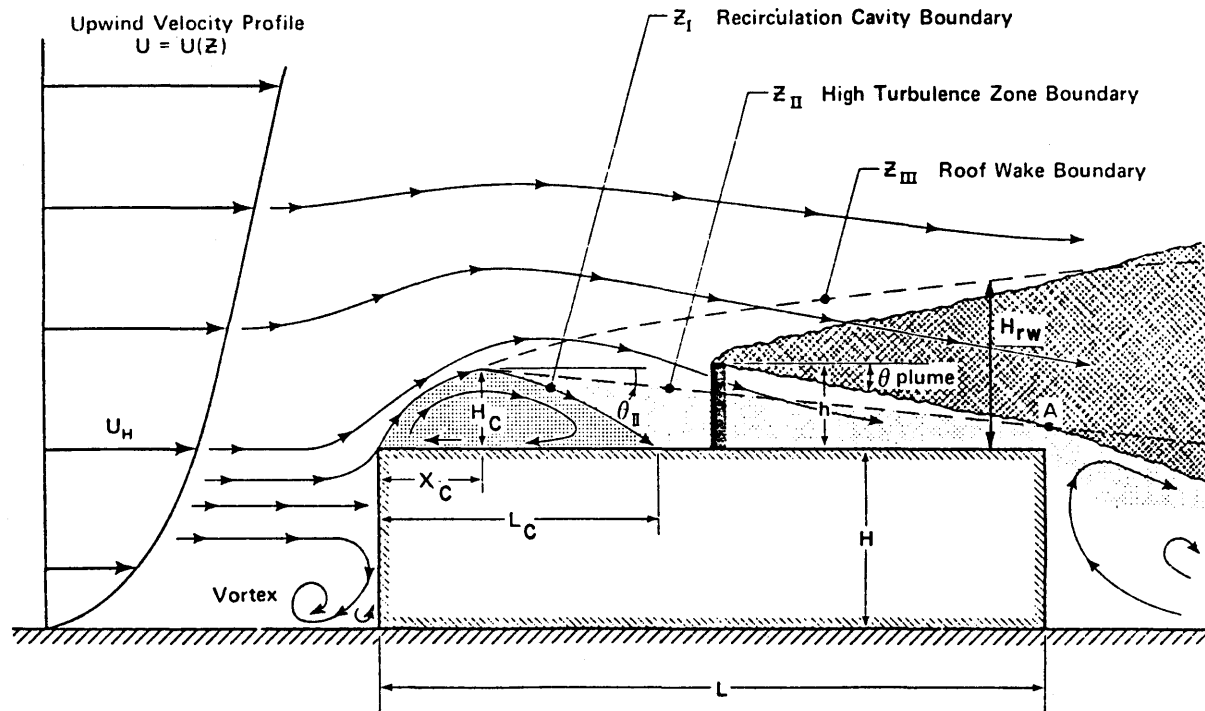
Figure 2.   The three flow zones over a building roof for $\theta = 0°$ orientation, Wilson (1979).
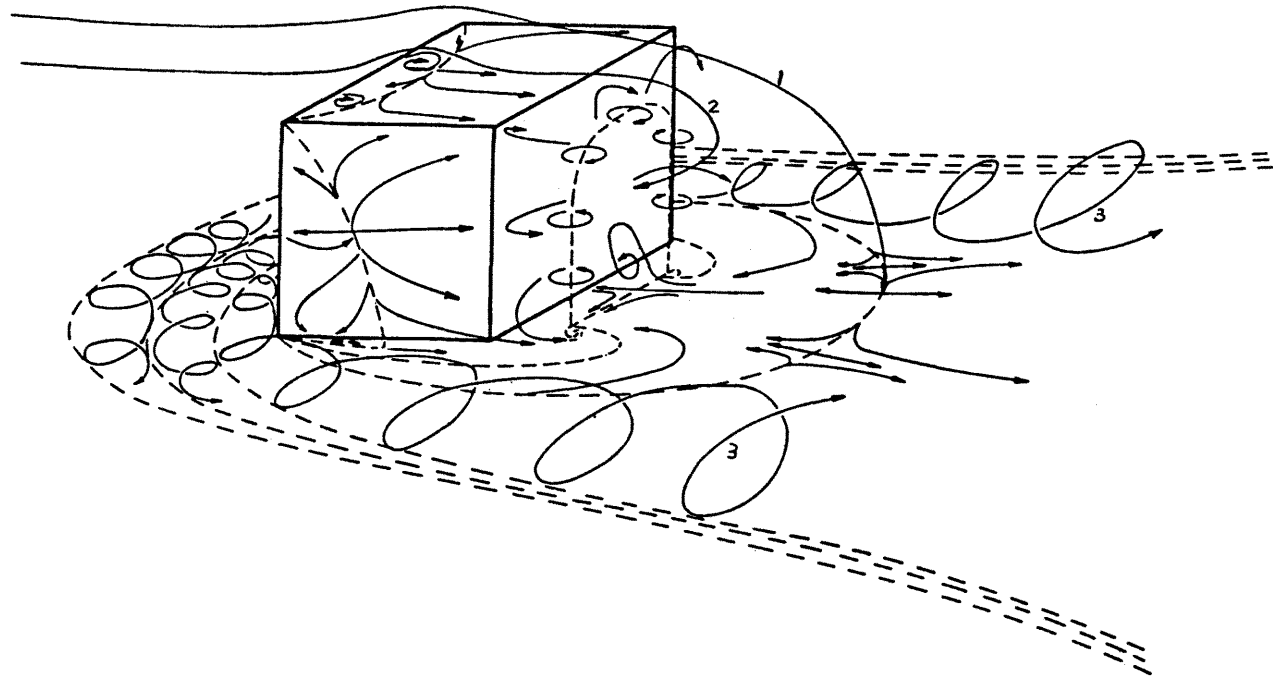
Figure 3. Flow pattern around a rectangular block with reattachment of the free shear layer, Woo, Peterka, and Cermak (1977).

23 Pieces of Silicone Heater
Plate Grid (Plate 17 × 24)

2 cm Honeycomb

1/2 hp Motor

Cross and Side
Supports

Silicone
Heating
Pad

122

55

Particle Board

Aluminum Tee

60

60

70

Particle
Board

SIDE VIEW

Water Cooled
Aluminum Plate

65 · 240 · 120 · 120 · 105 · 60
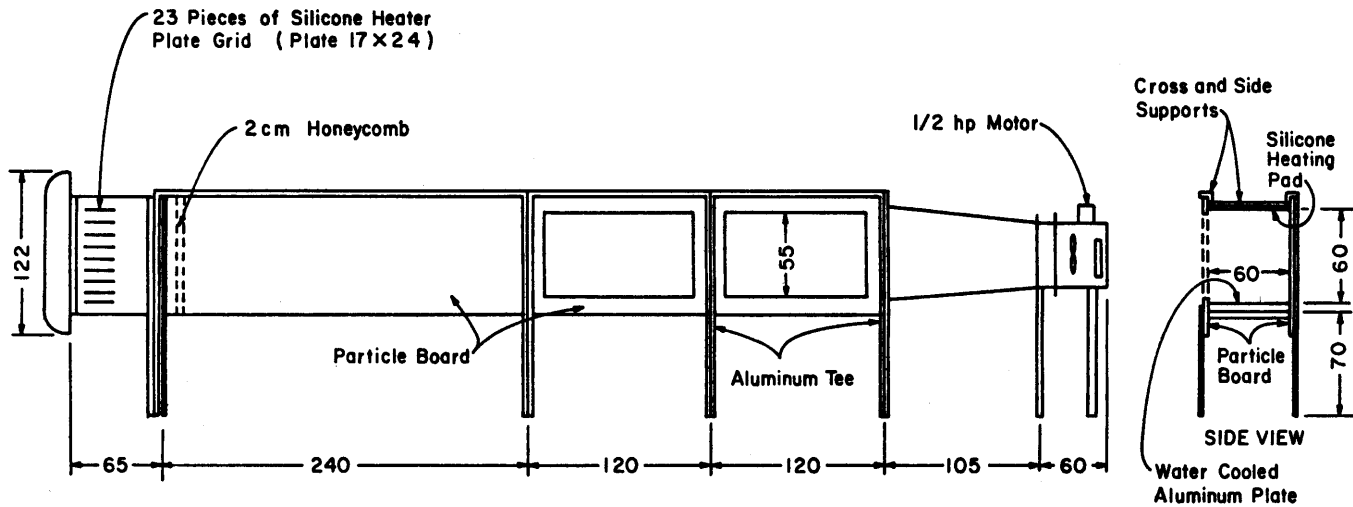
Note: 1. All Dimensions in cm
2. Interior Particle Board
Surfaces Formica Covered

45

Figure 4a. The thermally-stratified wind tunnel (TSWT).
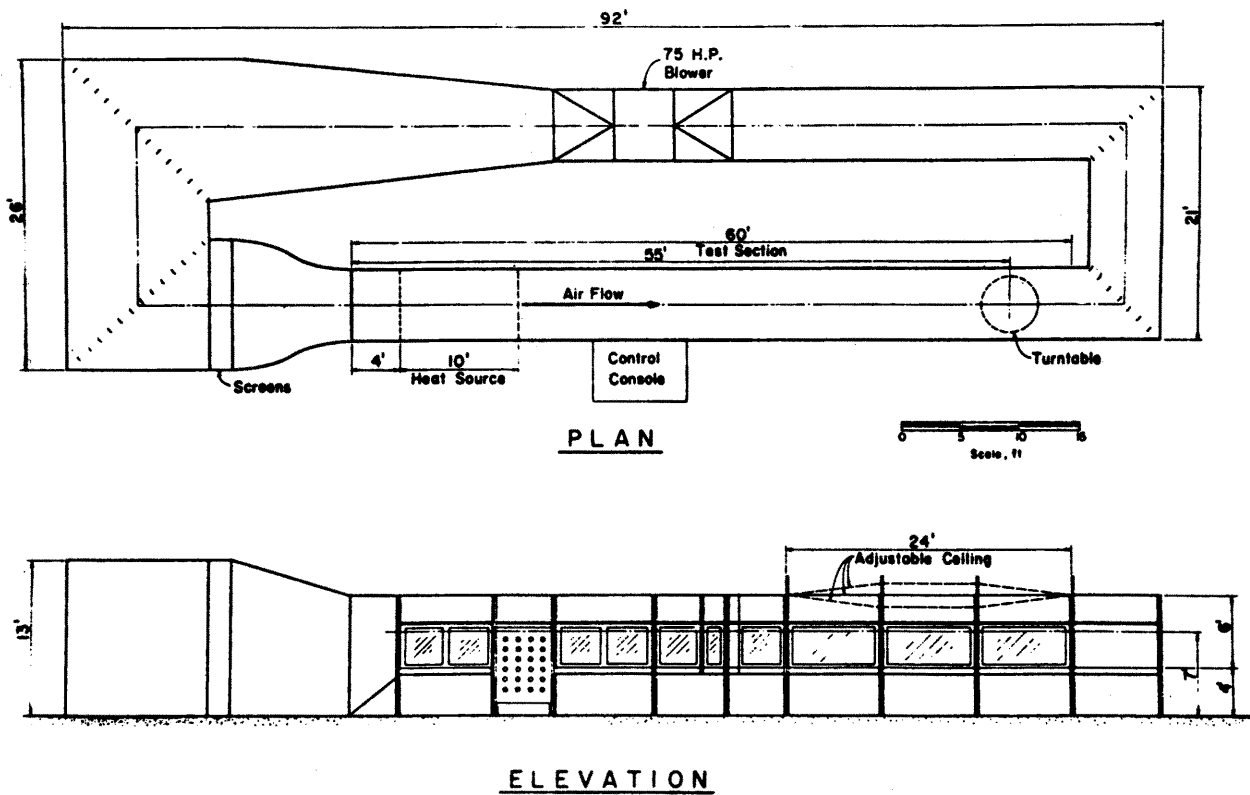
Figure 4b. Industrial Areodynamics Wind Tunnel (IAWT).
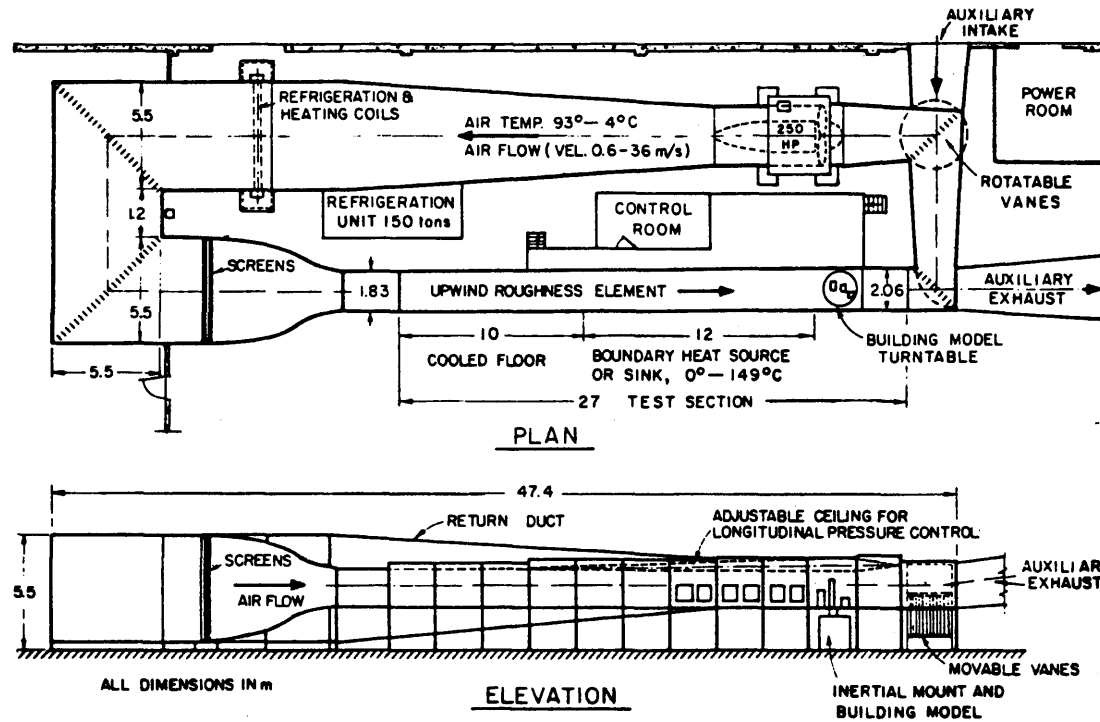
Figure 4c. Meteorological Wind Tunnel (MWT).
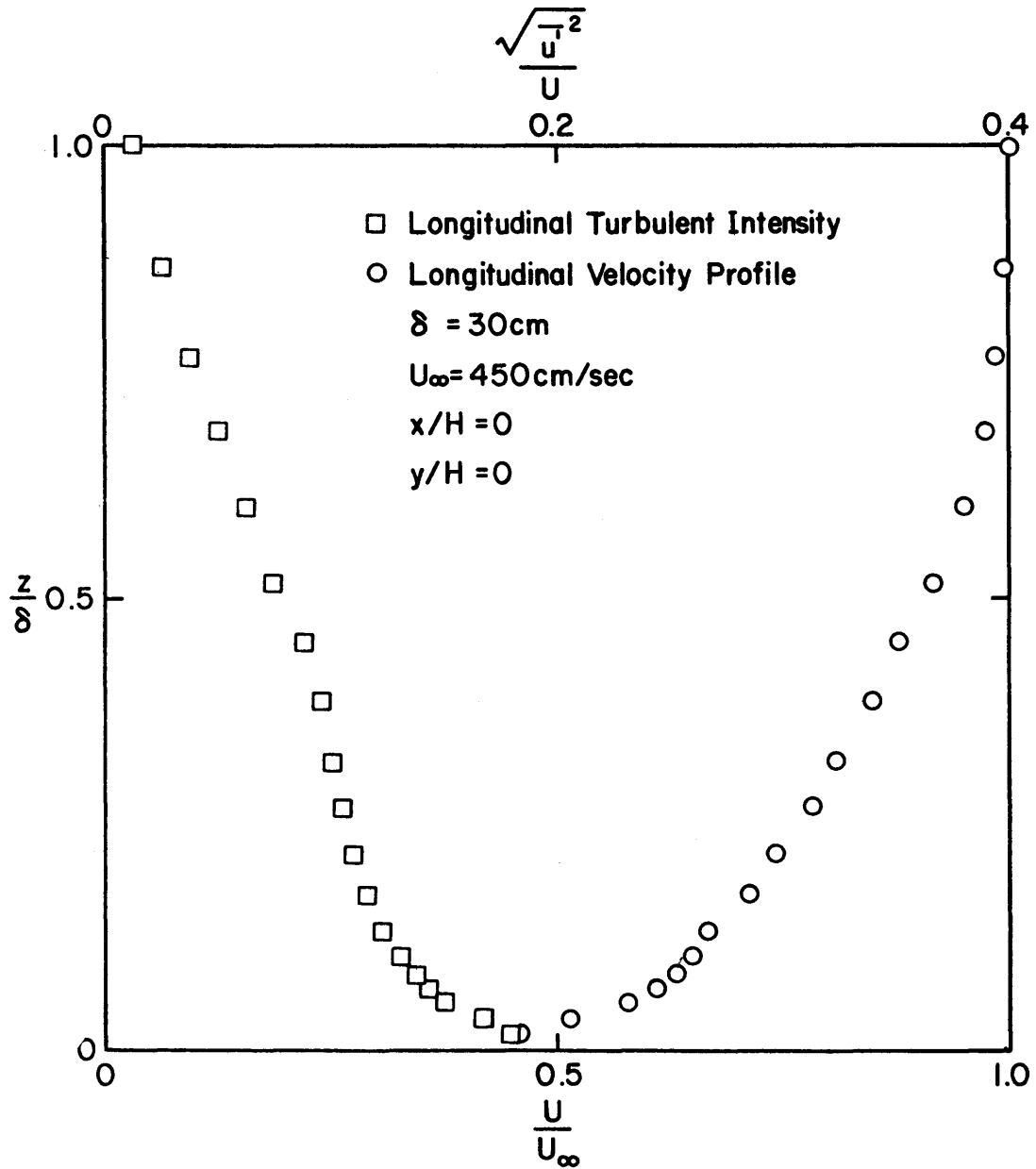
Figure 5. Mean velocity and turbulent intensity profiles.
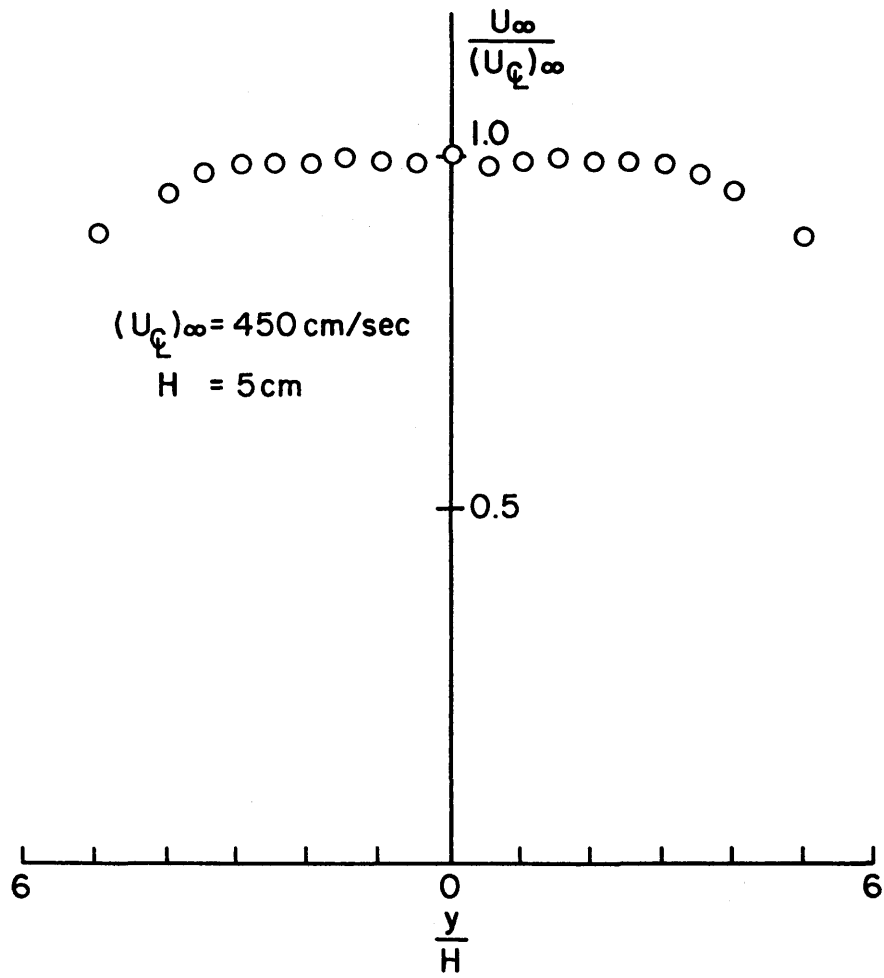
Figure 6. Lateral velocity profile across the TSWT.
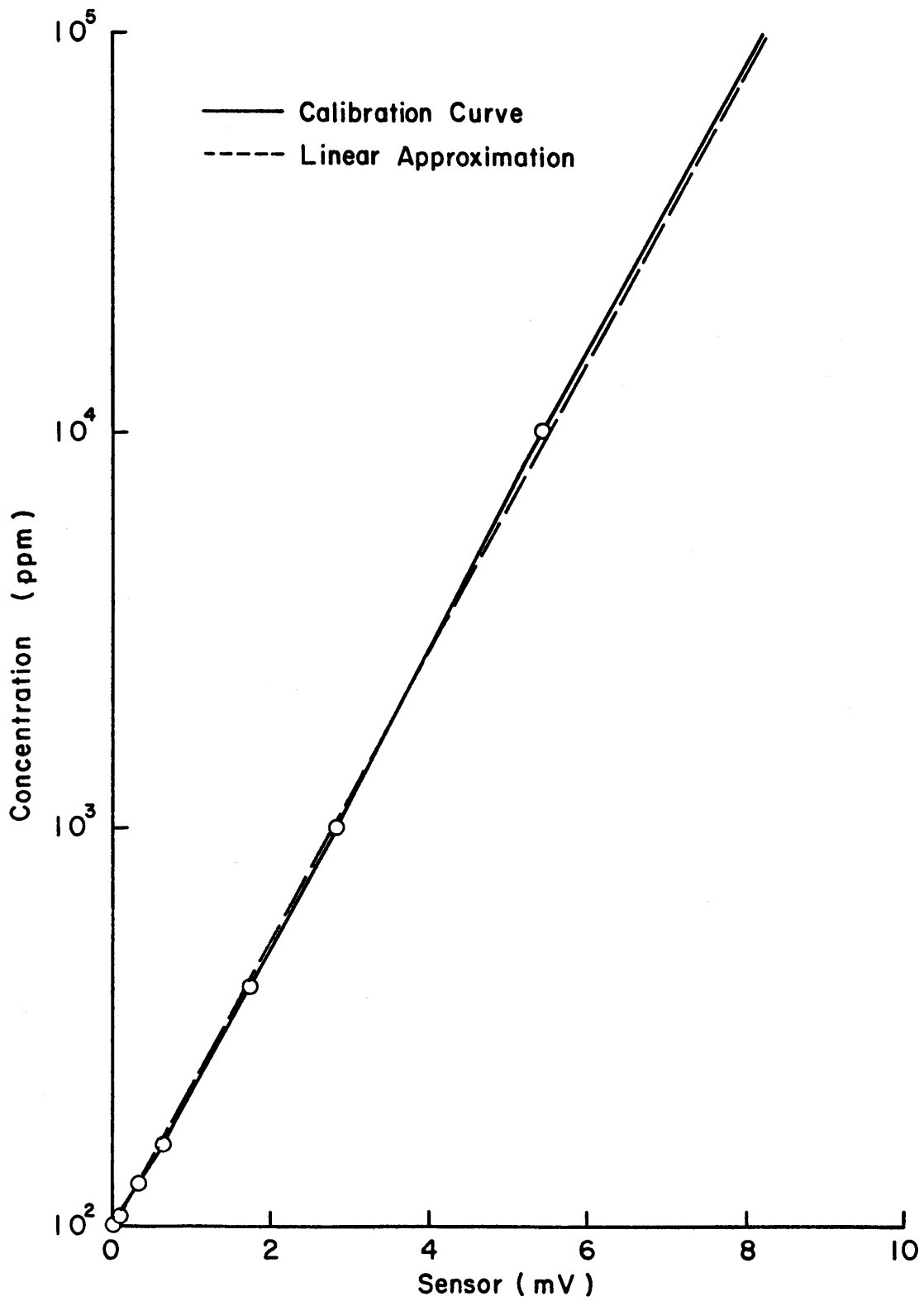
Figure 7. Calibration curve of mean concentration measurements.

a)   θ = 0°

b)   θ = 22.5°
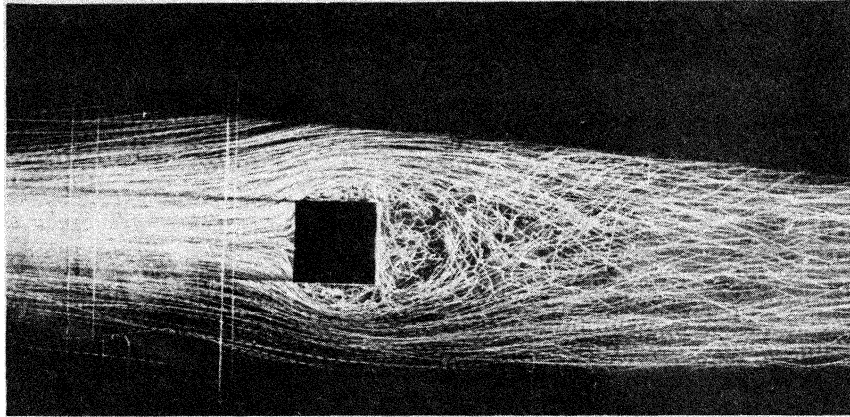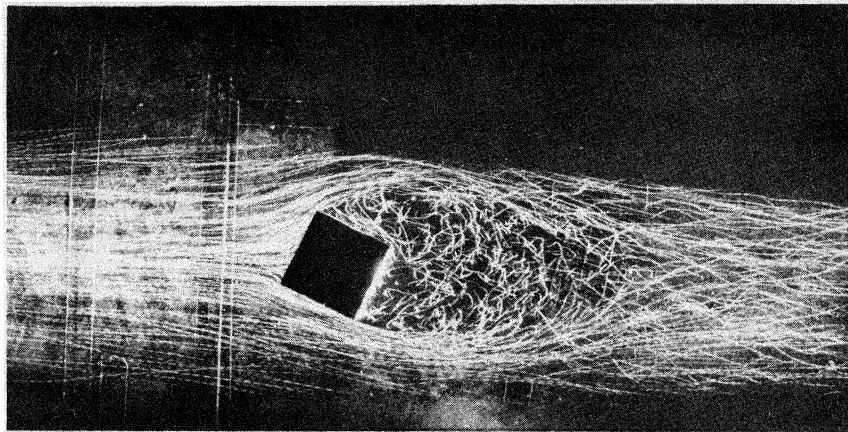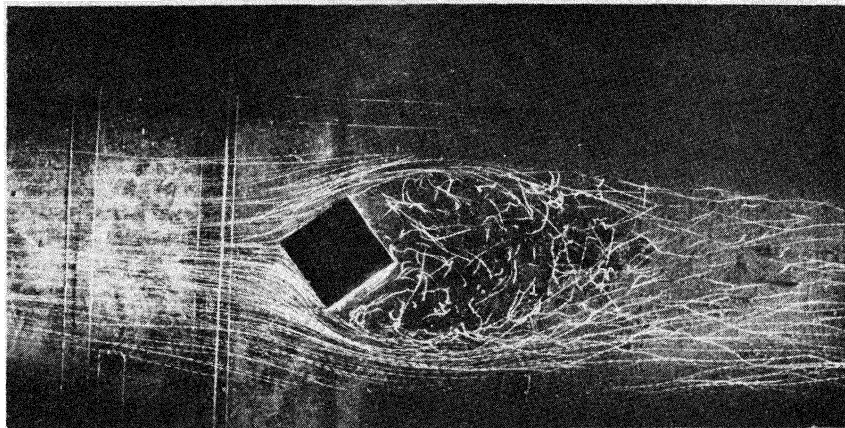
c)   θ = 45°

Figure 8.   Flow visualization photographs using helium bubble
technique (top view)(z = H/2).

a) θ = 0°

b) θ = 22.5°
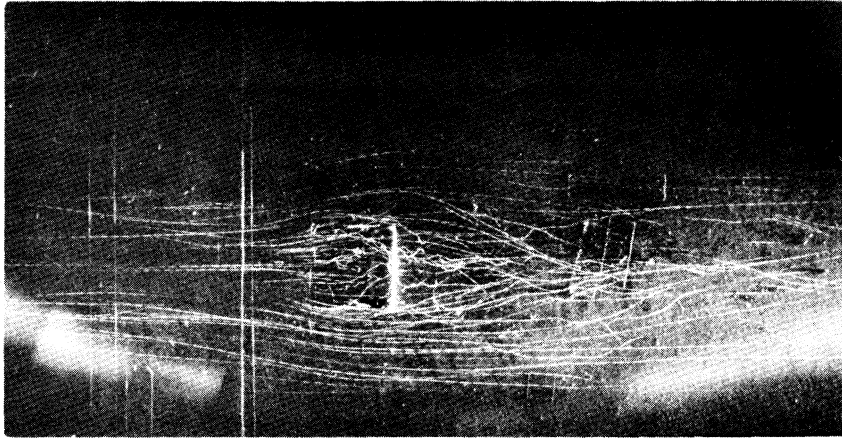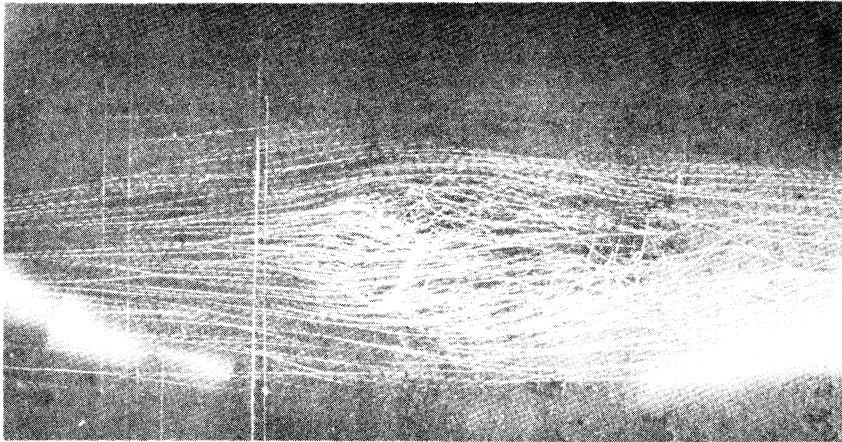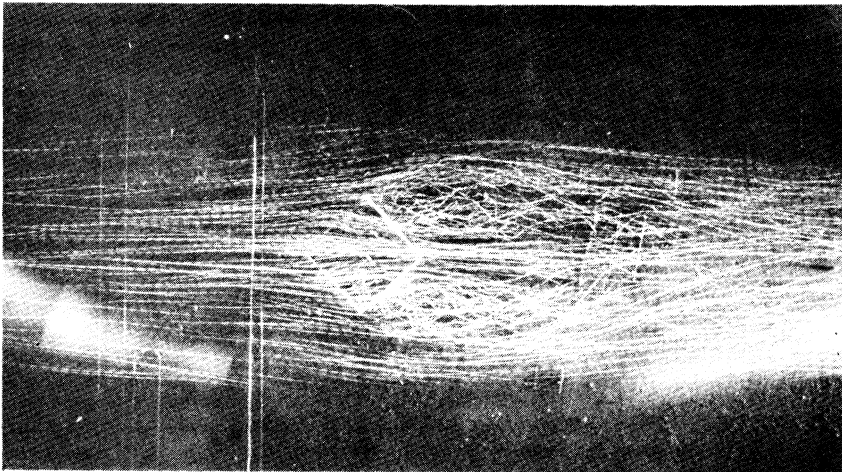
c) θ = 45°

Figure 8. Continued.
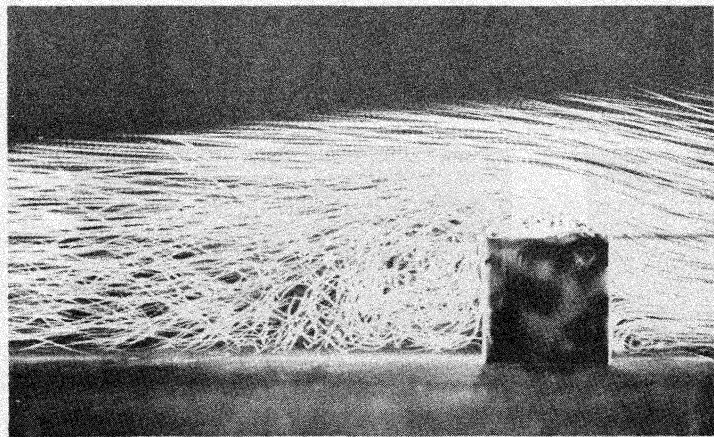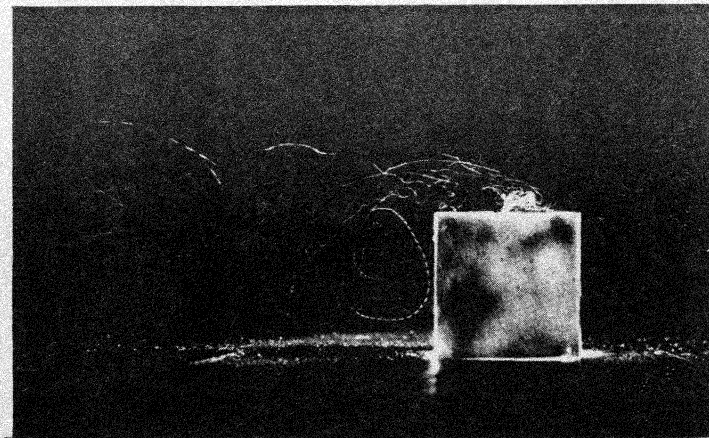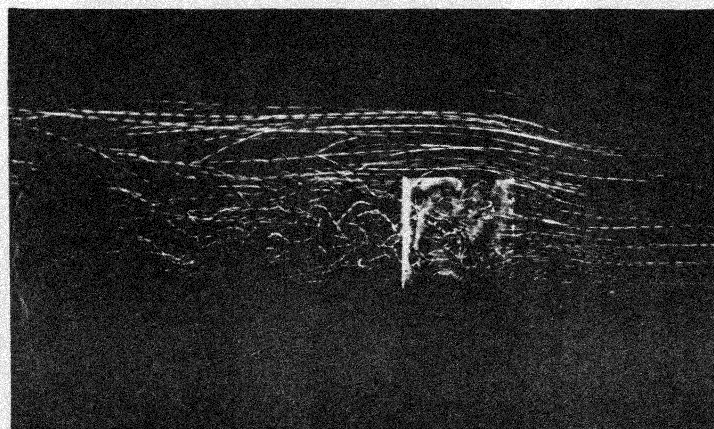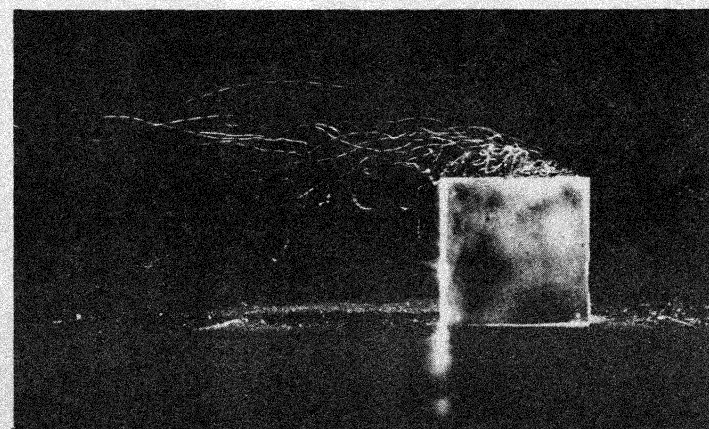
Figure 9. Flow visualization photographs using helium bubble technique
(side view)(θ = 0°).

a) θ = 0°

b) θ = 22.5°
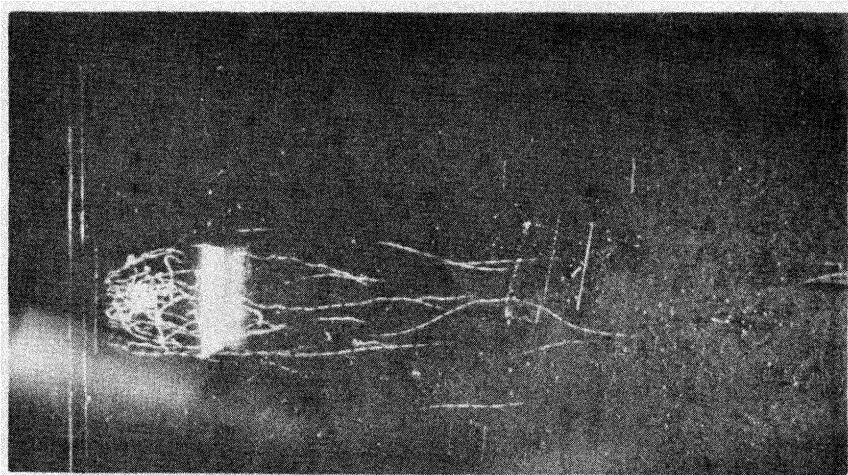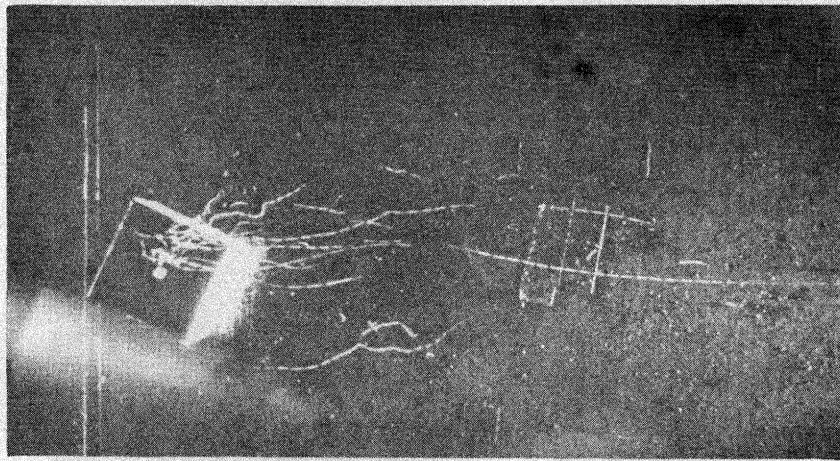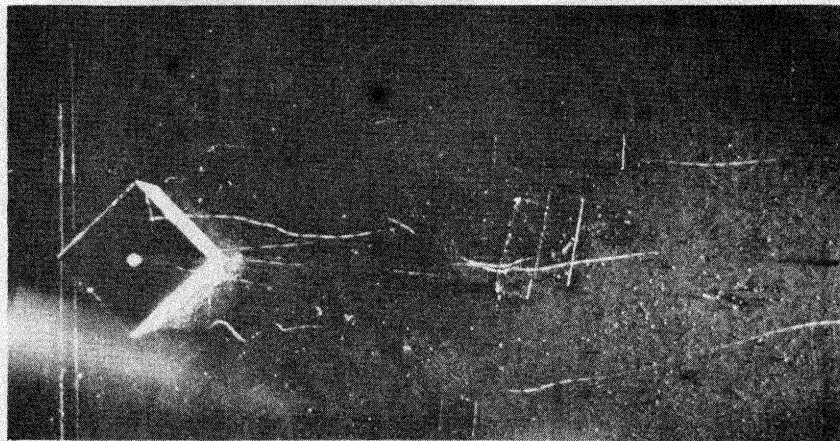
c) θ = 45°

Figure 10. Flow visualization photographs of roof central release (z = H).
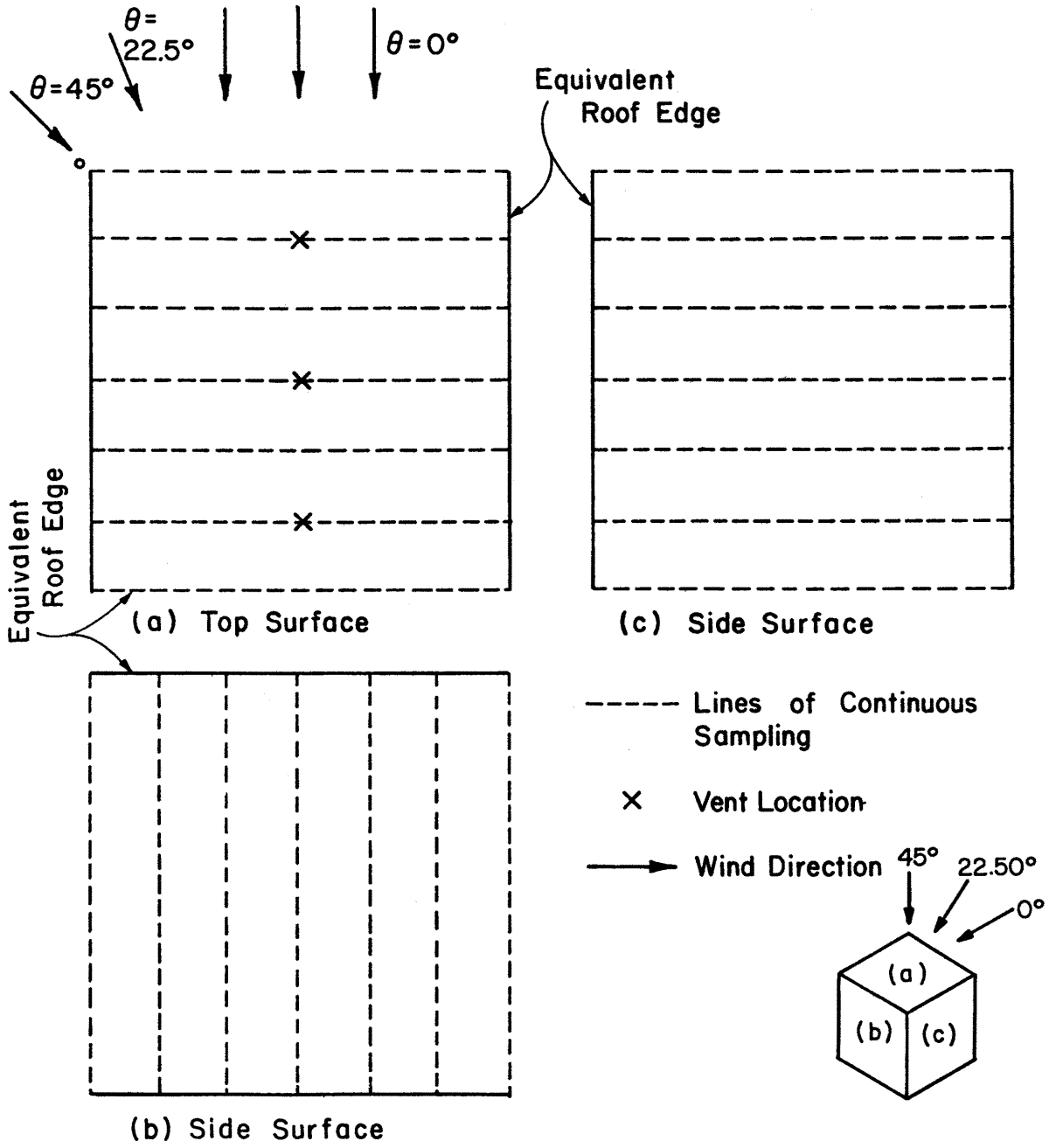
Figure 11. Wind directions and vent locations for building surface measurements.
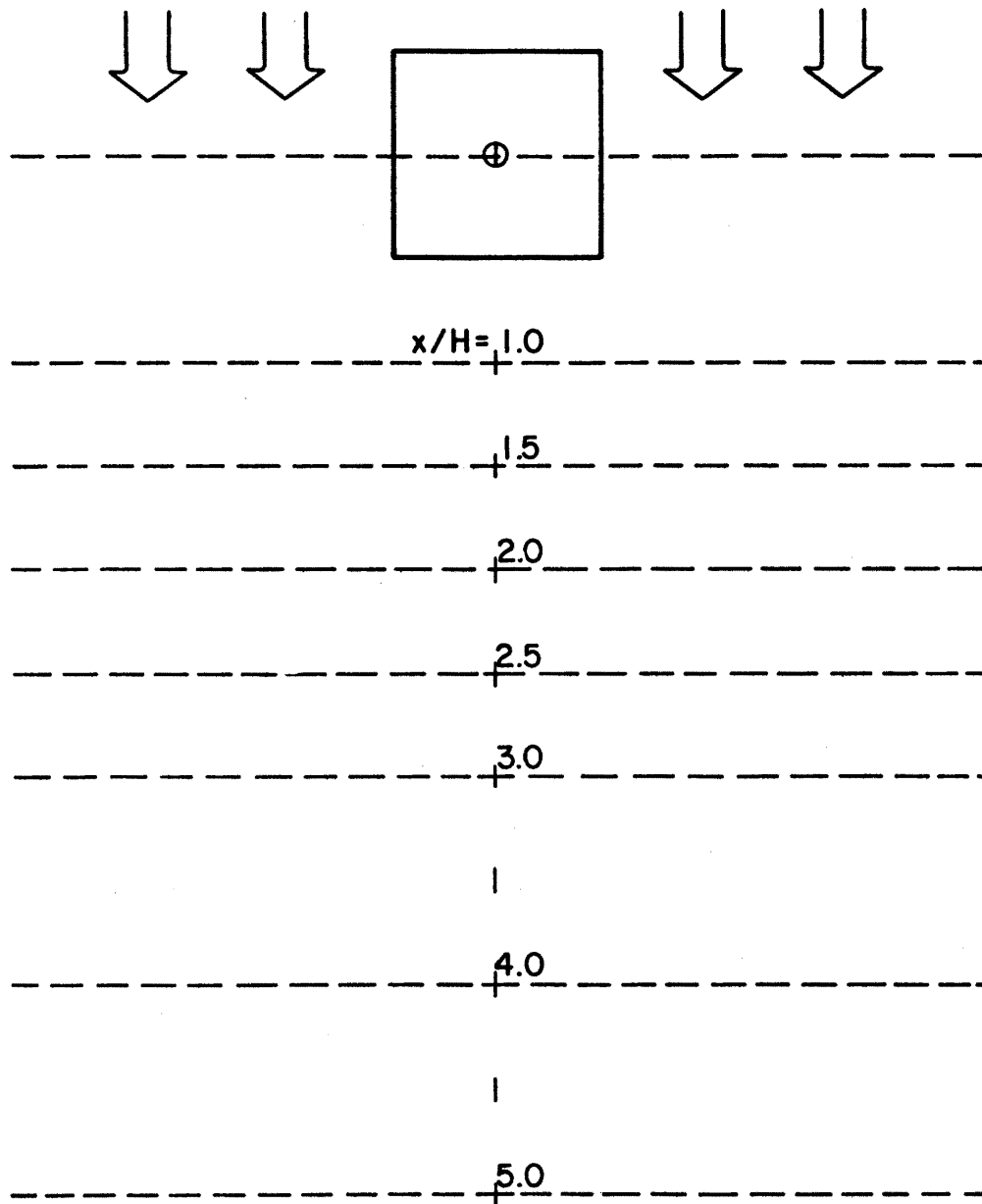
Figure 12. Sampling locations for measurements in the near wake region.
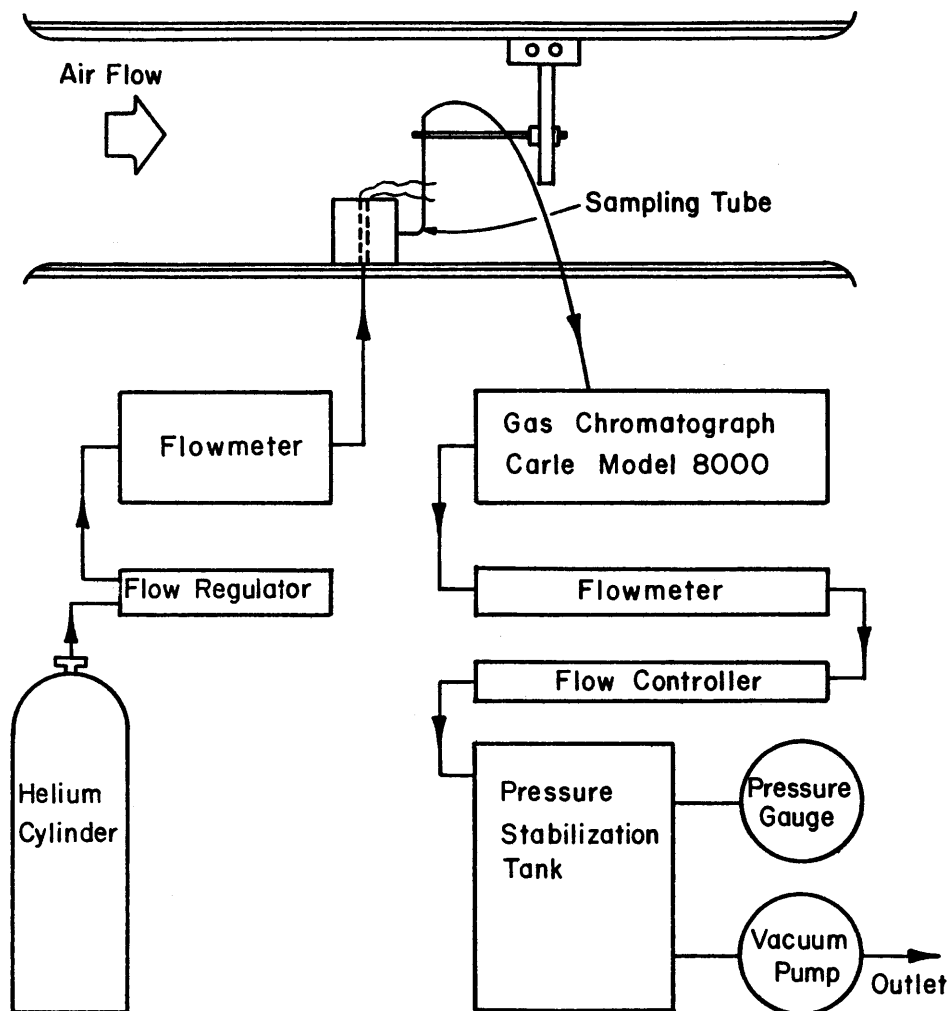
Figure 13. Setup of measuring apparatus.

$\theta = 0°$

(a)

(c)

(b)
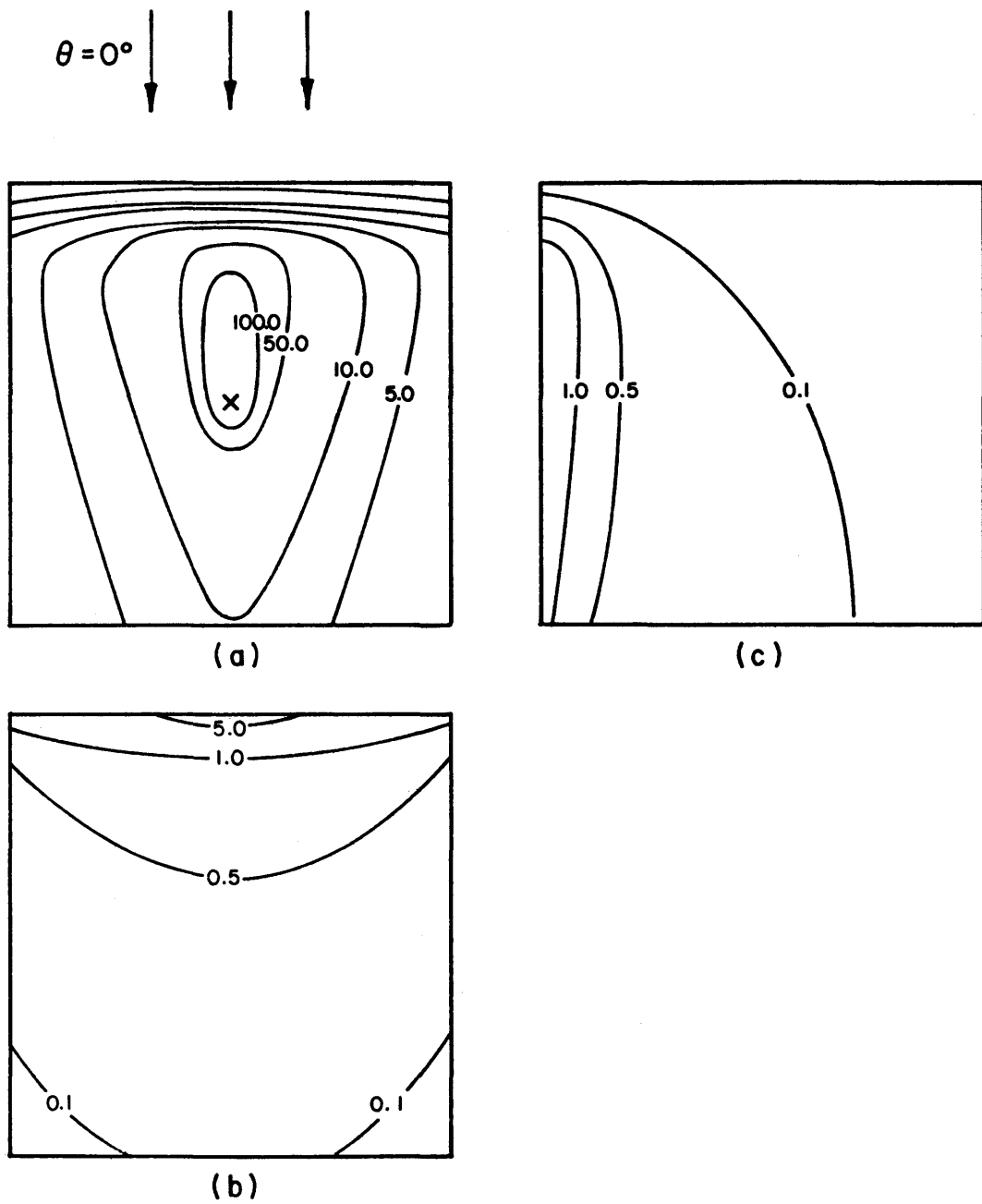
Figure 14.   Concentration coefficient isopleths on a cubical
building (θ = 0°, central roof vent release).

$\theta = 0°$
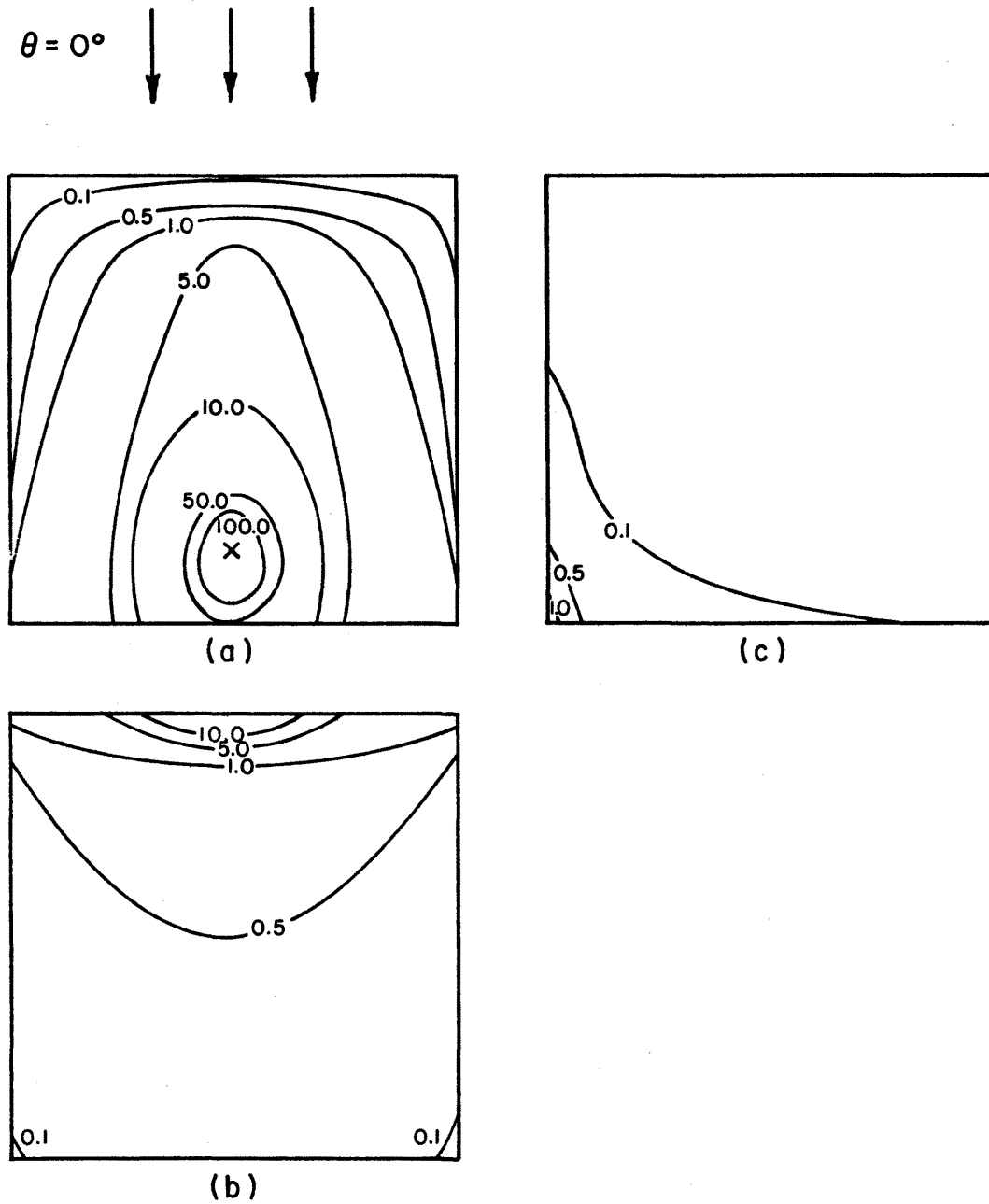
Figure 15. Concentration coefficient isopleths on a cubical building ($\theta = 0°$, downwind roof vent release).
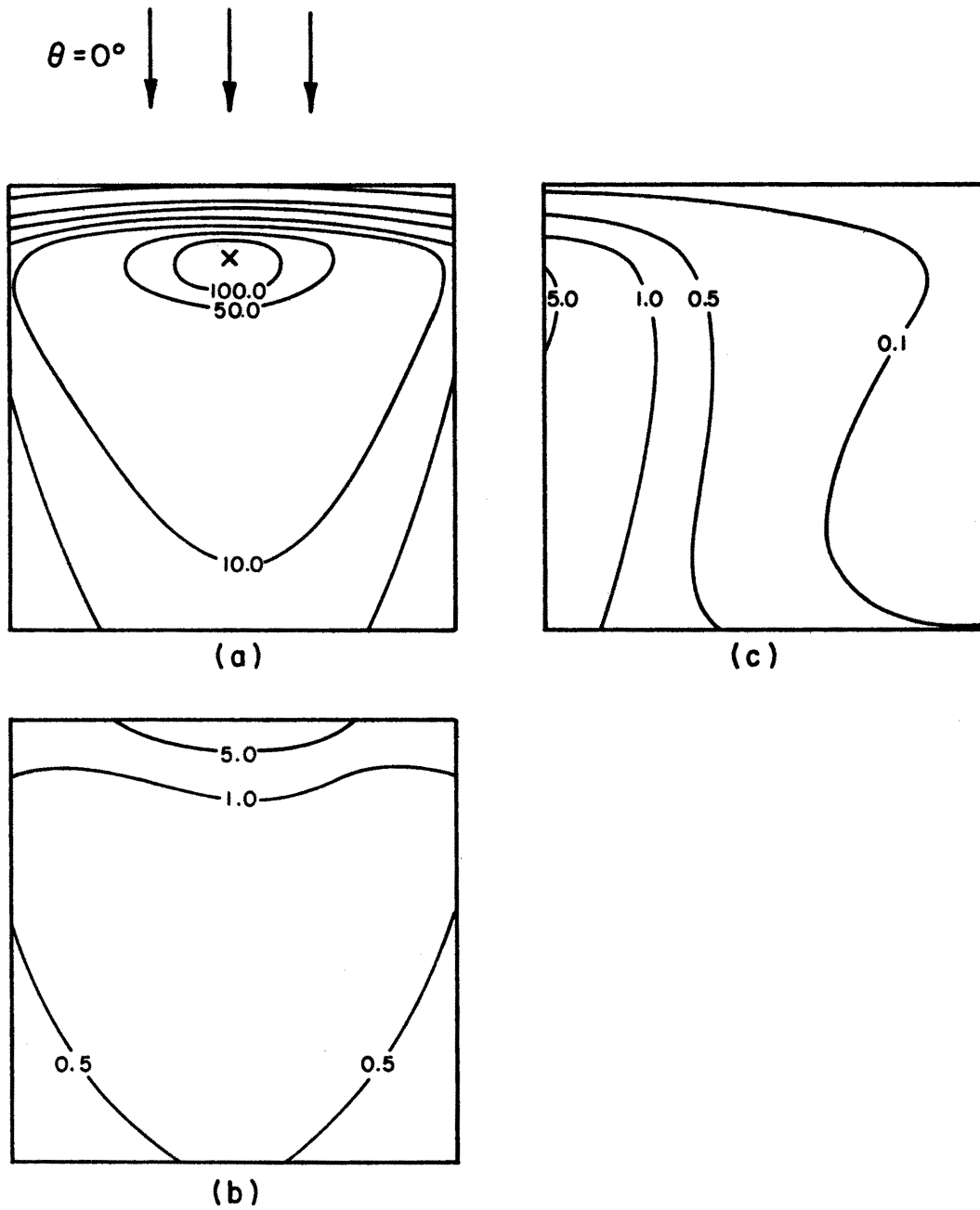
Figure 16. Concentration coefficient isopleths on a cubical
building (θ = 0°, upwind roof vent release).
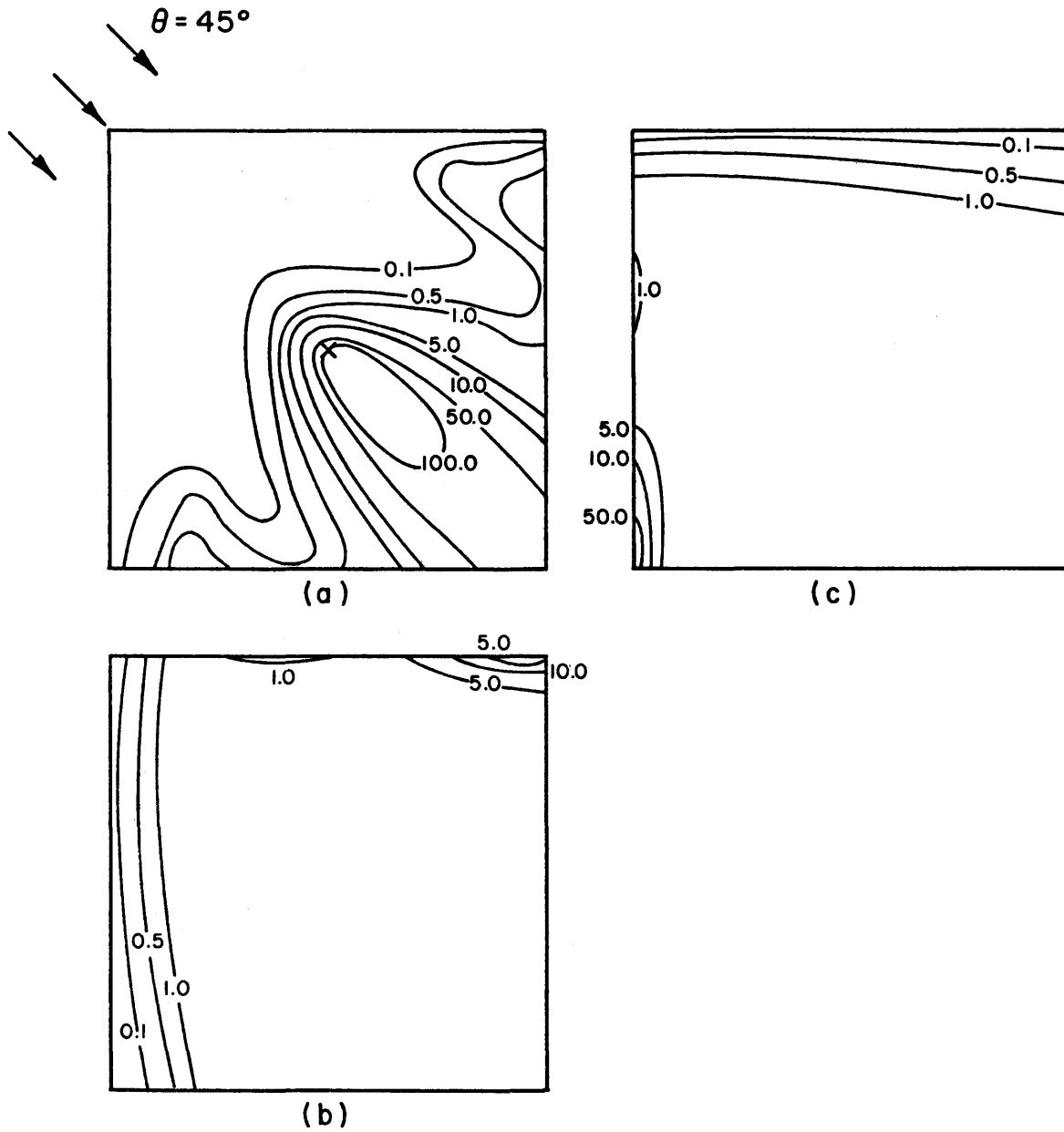
Figure 17. Concentration coefficient isopleths on a cubical
building (θ = 45°, central roof vent release).
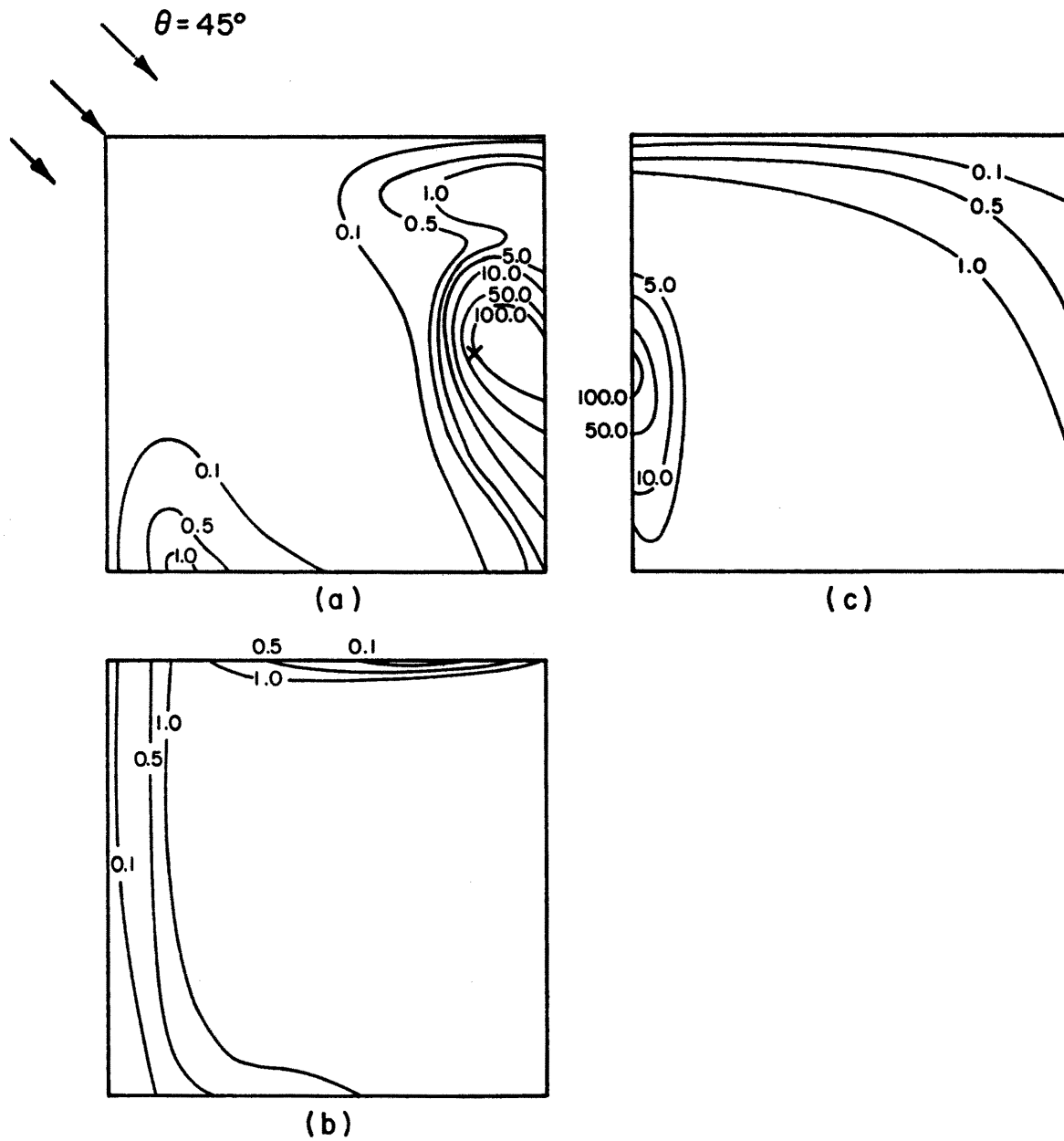
Figure 18. Concentration coefficient isopleths on a cubical building (θ = 45°, downwind roof vent release).
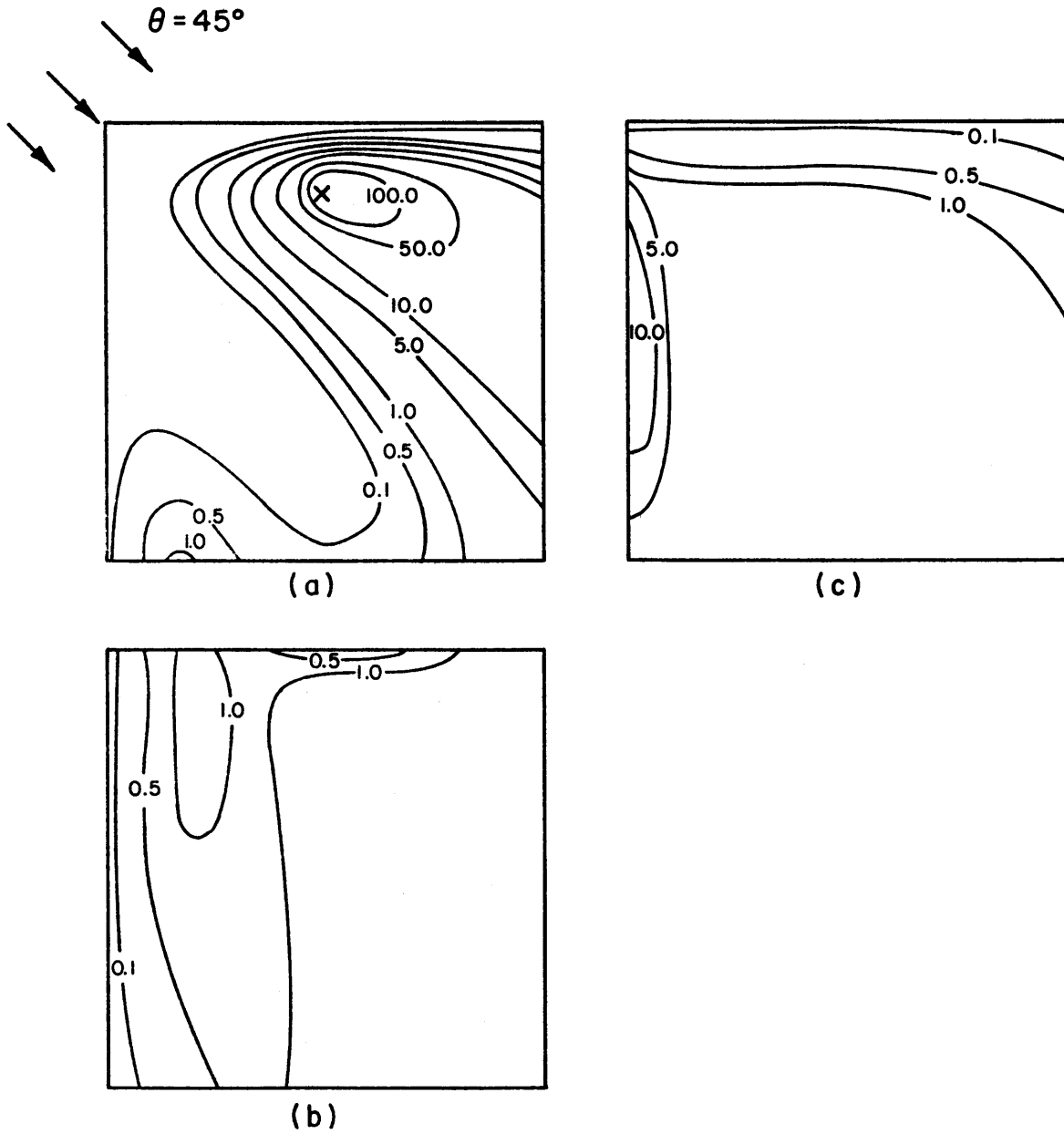
Figure 19. Concentration coefficient isopleths on a cubical building (θ = 45°, upwind roof vent release).
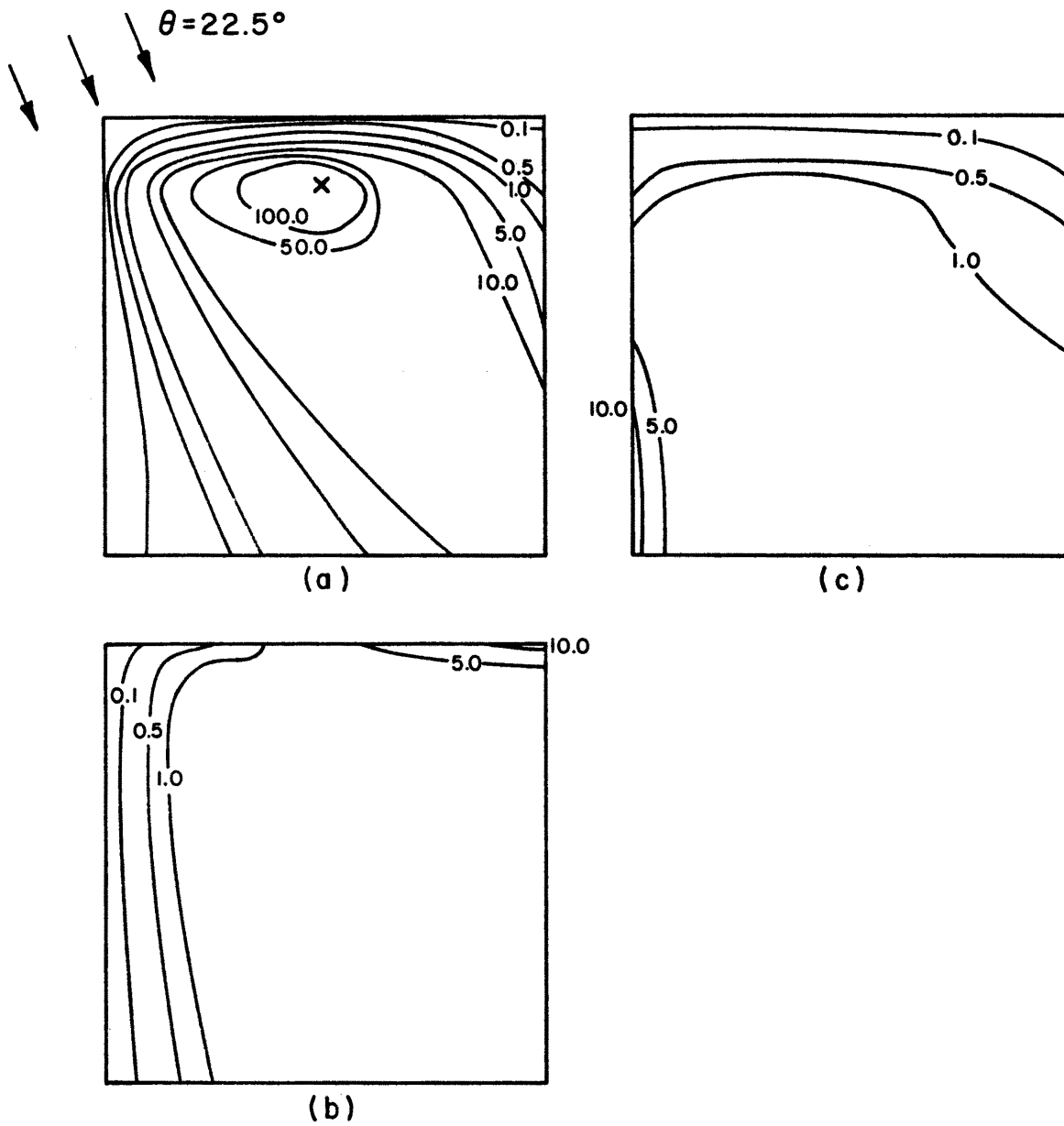
Figure 20. Concentration coefficient isopleths on a cubical
building (θ = 22.5°, upwind roof vent release).
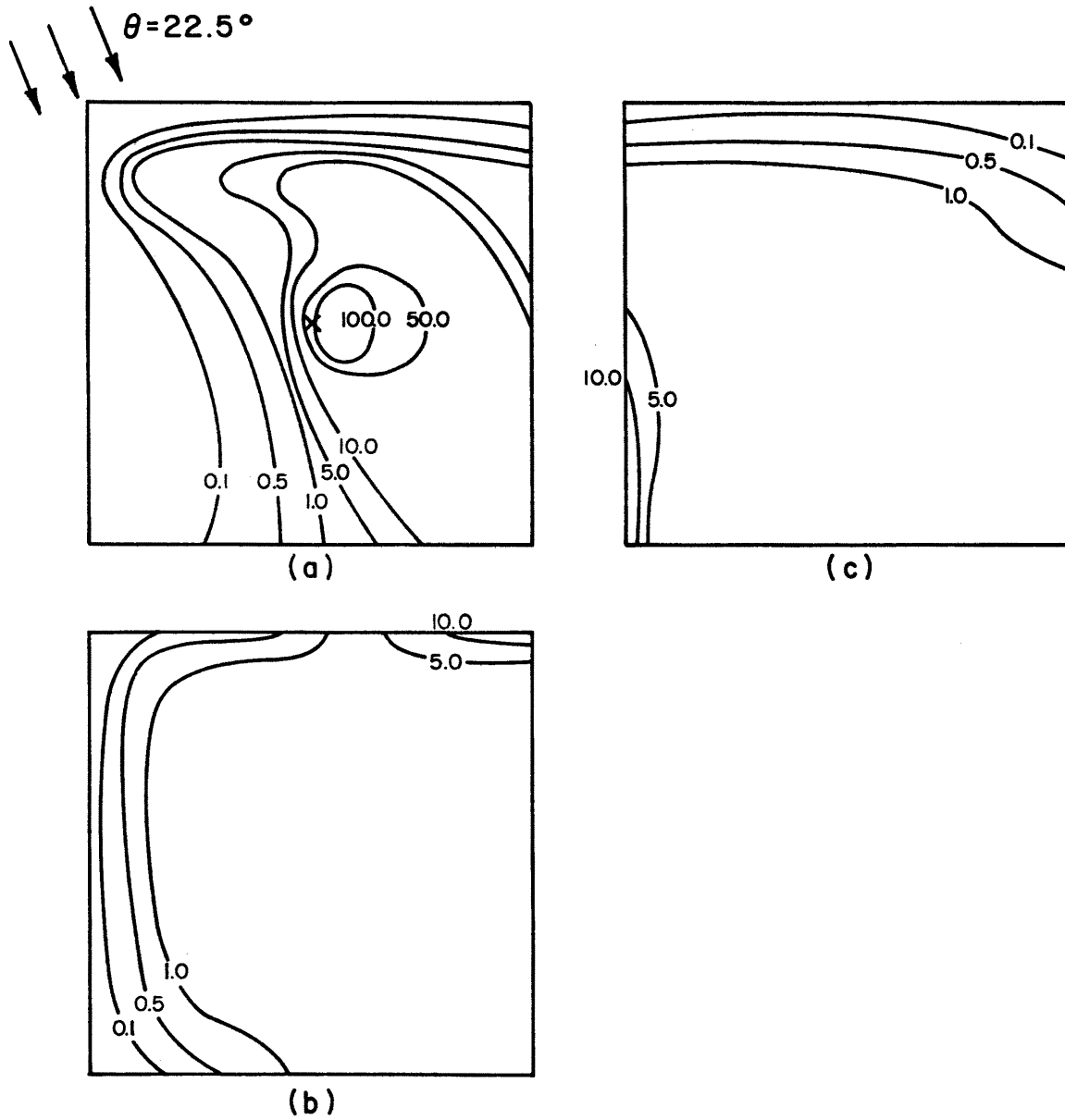
Figure 21. Concentration coefficient isopleths on a cubical
            building (θ = 22.5°, downwind roof vent release).
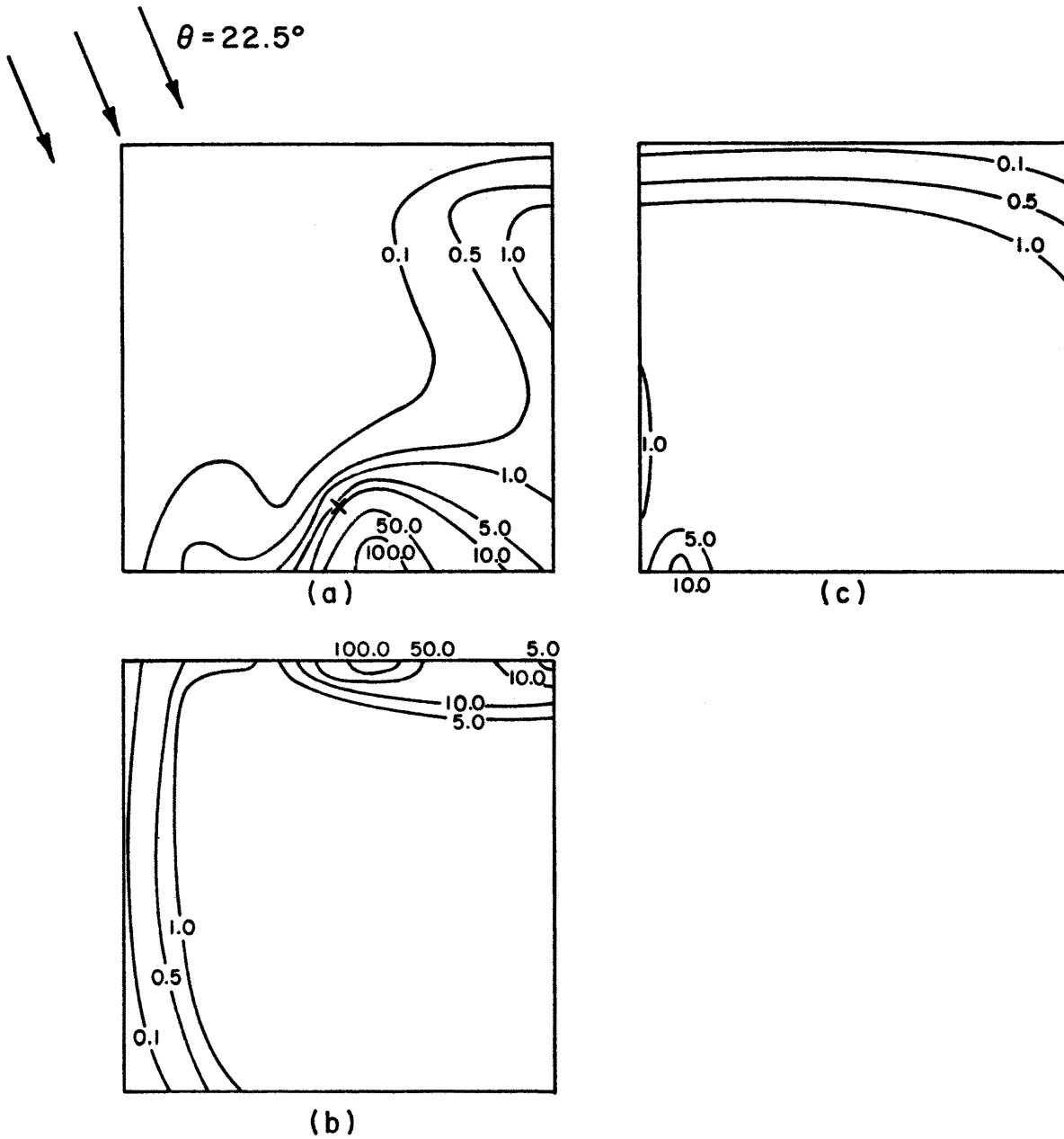
Figure 22.   Concentration coefficient isopleths on a cubical
             building (θ = 22.5°, downwind roof vent release).
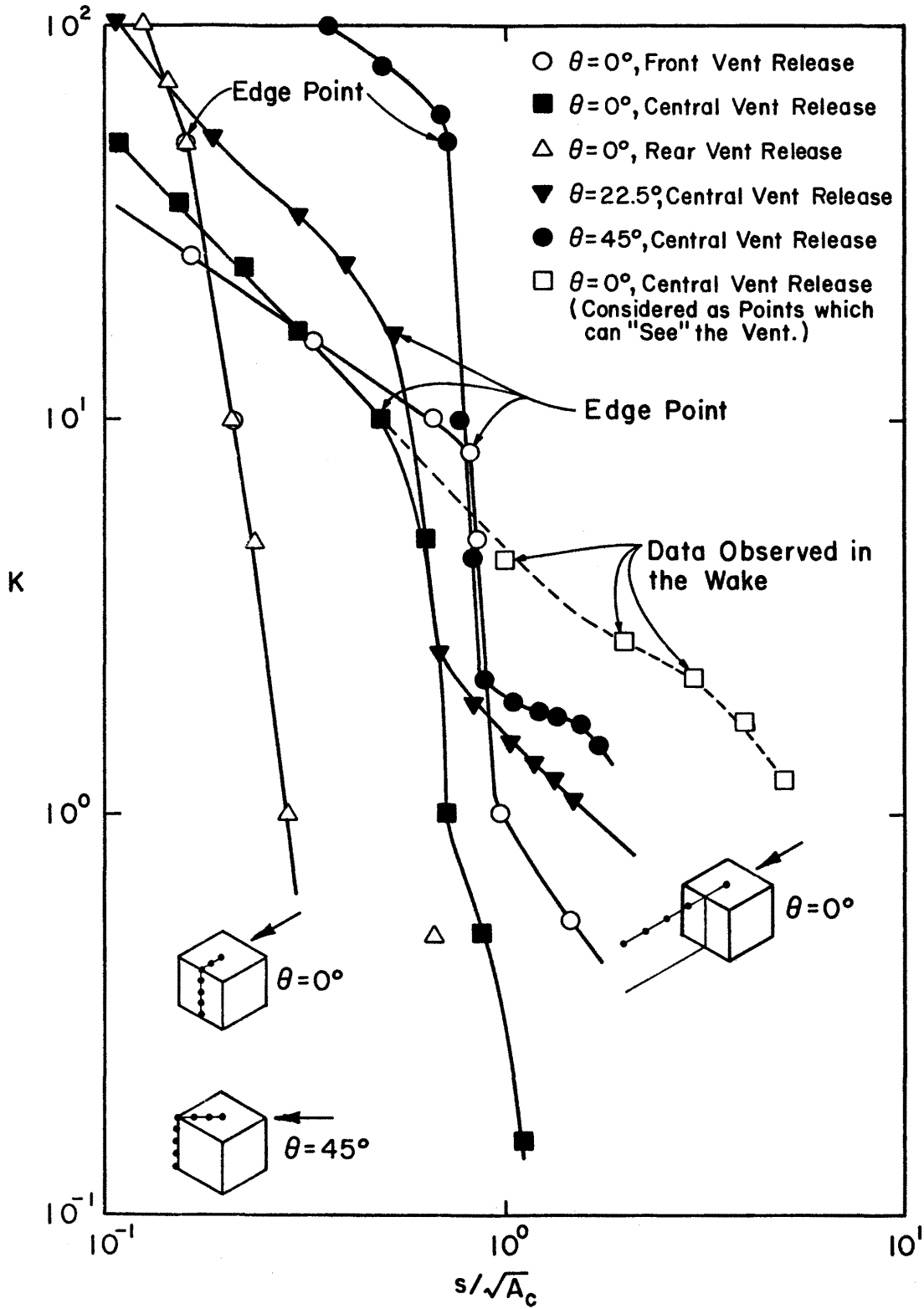
Figure 23. Surface concentration coefficients vs. distance from the vent.
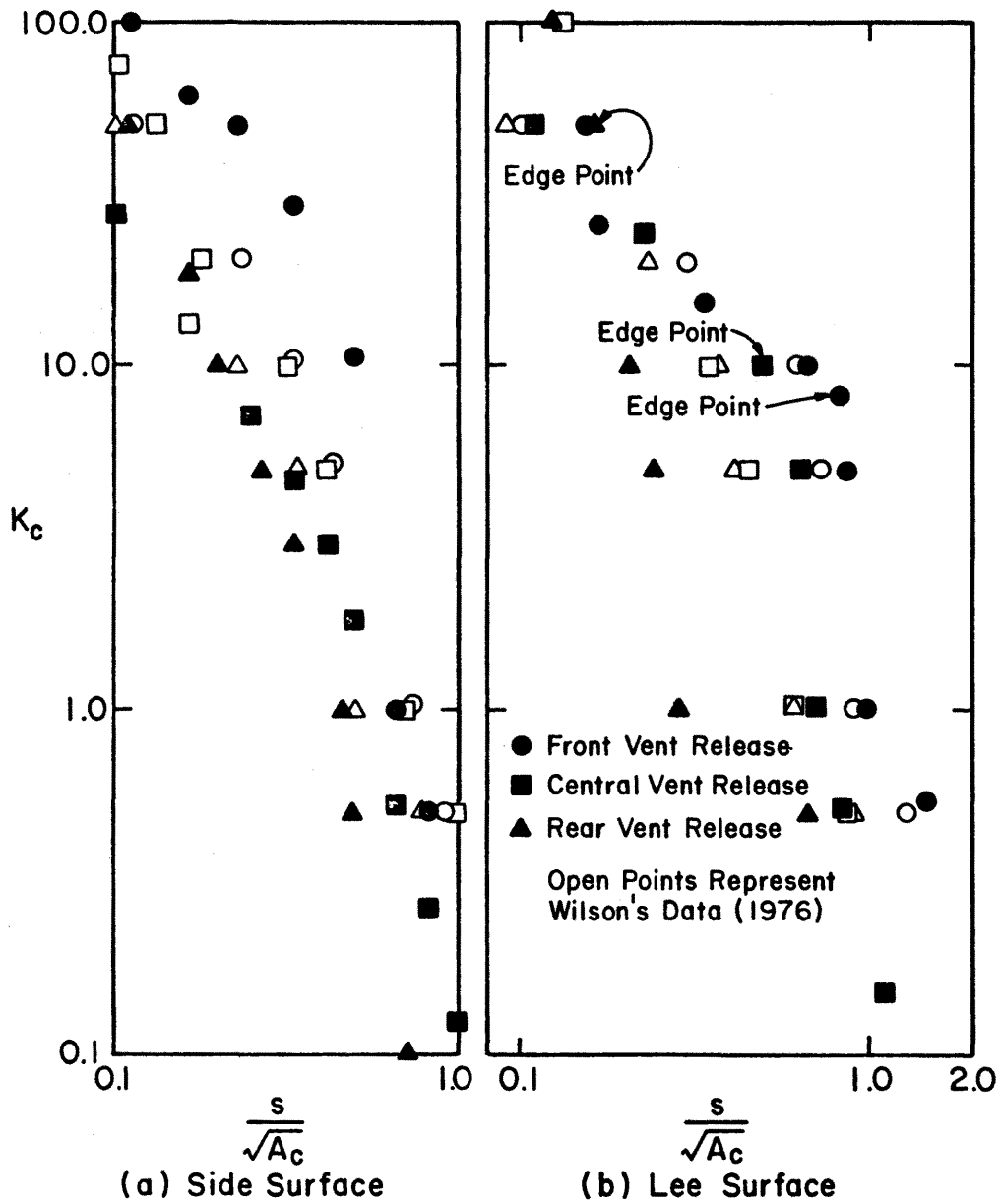
Figure 24. Concentration coefficients on the building surface along the wind direction, θ = 0°.
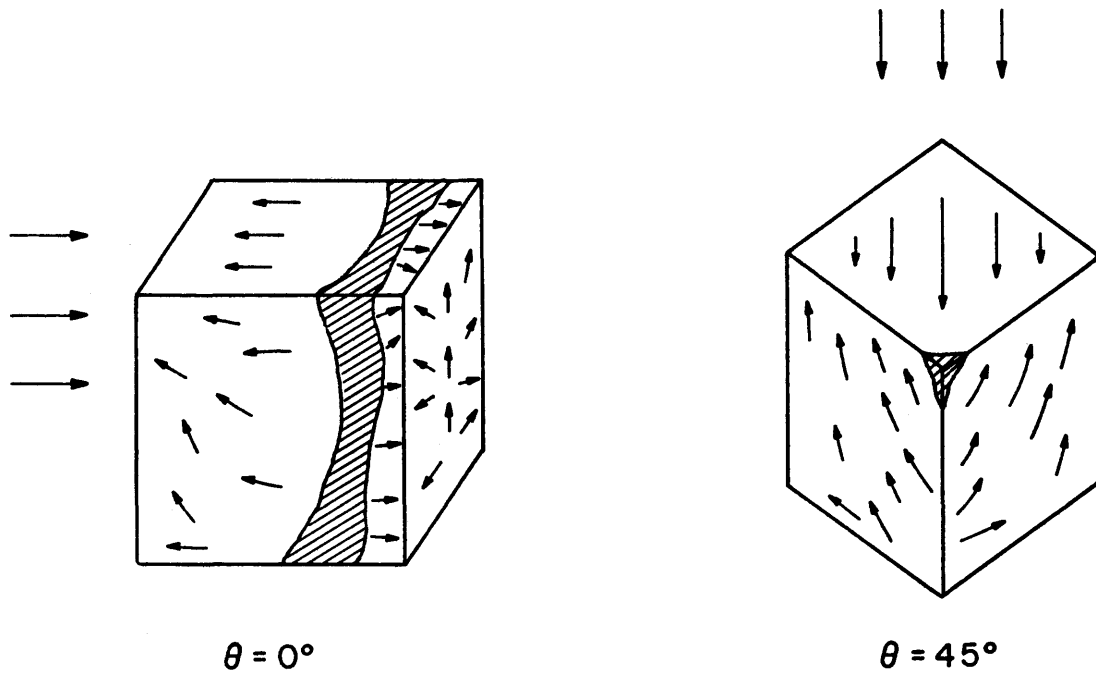
$\theta = 0°$

$\theta = 45°$
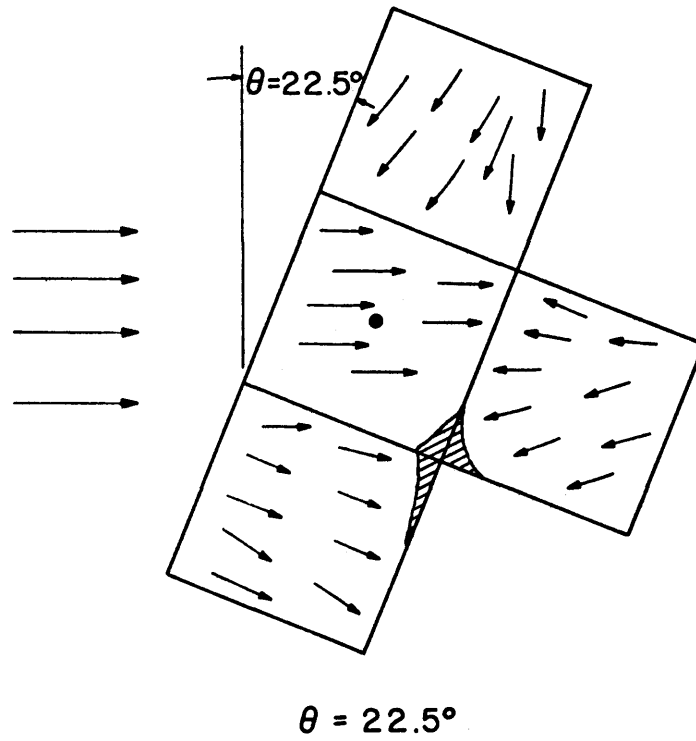
$\theta = 22.5°$

Figure 25. Surface flow patterns and reattachment zones.
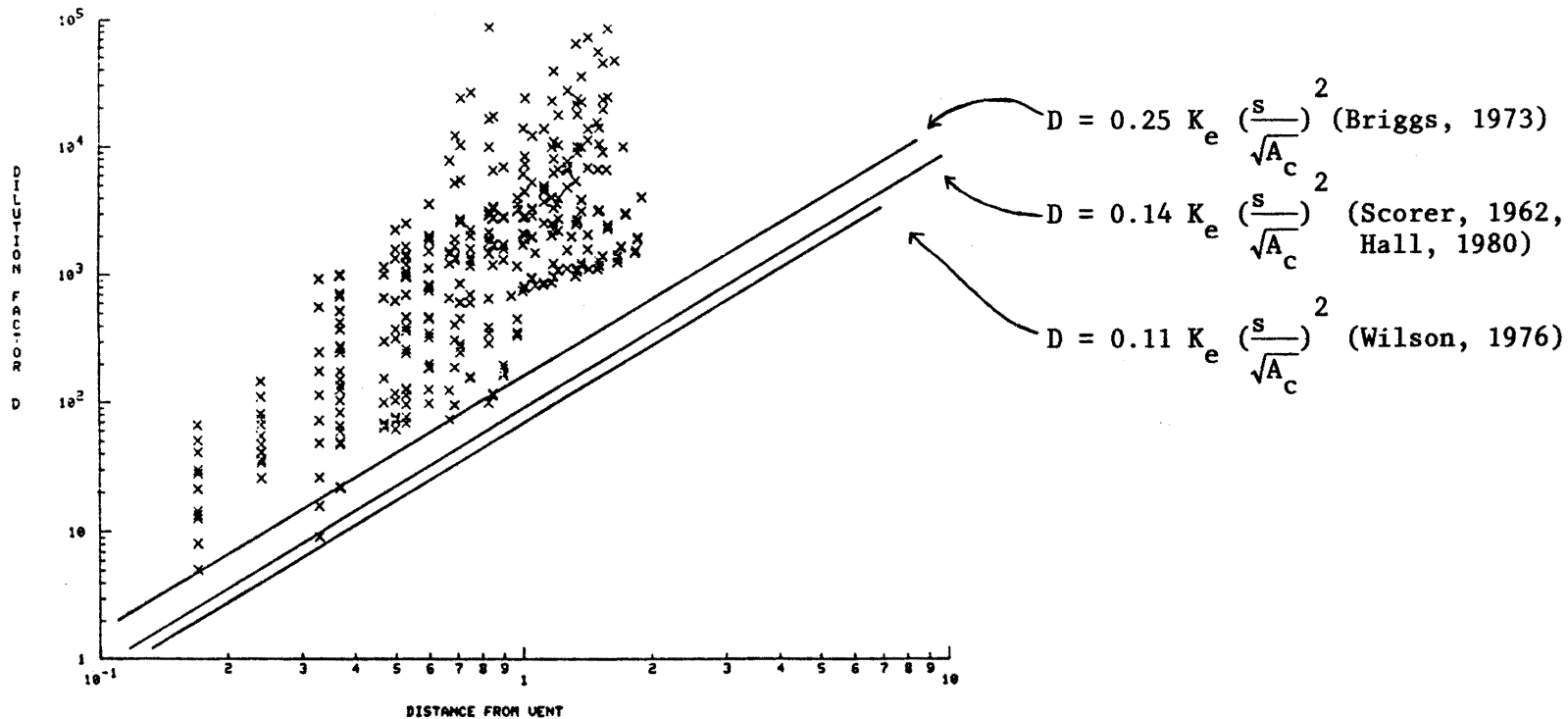
Figure 26. Dilution factors on the building for $\theta = 0°$ orientation.
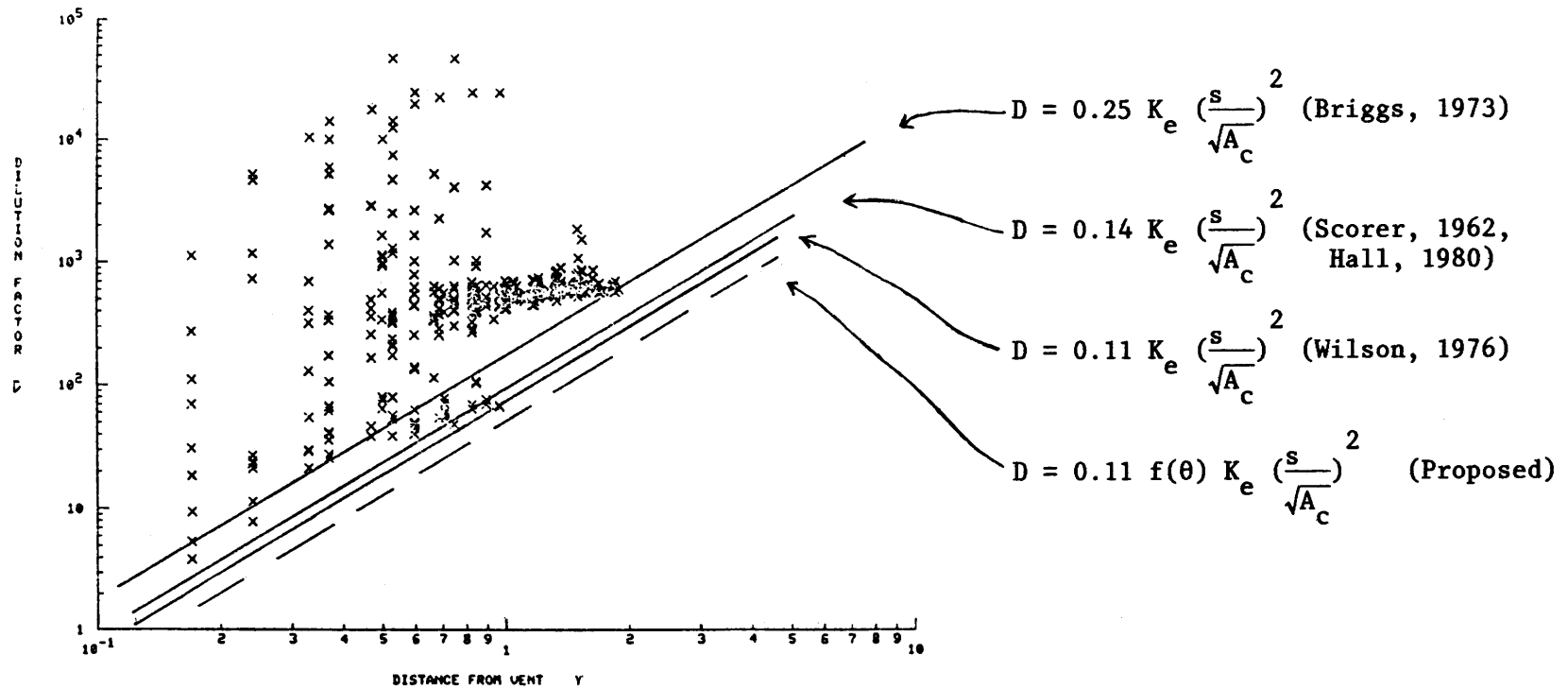
Figure 27. Dilution factors on the building for θ = 22.5° orientation.
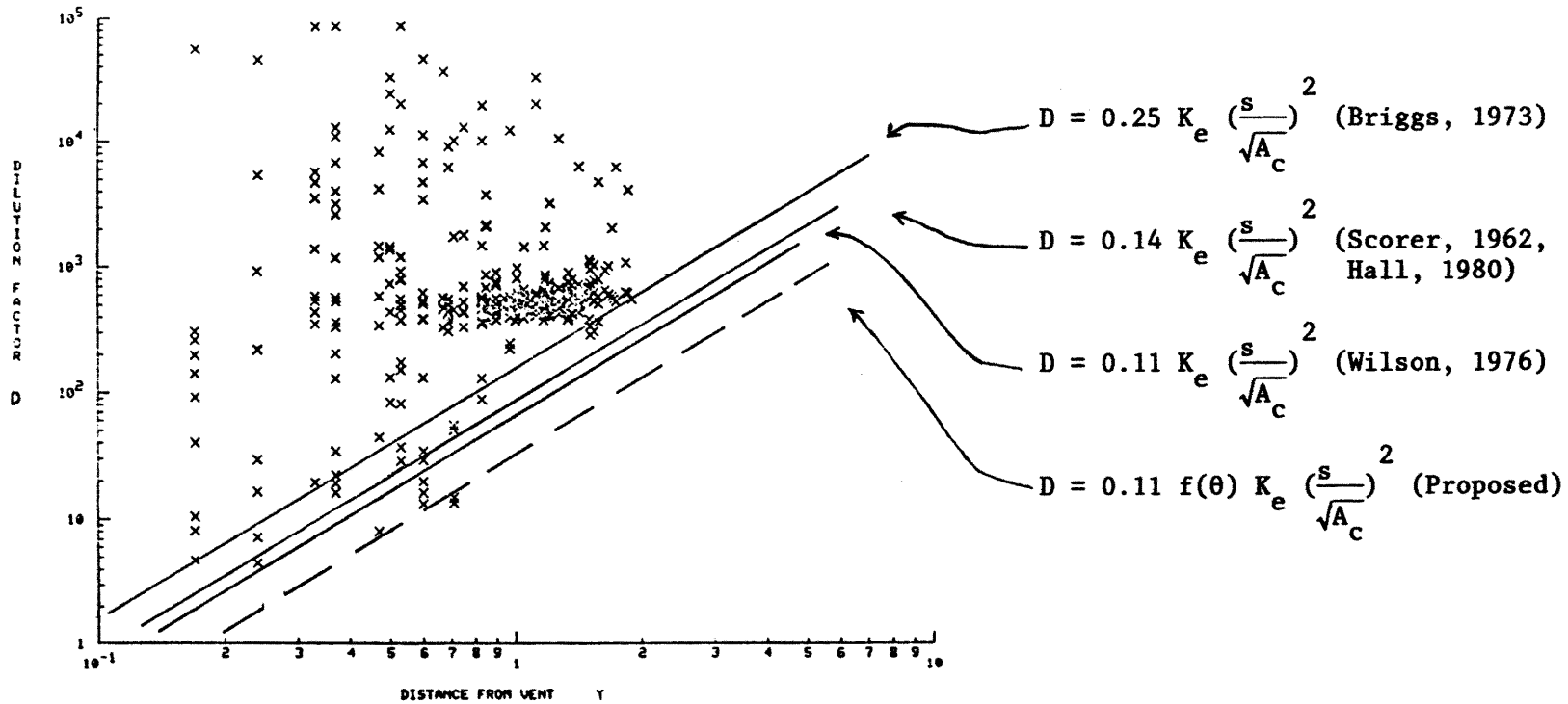
Figure 28. Dilution factors on the building for $\theta = 45°$ orientation.
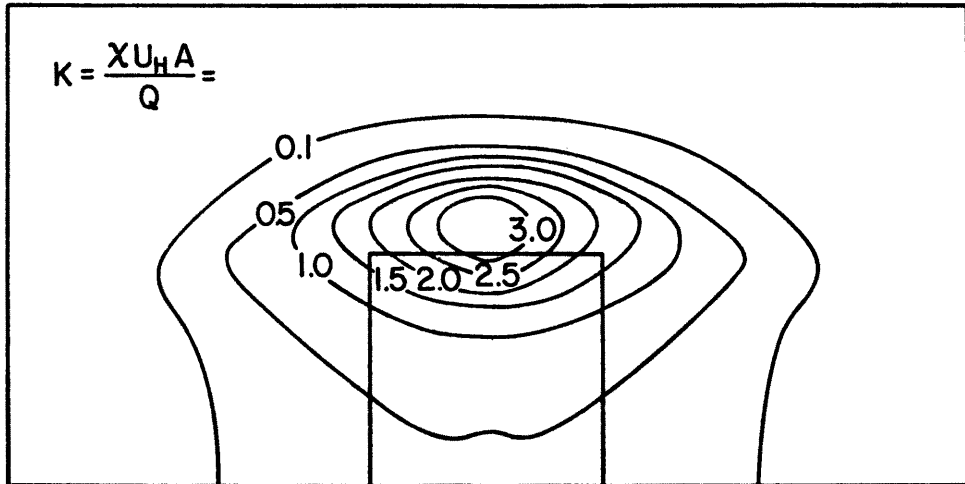
(a) x/H = 1.0
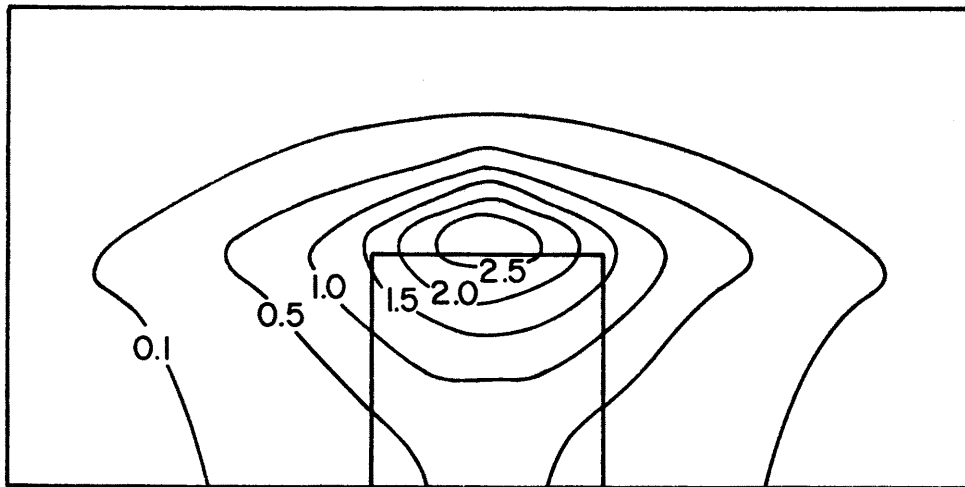
(b) x/H = 1.5
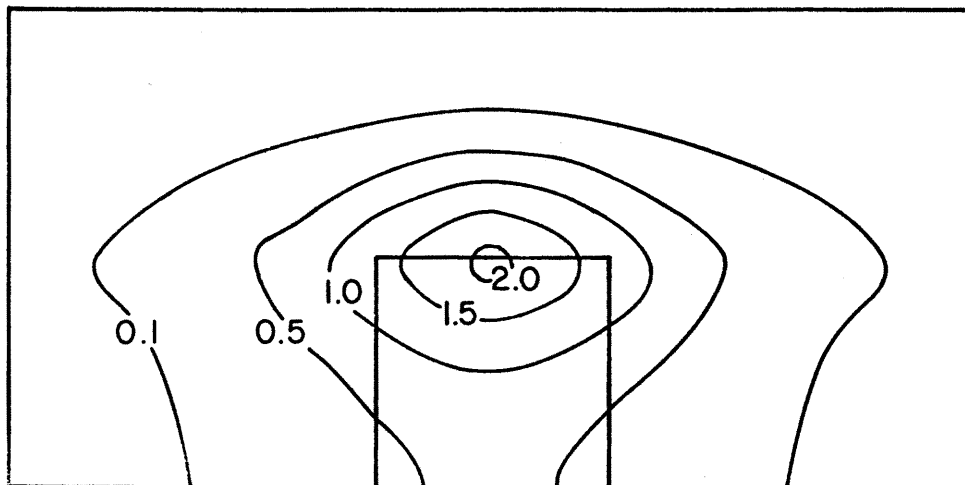
(c) x/H = 2.0

Figure 29. Concentration coefficient isopleths in the near wake
region for $\theta = 0°$, central roof vent release.
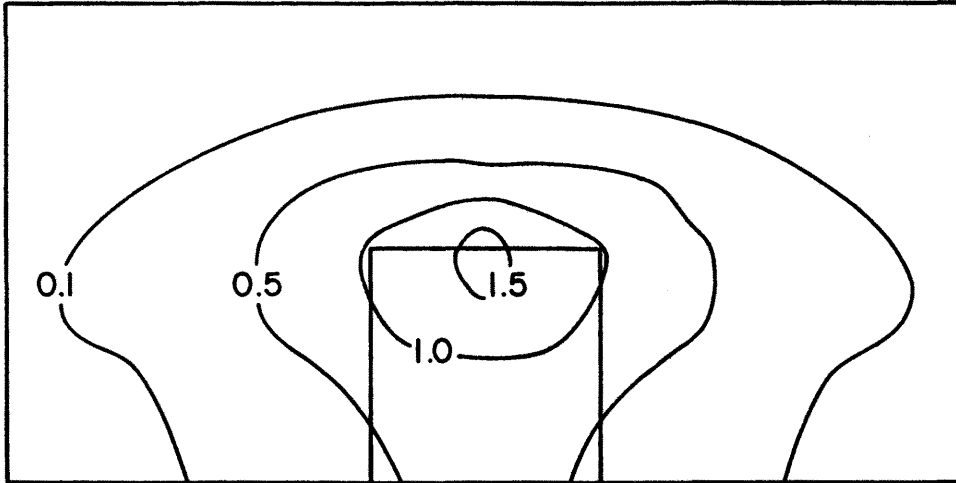
(d) x/H = 2.5
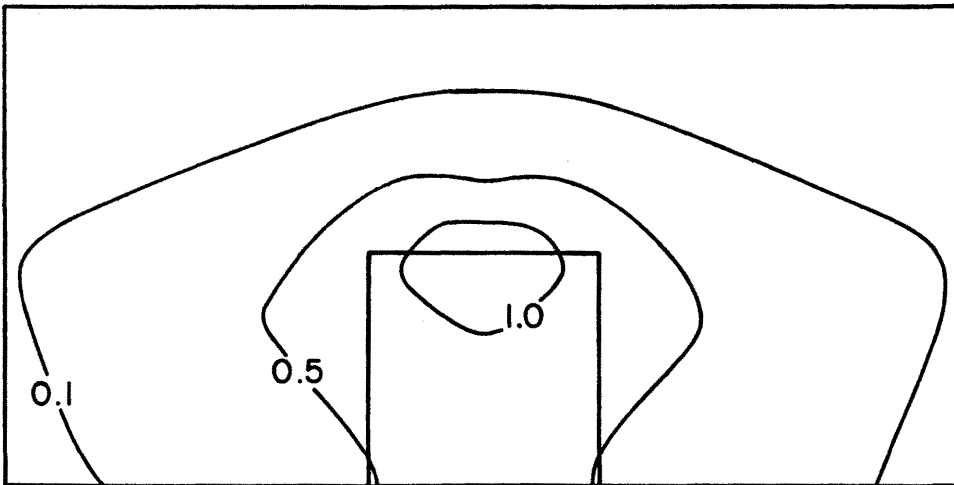
(e) x/H = 3.0
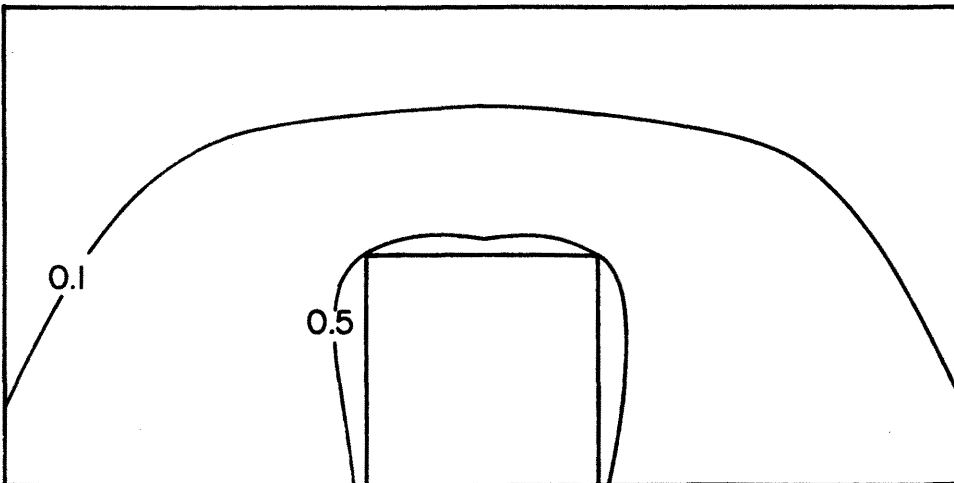
(f) x/H = 4.0

Figure 29. Continued.

(g) x/H = 5.0
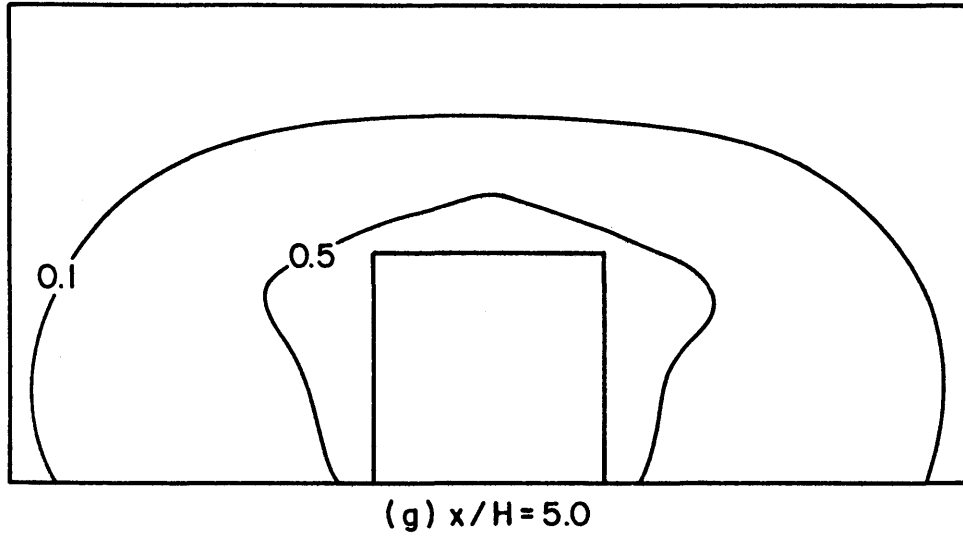
Figure 29. Continued.
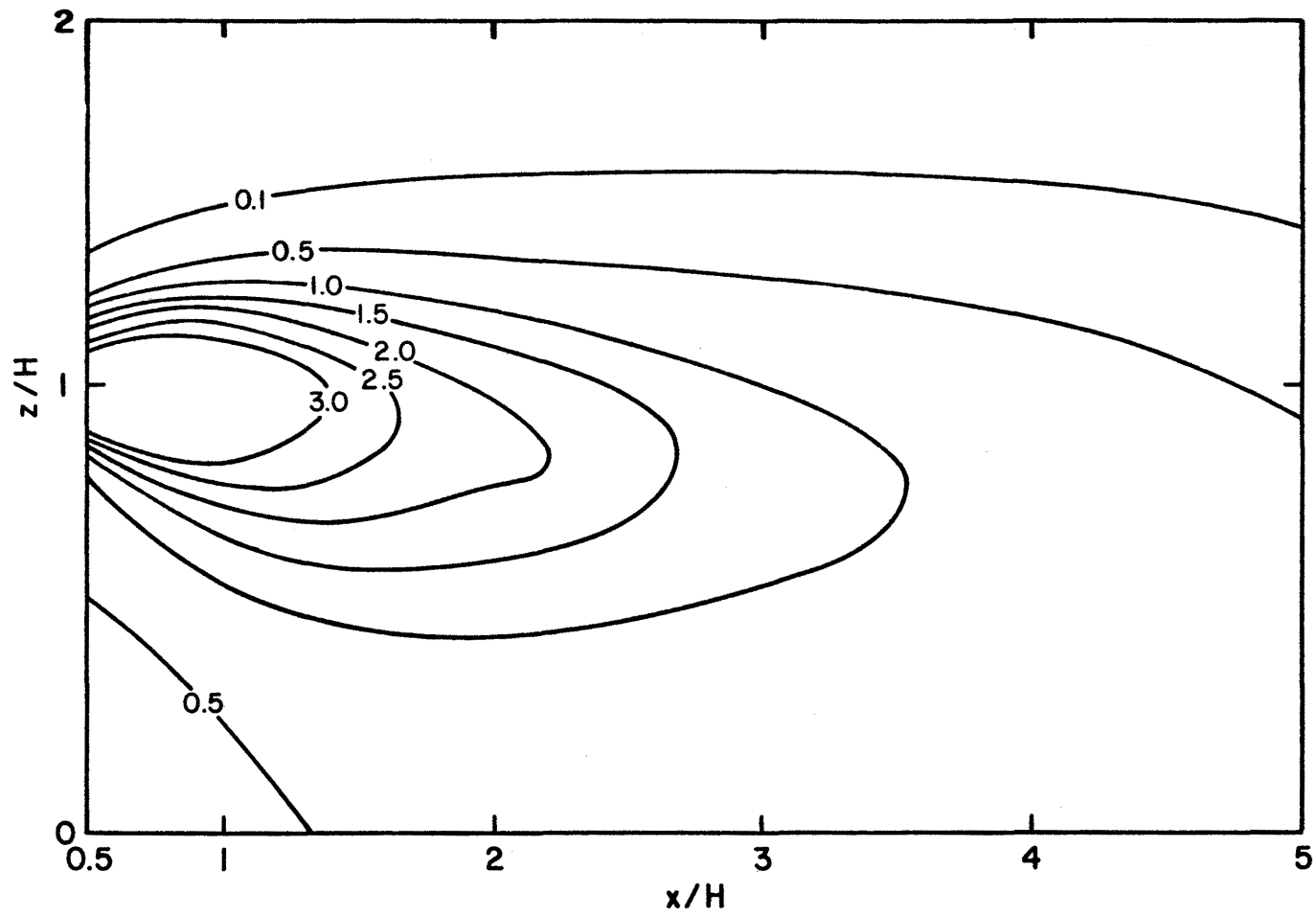
Figure 30. Longitudinal concentration coefficient distributions at y = 0 for
θ = 0° orientation.
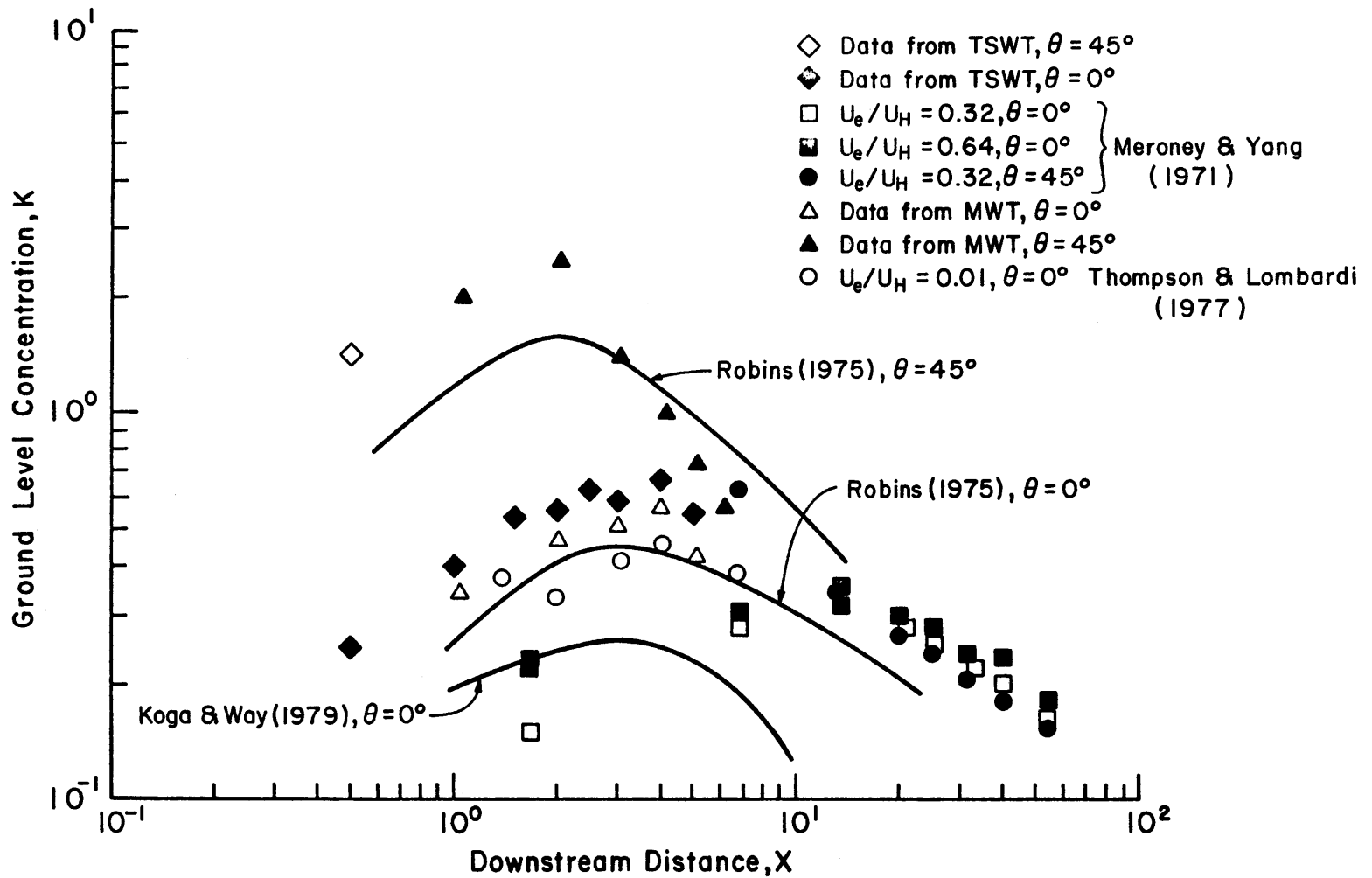
Figure 31. Centerline ground concentrations in the near wake region for θ = 0°, central roof vent release.
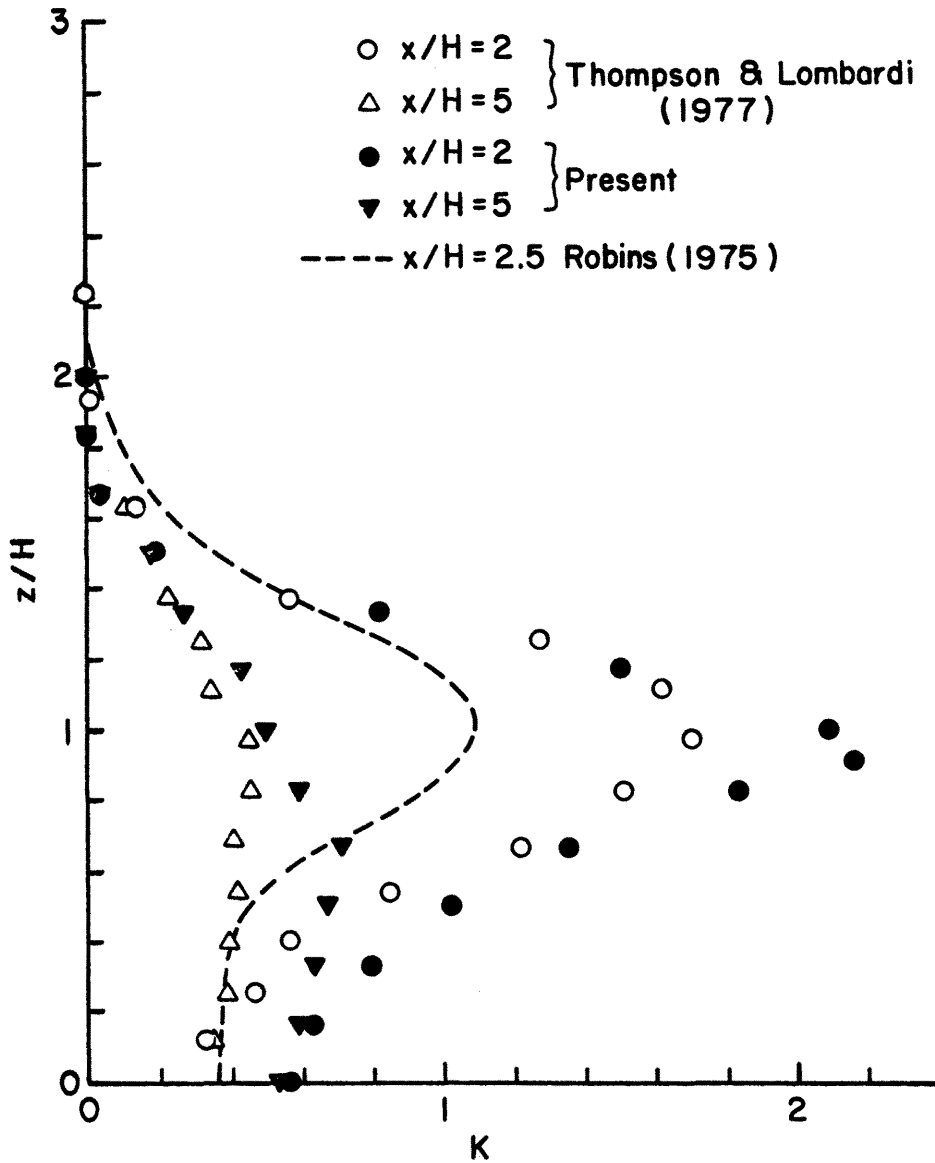
Figure 32. Vertical concentration coefficient profile for y = 0
and θ = 0°, central roof vent release.
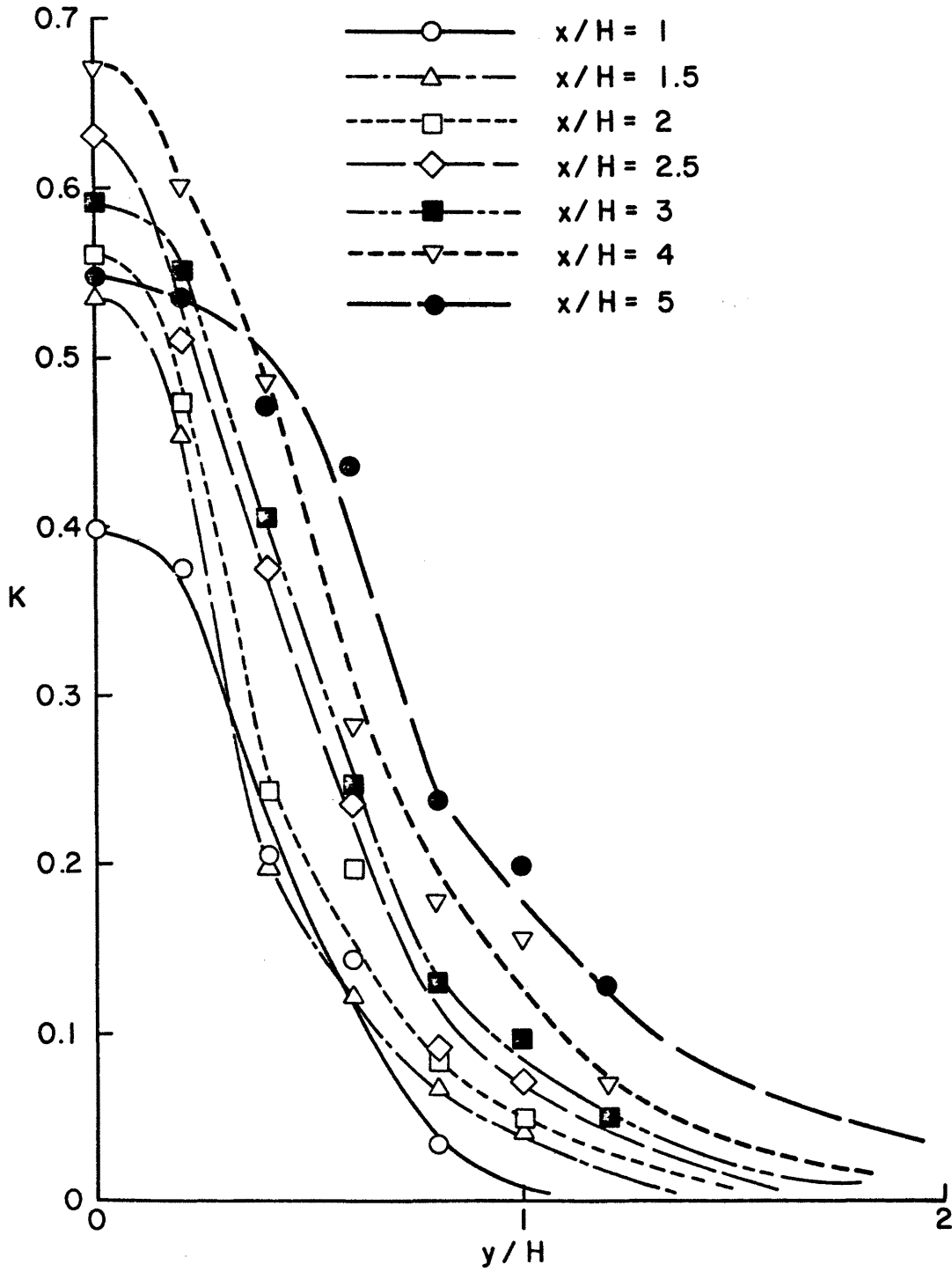
Figure 33. Lateral ground-level concentration coefficient distributions.
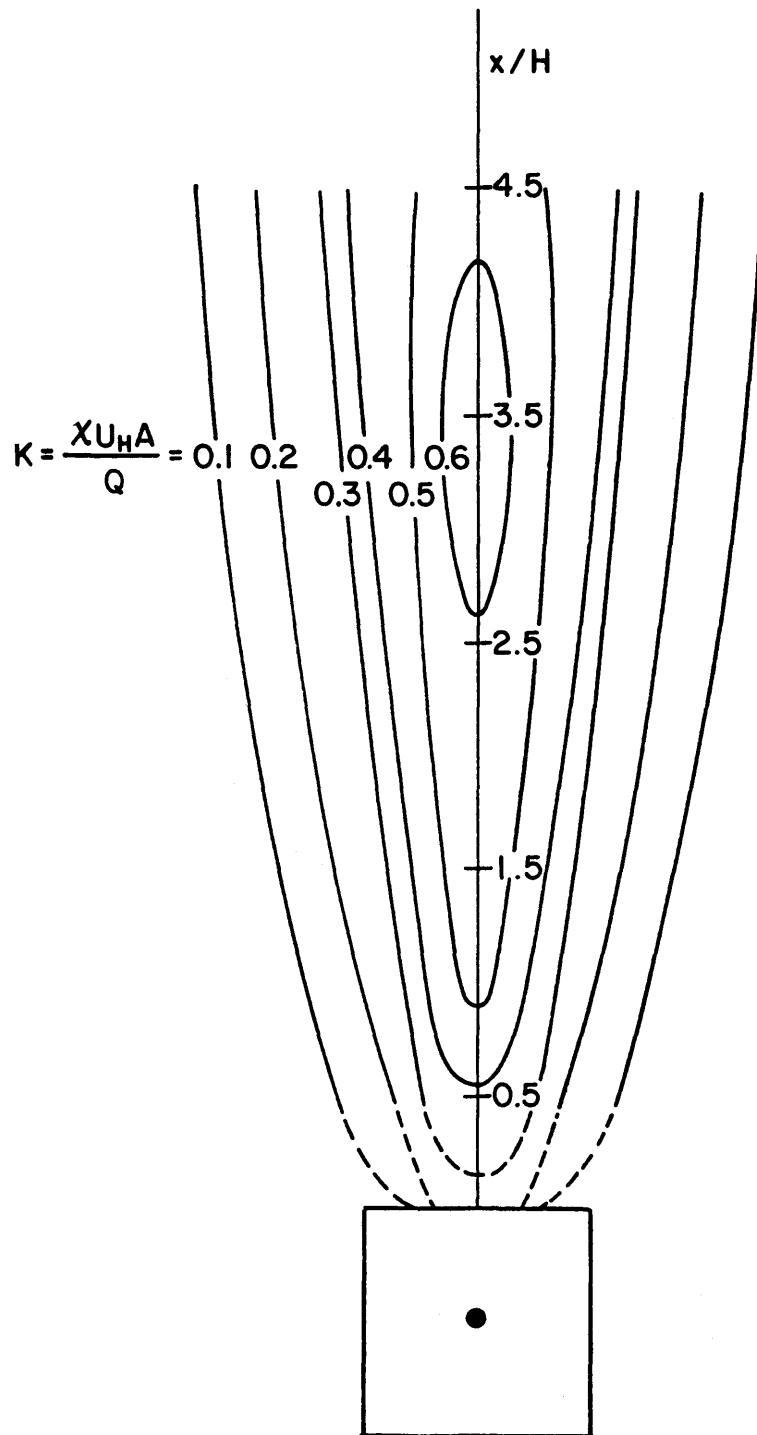
Figure 34. Ground-level concentration coefficients in the near wake for z = 0, θ = 0°, central roof vent release.
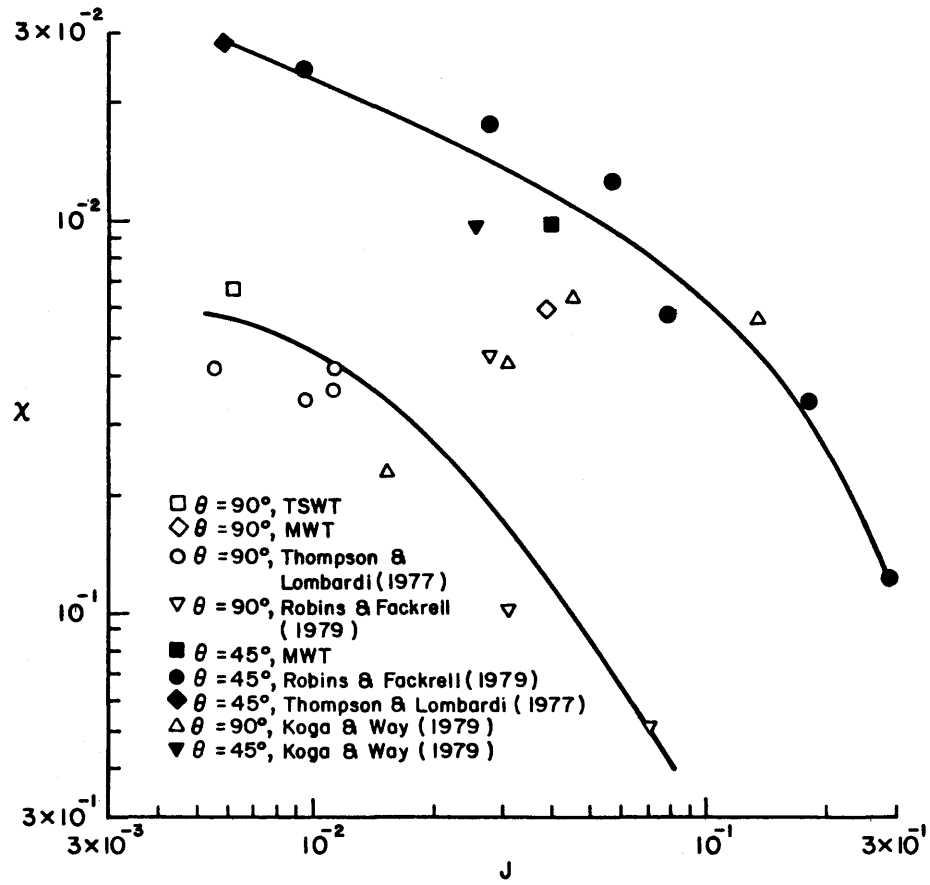
Figure 35. Maximum ground-level concentration coefficients vs. jet momentum parameter.
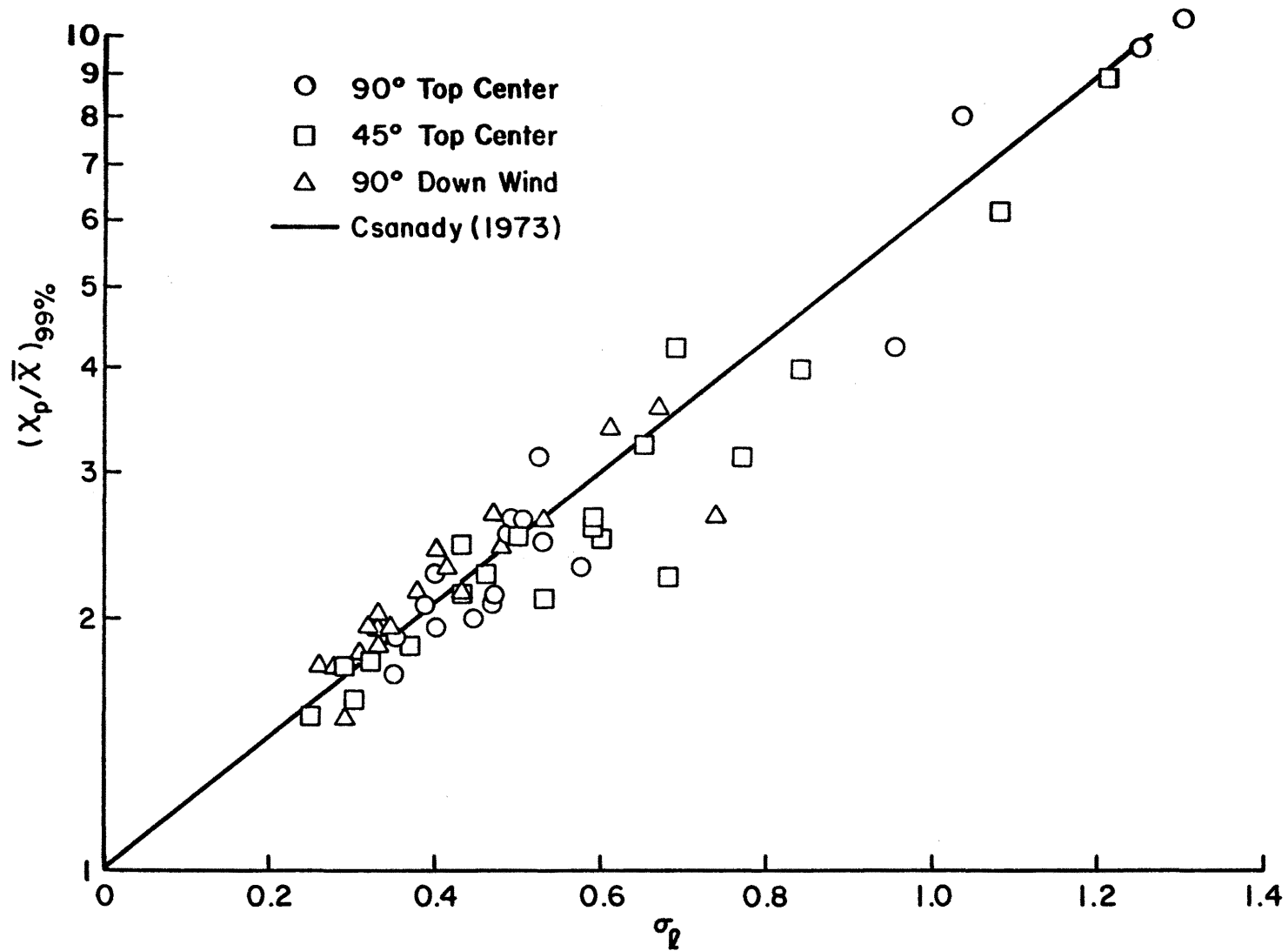
Figure 36. 99% peak-to-mean concentration ratio vs. logarithmic standard deviation.
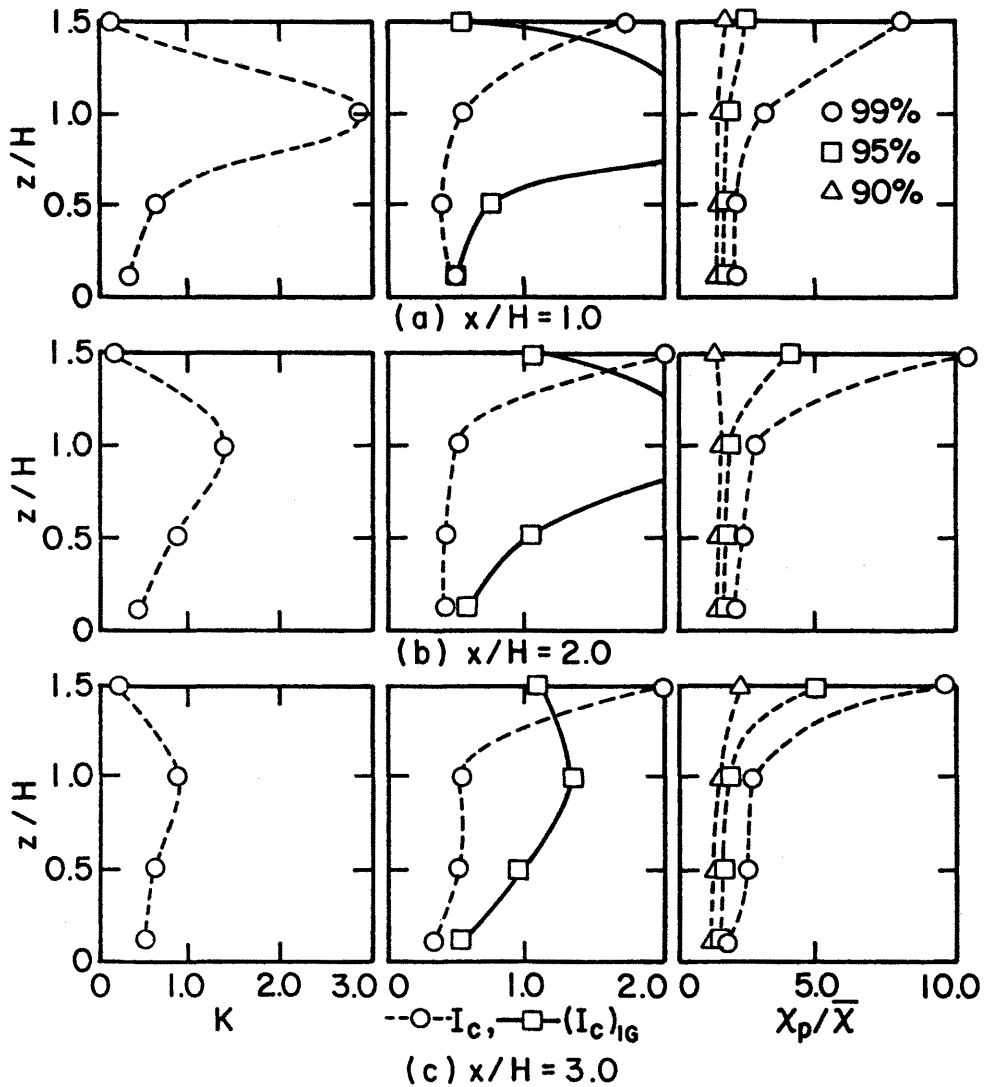
Figure 37. Vertical profiles of mean concentration, concentration fluctuation intensity, and peak-to-mean concentration ratio at several downwind points on wake centerline for $\theta = 0°$, central roof vent release.

(d) x/H=4.0

(e) x/H=5.0
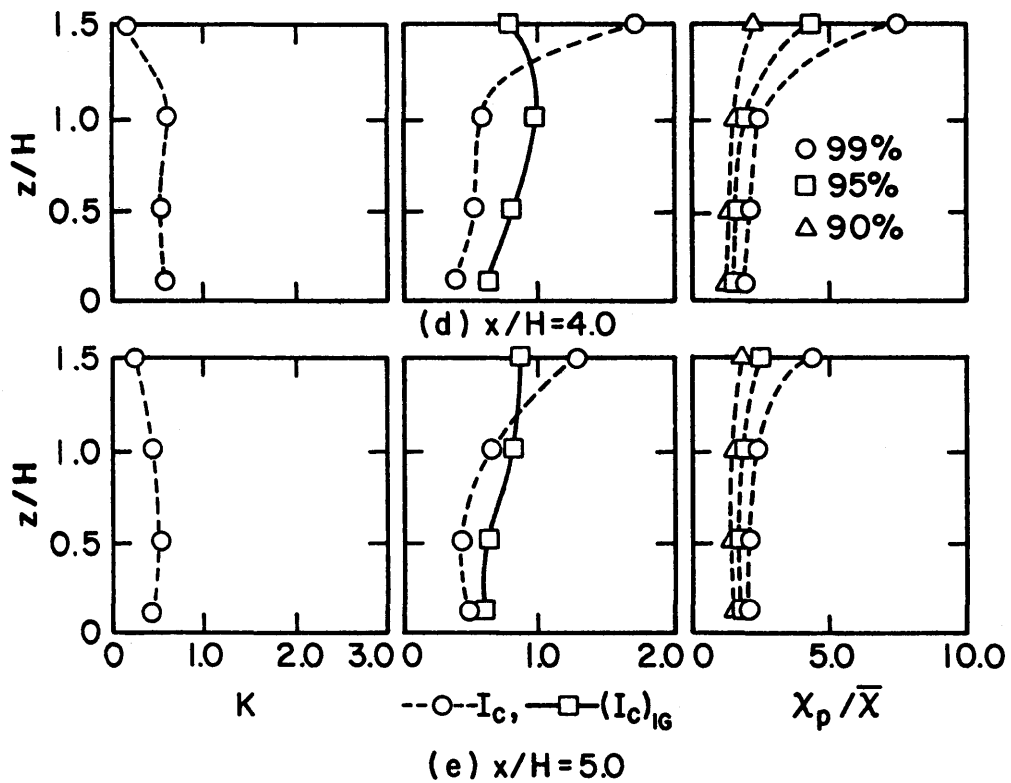
Figure 37. Continued.
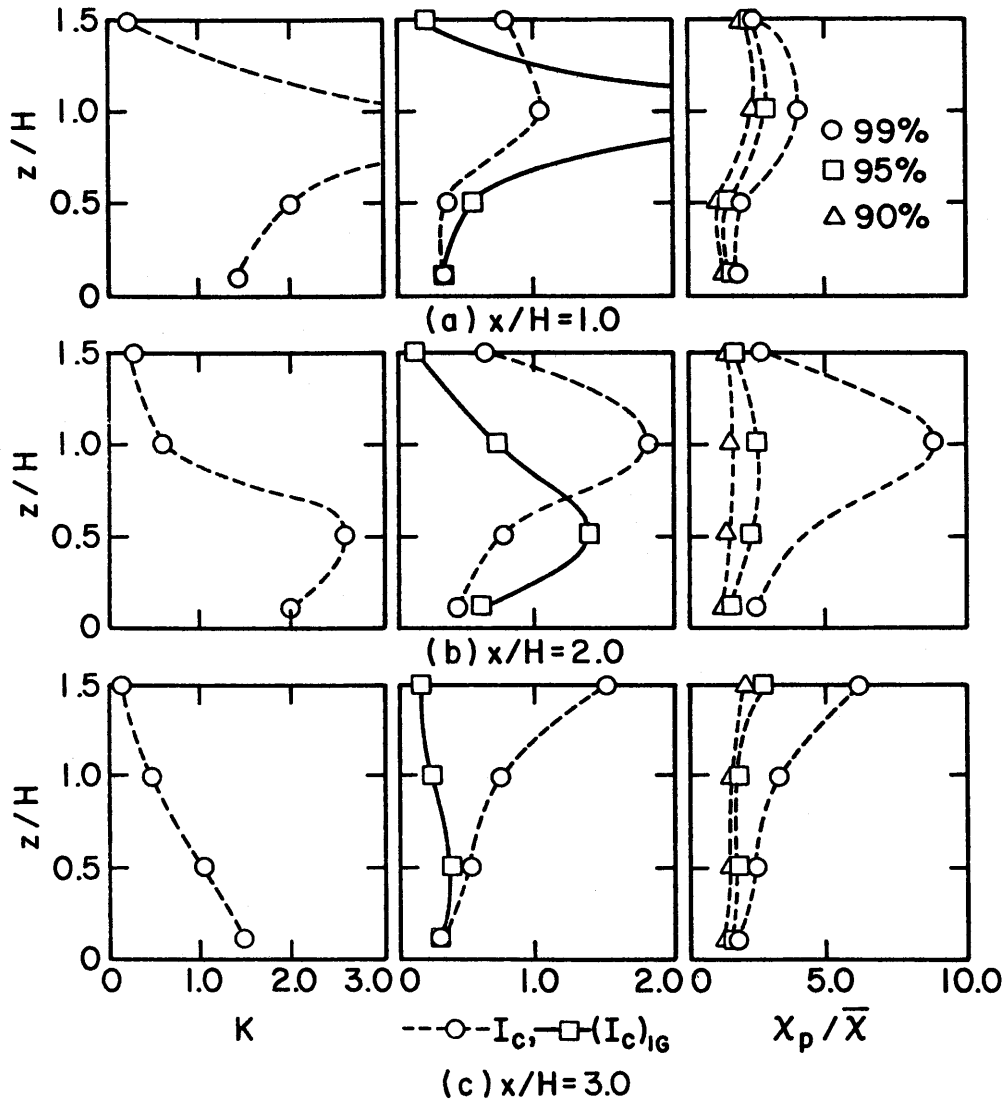
Figure 38. Vertical profiles of mean concentration, concentration
fluctuation intensity, and peak-to-mean concentration
ratio at several downwind points on wake centerline
for θ = 45°, central roof vent release.

(d) x/H=4.0

(e) x/H=5.0
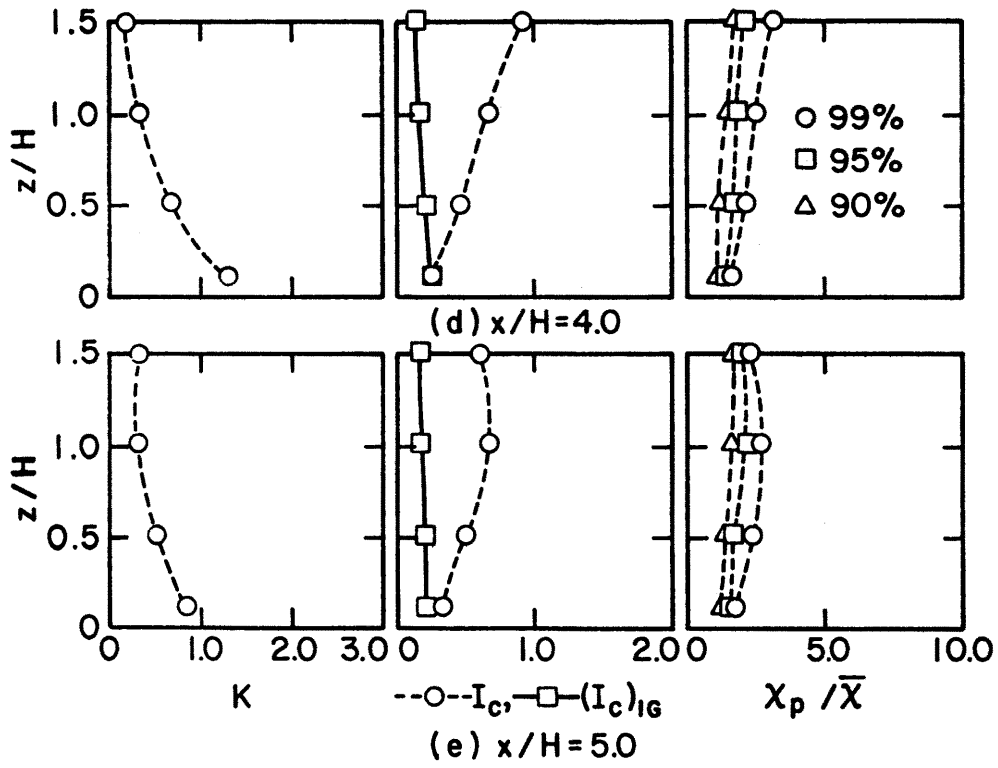
Figure 38. Continued.
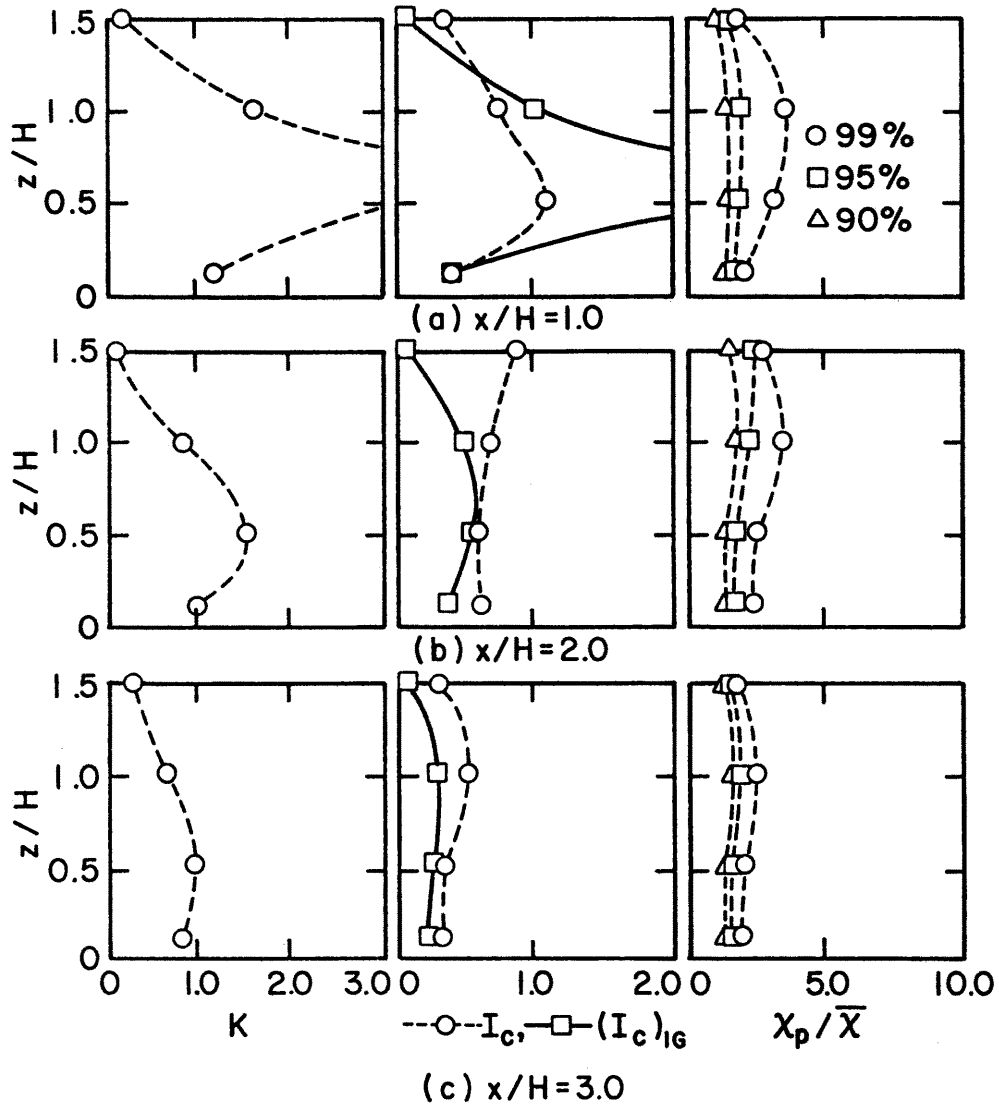
Figure 39. Vertical profiles of mean concentration,
concentration fluctuation intensity, and
peak-to-mean concentration ratio at several
downwind points on wake centerline for
$\theta = 0°$, downwind roof vent release.
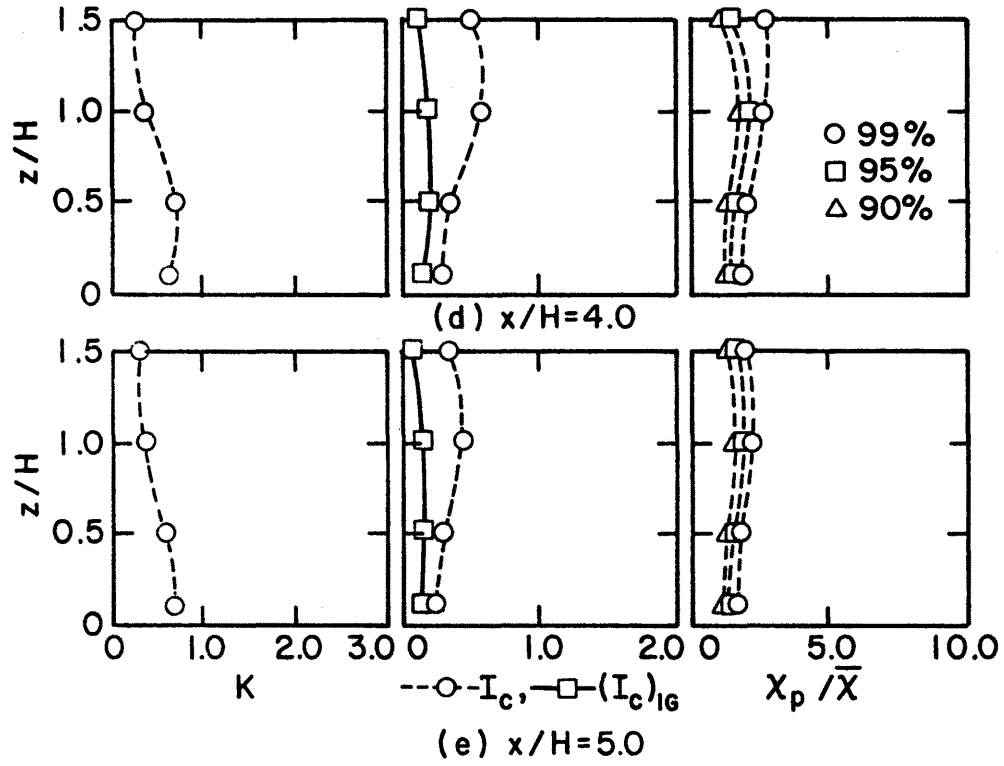
Figure 39. Continued.
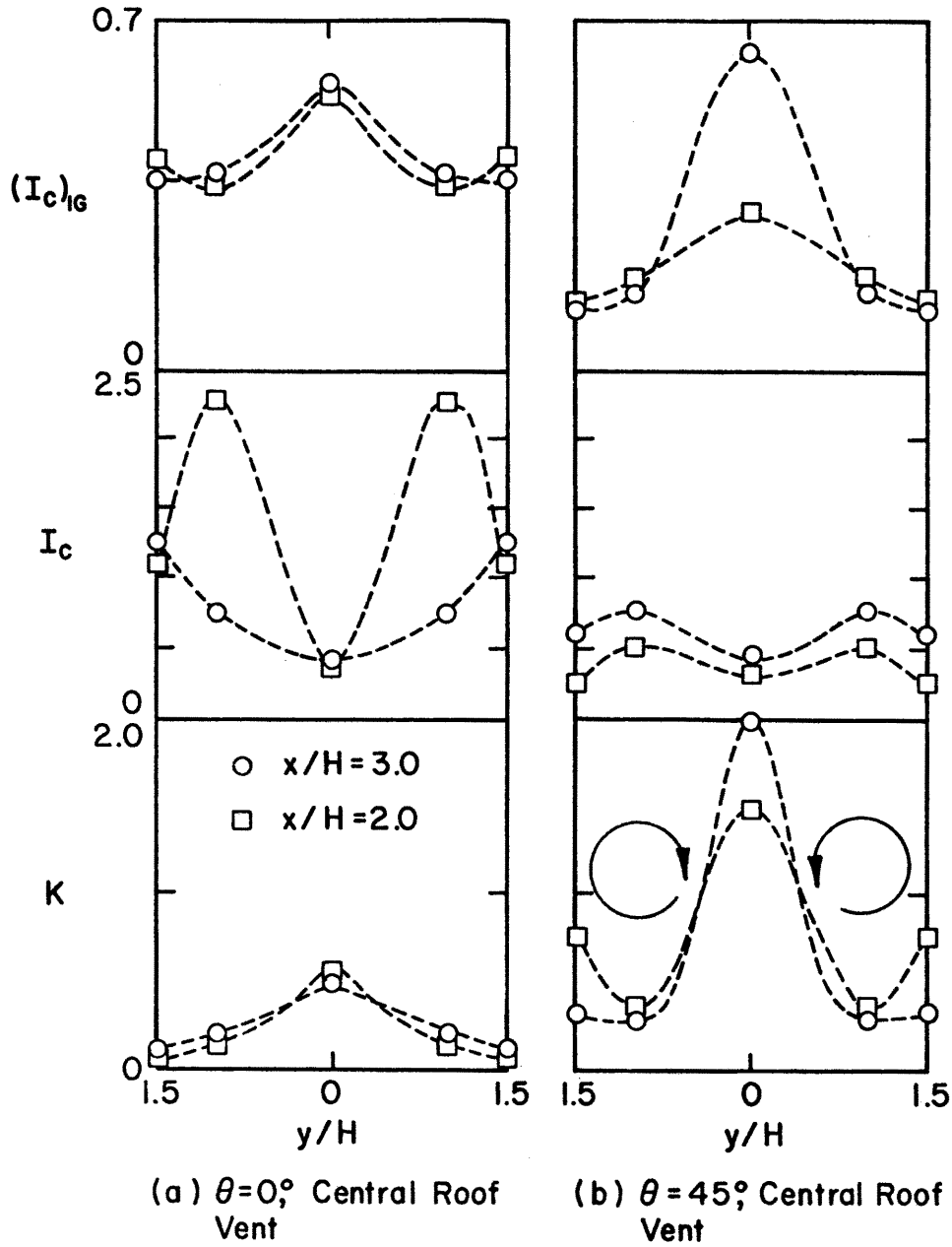
Figure 40. Cross-wind profiles of mean concentration
coefficients and concentration fluctuation
intensity.
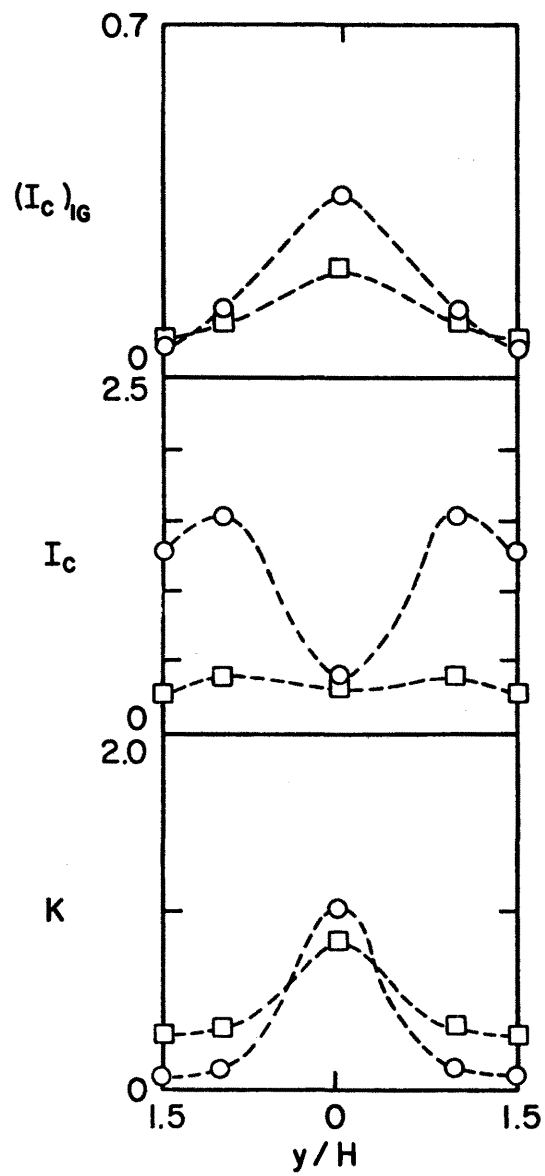
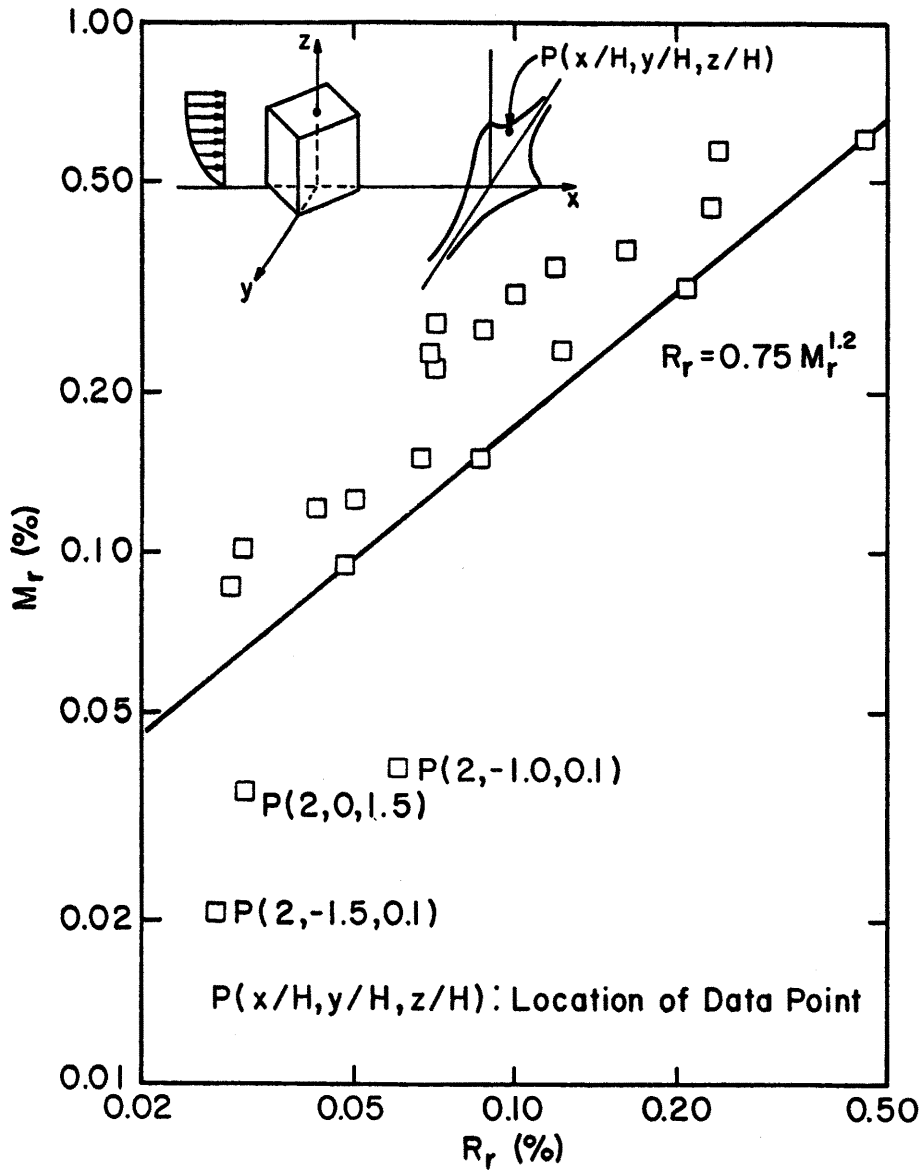(c) $\theta = 0°$, Downwind
Roof Vent

Figure 40. Continued.

Figure 41. RMS concentration vs. mean concentration in the near wake region for θ = 0°, central roof vent release.

Figure 42. RMS concentration vs. mean concentration in the near wake region for θ = 0°, downwind roof vent release.

$$R_r = 0.75 M_r^{1.2}$$

$P(2,-1.0,0.1)$

$P(2,0,1.5)$

$P(2,-1.5,0.1)$

$P(x/H, y/H, z/H)$: Location of Data Point
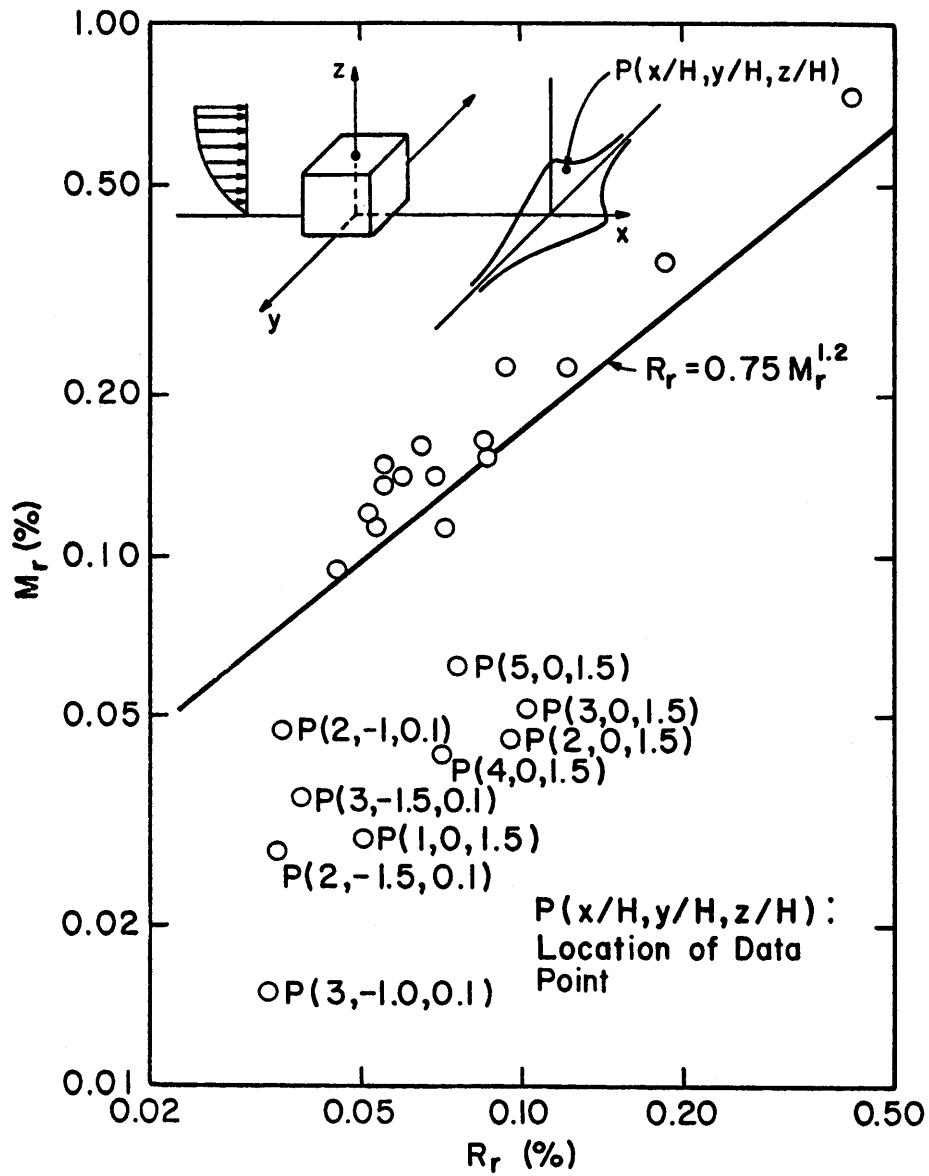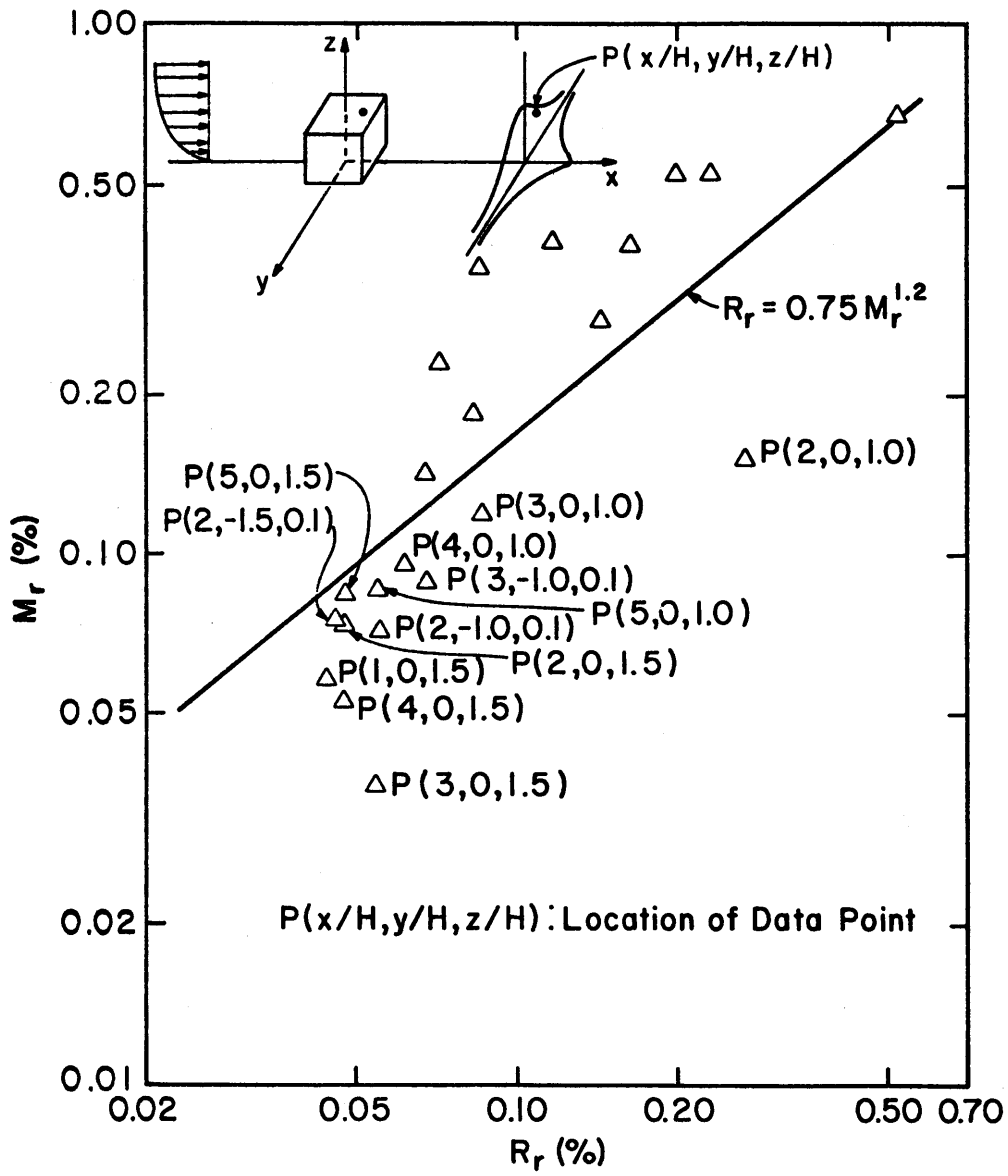
Note: See discussion, Section 4.4.1.

Figure 43. RMS concentration vs. mean concentration in the near wake region for $\theta = 45°$, central roof vent release.
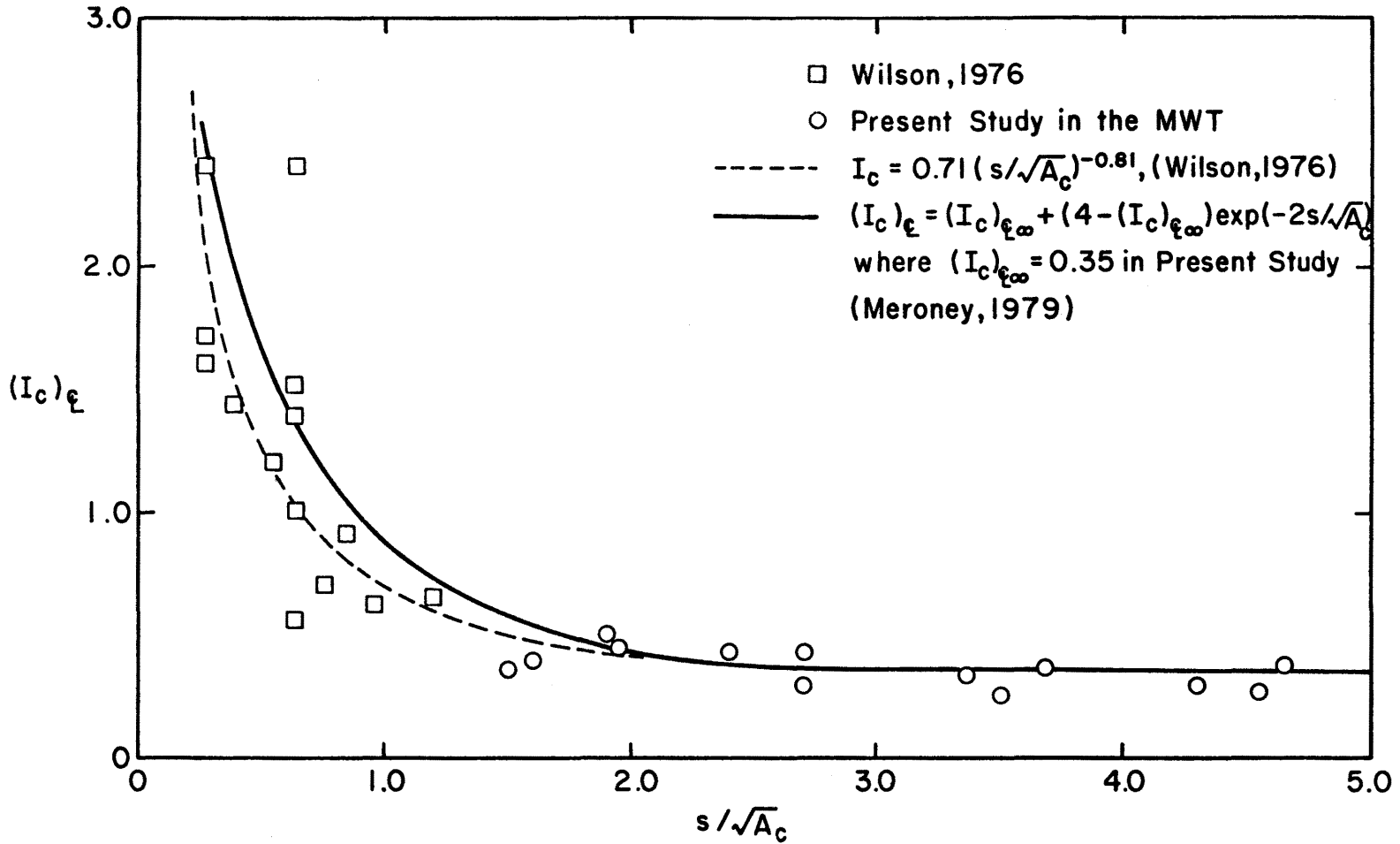
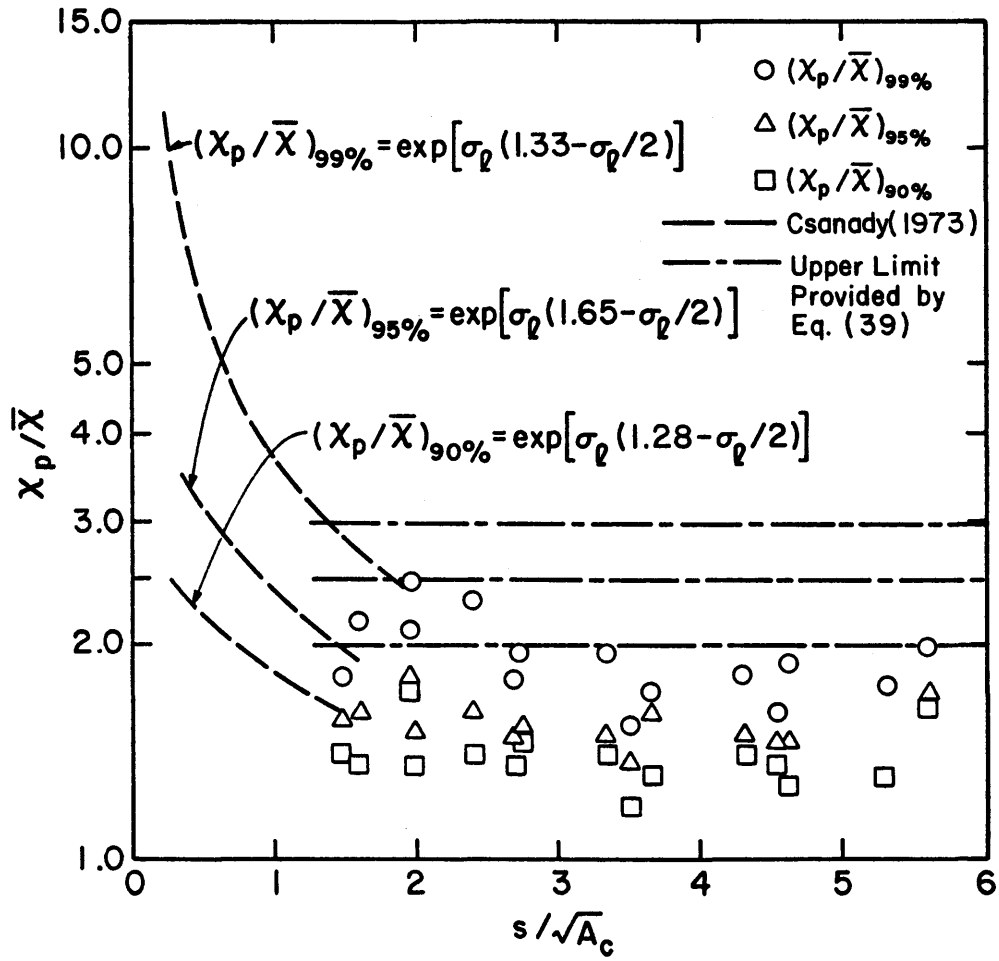Figure 44. Concentration fluctuation intensity at ground centerline vs. $s/\sqrt{A}$.

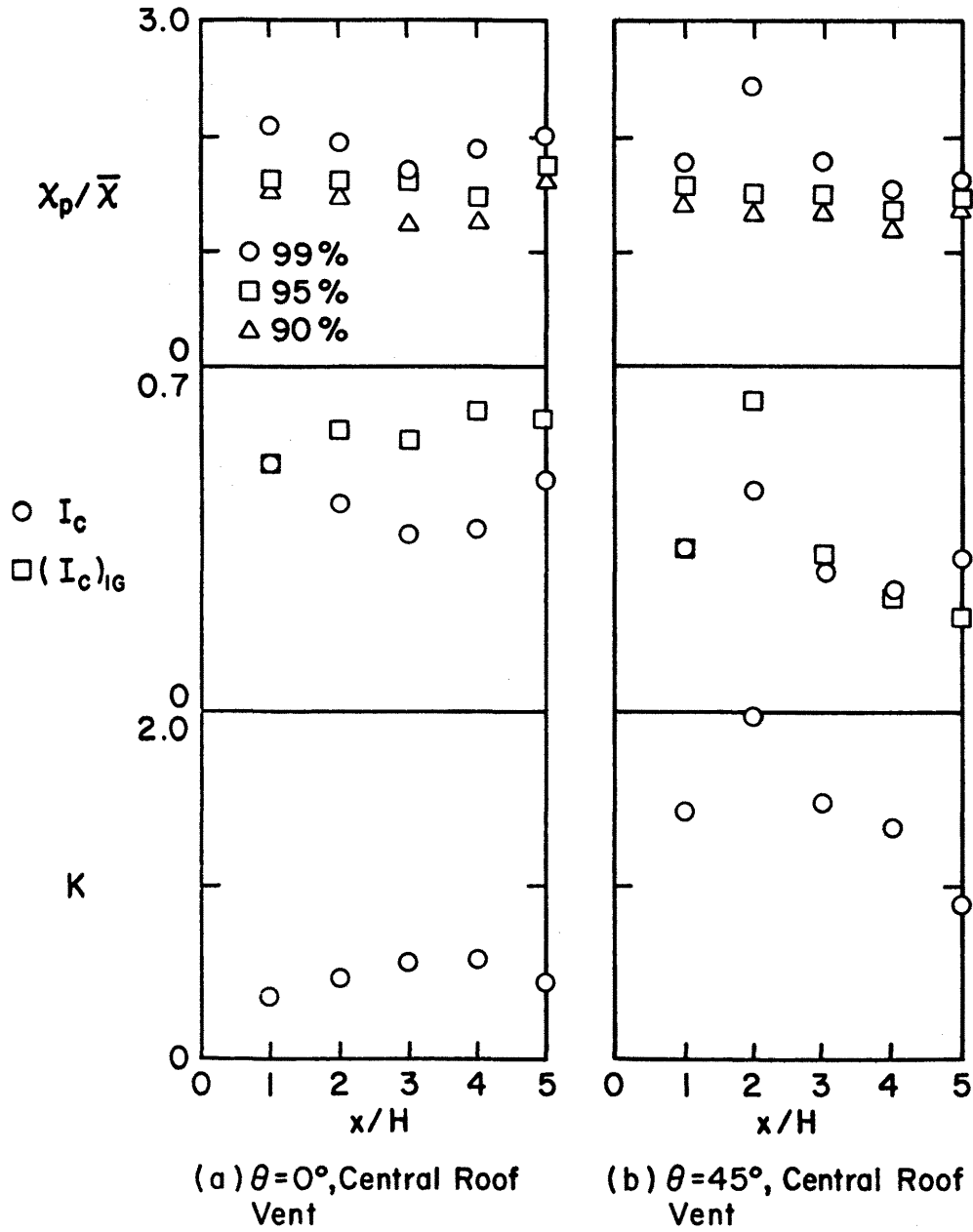Figure 45. Peak-to-mean concentration ratio at ground-level wake centerline vs. $s/\sqrt{A}$.
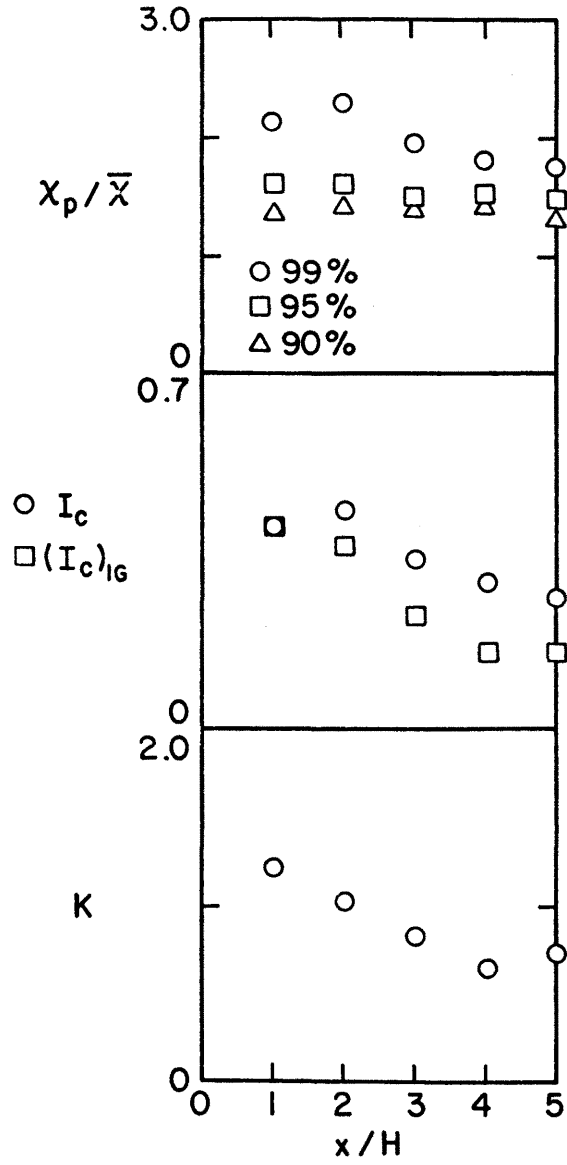
Figure 46. Longitudinal ground-level profile of mean concentration coefficient, concentration fluctuation intensity, and peak-to-mean concentration ratio at y/H = 0, z/H = 0.1.

(c) $\theta = 22.5°$, Central Roof
Vent

Figure 46. Continued.